



University of Kentucky
UKnowledge

Theses and Dissertations--Mechanical
Engineering

Mechanical Engineering


2020

MODELING THIN FLUID FILM ON A ROTARY BELL

Mark Doerre

University of Kentucky, mark.doerre@uky.edu

Author ORCID Identifier:

 <https://orcid.org/0000-0003-1105-3522>

Digital Object Identifier: <https://doi.org/10.13023/etd.2020.148>

[Right click to open a feedback form in a new tab to let us know how this document benefits you.](#)

Recommended Citation

Doerre, Mark, "MODELING THIN FLUID FILM ON A ROTARY BELL" (2020). *Theses and Dissertations--Mechanical Engineering*. 150.

https://uknowledge.uky.edu/me_etds/150

This Doctoral Dissertation is brought to you for free and open access by the Mechanical Engineering at UKnowledge. It has been accepted for inclusion in Theses and Dissertations--Mechanical Engineering by an authorized administrator of UKnowledge. For more information, please contact UKnowledge@lsv.uky.edu.

STUDENT AGREEMENT:

I represent that my thesis or dissertation and abstract are my original work. Proper attribution has been given to all outside sources. I understand that I am solely responsible for obtaining any needed copyright permissions. I have obtained needed written permission statement(s) from the owner(s) of each third-party copyrighted matter to be included in my work, allowing electronic distribution (if such use is not permitted by the fair use doctrine) which will be submitted to UKnowledge as Additional File.

I hereby grant to The University of Kentucky and its agents the irrevocable, non-exclusive, and royalty-free license to archive and make accessible my work in whole or in part in all forms of media, now or hereafter known. I agree that the document mentioned above may be made available immediately for worldwide access unless an embargo applies.

I retain all other ownership rights to the copyright of my work. I also retain the right to use in future works (such as articles or books) all or part of my work. I understand that I am free to register the copyright to my work.

REVIEW, APPROVAL AND ACCEPTANCE

The document mentioned above has been reviewed and accepted by the student's advisor, on behalf of the advisory committee, and by the Director of Graduate Studies (DGS), on behalf of the program; we verify that this is the final, approved version of the student's thesis including all changes required by the advisory committee. The undersigned agree to abide by the statements above.

Mark Doerre, Student

Dr. Kozo Saito, Major Professor

Dr. Alexandre Martin, Director of Graduate Studies

MODELING THIN FLUID FILM
ON A ROTARY BELL

DISSERTATION

A dissertation submitted in partial fulfillment of the
requirements for the degree of Doctor of Philosophy in the
College of Engineering
at the University of Kentucky

By

Mark Doerre

Lexington, Kentucky

Co-Directors: Dr. Kozo Saito, TVA Professor of Mechanical Engineering
and Dr. Nelson Akafuah, Professor of Mechanical Engineering

Lexington, Kentucky

2020

Copyright © Mark Doerre 2020
<https://orcid.org/0000-0003-1105-3522>

ABSTRACT OF DISSERTATION

MODELING THIN FLUID FILM ON A ROTARY BELL

A component of the mission in the Institute of Research for Technology Development at the University of Kentucky is advancing research and development and bringing it to the factory floor for continuous improvement. This dissertation delves into the art and science of rotational fluid mechanics in the context of rotary bell atomizers. One outcome proves that an approximation for calculating fluid film thicknesses on high-speed spinning surfaces inferred while working in cylindrical and spherical coordinate systems can be applied to an arbitrary bell profile. However, the analytical limits of this approximation were not investigated. In all cases, a restriction exists that the bell profile curvature is much greater than the fluid film thickness. The validity of this approximation was supported by findings in publications employing curvilinear coordinates created by axisymmetric revolution of a planar curve. This validation enabled rigorous analyses of bell profiles beyond the common cylindrical or spherical profiles. A curvilinear system containing a coordinate of arc length along the bell profile is the arbitrary case, and the most reduced high-speed case collapses to an approximation from an observed pattern in simpler coordinate systems. The jump to varying curvature curvilinear coordinates requires additional mathematics to calculate metric tensor coefficients and spatial derivatives of directional unit vectors, and to develop lengthy vector invariants. Another outcome was to explain the underlying symmetry in the reduced order solution for a coupled rotary system that included centrifugal and Coriolis effects on a conical rotary bell.

KEYWORDS: curvilinear, metric tensor, vector invariant, Navier-Stokes, rotary bell

Mark Doerre

5/3/2020

Date

MODELING THIN FLUID FILM
ON A ROTARY BELL

By
Mark Doerre

Dr. Kozo Saito

Co-Director of Thesis

Dr. Nelson Akafuah

Co-Director of Thesis

Dr. Alexandre Martin

Director of Graduate Studies

5/3//2020

Date

DEDICATION

To Mom (3/31/2013) and Dad (4/2/2019)

And

My wife, Ollie

And

Samantha & Paul, Richard & Maddie, Lily and Gabby

And

John, George, Debbie, Barbara, George III, Theresa, Rick, Cailyn, Mallory, James
And James Jr. and Olivia

ACKNOWLEDGMENTS

I would like to thank the University of Kentucky and Toyota for establishing the IR4TD Toyota Paint Lab.

Professor Dr. Kozo Saito is owed a debt of gratitude that cannot be repaid. However, I can pay it forward by using a lifetime of engineering to educate the next generation, and to engage in service for students, scholars, and practitioners in rotating thin film research and development.

Professor Dr. Nelson Akafuah has been invaluable in teaching the art of publication and academic writing; thank you. His story as a “kid from Ghana” that used the pensions of family members as collateral to pay for his education, to having his PhD interrupted by Hurricane Katrina, to transferring to UK and repeating his qualifying exams, and finally finishing his doctorate at U.K is an inspiration.

Thank you to Professor Dr. John Wenk for the formalism of your teachings in ME640, Foundations of Solid Mechanics, and ME601, Theory of Plasticity. Learning the art and science of indicial notation was essential to understanding the mathematics contained in this dissertation. This dissertation used those teachings to extrapolate from Cartesian coordinate systems, and into a surface following varying curvature curvilinear coordinate system.

Thank you to Dr. John Stencil for reviewing manuscripts and sharing wisdom that can only come from years of experience. Thank you to Research Professor Dr. Ahmad Salaimh for his guidance and expertise in the area of automotive paint processes.

Thank you to Adnan Darwish Ahmad - I have known you the longest as a graduate student and colleague - for friendship and all the discussions and cultural exchanges between the USA and Middle East.

Thank you to Essa Khalid, Ahmad Abubaker, Masoud Arabghahestani, Helmut Koch, Dr. Zhaojin Diao, and Ricky Green, “you all” made our office a great place to work and learn.

Thank you to my committee members:

Dr. Saito	Mechanical Engineering
Dr. Akafuah	Mechanical Engineering
Dr. Bailey	Mechanical Engineering
Dr. Salaimah	Mechanical Engineering
Dr. Perry	Mathematics
Dr. Harik	Civil Engineering - External Examiner

TABLE OF CONTENTS

ACKNOWLEDGMENTS iii

LIST OF TABLES viii

LIST OF FIGURES ix

NOMENCLATURE..... x

CHAPTER 1. INTRODUCTION..... 1

 1.1 Summary of Chapters 1

 1.2 Map of Dissertation 11

CHAPTER 2. PATENT HISTORY 14

 2.1 Introduction 14

 2.2 US Patent Database 15

CHAPTER 3. LITERATURE REVIEW 21

 3.1 Introduction 21

 3.2 Literature Review 23

CHAPTER 4. PRELIMINARIES 42

 4.1 Introduction 42

 4.2 Non-Inertial Rotating Frame - Cylindrical Coordinate System 43

 4.3 Thin Film Approximation – Cylindrical Coordinate System 46

 4.4 Non-Inertial Rotating Frame - Spherical Coordinate System 47

 4.5 Thin Film Approximation – Spherical Coordinate System 50

 4.6 Cylindrical Navier-Stokes – Rotating System 52

 4.7 Spherical Navier-Stokes – Rotating System 53

CHAPTER 5. VON KARMAN MODEL 54

 5.1 Introduction 54

 5.2 Continuity Equation of Infinite Fluid on Spinning Boundary 56

 5.3 Radial Navier-Stokes Equation of Infinite Fluid on Spinning Boundary 57

5.4	Tangential Navier-Stokes Equation of Infinite Fluid on Spinning Boundary	59
5.5	Solution to the System of Ordinary Differential Equations.....	60
CHAPTER 6. The Ekman Number		64
6.1	Introduction	64
CHAPTER 7. Greenspan Formulation		69
7.1	Introduction	69
7.2	Coriolis Terms – Spherical Vector Cross Product.....	72
7.3	Centrifugal Terms – Spherical Vector Cross Product	75
CHAPTER 8. Thin Film Model		78
8.1	Introduction	78
8.2	Disk Model of Rotary Bell	79
8.3	Conical Model of Rotary Bell	83
8.4	Spherical Model of Rotary Bell.....	87
8.5	Non-Dimensional Forms	92
8.6	Coupled Differential Equations – Conical Model of Rotary Bell	95
8.7	Discussion and Numerical Results	101
8.8	Reduction of order.....	104
8.9	Conclusion.....	107
CHAPTER 9. Curvilinear Model.....		108
9.1	Introduction	108
9.2	Order of Magnitude Analysis	111
9.3	Curvilinear Coordinates	122
9.4	Metric Tensor Coefficients.....	126
9.5	Unit Vector Derivatives in Curvilinear Coordinates	134
9.6	Vector Invariants	143
9.7	Navier-Stokes in a Curvilinear System	146
9.8	Convergence of High Speed Cases.....	154
CHAPTER 10. Comparison of Approximation to published data		162
10.1	Film thickness Calculation	162
10.2	Conclusion.....	166
CHAPTER 11. Publication Abstracts.....		168
11.1	Publication I	168

11.2	Publication II.....	169
11.3	Publication III.....	170
REFERENCES.....		171
VITA.....		176

LIST OF TABLES

Table 8.7-1 Disk, Cone, and Hemisphere Film Characterization.....	101
---	-----

LIST OF FIGURES

Figure 1.2-1	Map of Dissertation.....	11
Figure 2.2-1	Disk Rotary Atomizer Insecticide Spray Bar [20]	15
Figure 2.2-2	Conical Rotary Atomizer, 1915 [21].....	16
Figure 2.2-3	Fluid supply [25].....	17
Figure 2.2-4	Atomizer [26]	18
Figure 2.2-5	Cup with serrations [27]	18
Figure 2.2-6	Cross Hatch Serrations [28].....	19
Figure 2.2-7	Powdered Metal [29]	20
Figure 4.2-1	Cylindrical Coordinate System	44
Figure 4.4-1	Spherical Coordinate System	47
Figure 5.5-1	Matlab Function solves system of ODE's	61
Figure 5.5-2	Solution to System of ODE's.....	62
Figure 5.5-3	Three dimensional flow field.....	63
Figure 6.1-1	Ekman spiral (axes scaled for illustration)	67
Figure 7.2-1	Symbolic Processor Calculation - Coriolis Terms	74
Figure 7.3-1	Symbolic Processor Calculation - Centrifugal Terms	76
Figure 8.3-1	Air/Fluid Boundary Condition Location	85
Figure 8.4-1	Spherical bell analysis.....	90
Figure 8.7-1	Film thickness vs R (distance from axis of rotation)	102
Figure 8.8-1	Complex Plane and roots of $\alpha^4 + 4 = 0$	105
Figure 9.3-1	Curvilinear Coordinates ξ, η	123
Figure 9.3-2	Differential quantities define proportions.....	124
Figure 9.3-3	Curvilinear Coordinates	124
Figure 9.8-1	Cylindrical System	156
Figure 9.8-2	Spherical System: Constant Polar Angle	157
Figure 9.8-3	Spherical System: Constant Radius.....	157
Figure 9.8-4	Bell profile as $f(x)$	159
Figure 9.8-5	Cartesian & Curvilinear Systems.....	160
Figure 10.1-1	Film Thickness Example.....	163

NOMENCLATURE

Alpha	Name	Description	Fundamental Units	Units
cup, bell, disk	surface profile	Synonyms for the spinning device with impermeable wetted inner surface with theoretical line source at center.	NA	NA
Re	Reynolds Number	viscous forces/inertial forces translational	dimensionless	NA
Ro	Rossby Number	viscous forces/inertial forces rotational	dimensionless	NA

Alphabet

H_0, H	thickness	Characteristic film thickness	length	m
q	coordinate	Generic coordinate	NA	NA
r		length (Cartesian, cylindrical, spherical dimension)	length	m
R	Radius	horizontal distance from rotation axis, or characteristic length	length	m
\mathcal{R}		Max horizontal distance, radius of spherical bell	length	m
u	velocity	Velocity coordinate direction 1 Coordinate system context	$\frac{\text{length}}{\text{time}}$	$\frac{\text{m}}{\text{s}}$
u, \mathbf{u} , \vec{u}	velocity vector	Velocity Vector Coordinate system context		
v	velocity	Velocity coordinate direction 2 Coordinate system context	$\frac{\text{length}}{\text{time}}$	$\frac{\text{m}}{\text{s}}$
w	velocity	Velocity coordinate direction 3 Coordinate system context	$\frac{\text{length}}{\text{time}}$	$\frac{\text{m}}{\text{s}}$
x, \mathbf{x} , \vec{x}	position vector	Position Vector Coordinate system context	length	context
z	position	length (Cartesian, cylindrical)	length	m

x	non-dim	Context dependent Non-dimensional arc length variable in curvilinear system	NA	NA
y	non-dim	Context dependent Non-dimensional arc length variable in curvilinear system	NA	NA

Greek

β	beta	cone half angle	dimensionless	radians
θ	theta	azimuthal angle of rotationally symmetric coordinate systems	dimensionless	radians
μ	mu	absolute (dynamic) viscosity	$\frac{\text{force time}}{\text{length}^2}$	$\frac{\text{N s}}{\text{m}^2}$
η	eta	absolute (dynamic) viscosity	$\frac{\text{force time}}{\text{length}^2}$	$\frac{\text{N s}}{\text{m}^2}$
ν	nu	Stokes - kinematic viscosity (μ/ρ)	$\frac{\text{length}^2}{\text{time}}$	$\frac{\text{m}^2}{\text{s}}$
λ	lambda	Describes curvature of bell surface in curvilinear coordinate system	$\frac{1}{\text{length}}$	$\frac{1}{\text{m}}$
ρ	rho	density	$\frac{\text{mass}}{\text{length}^3}$	$\frac{\text{kg}}{\text{m}^3}$
ϕ	phi	Context dependent coordinate angle	dimensionless	radians
ω	omega	angular velocity	$\frac{1}{\text{time}}$	$\frac{1}{\text{sec}}$
ξ	xi	Arc length coordinate along bell profile in curvilinear system	length	m
η	eta	Normal outward coordinate along bell profile in curvilinear system	length	m

Sub Script

r, θ, ϕ	r theta	Indicates coordinate or differentiation	context dependent	context dependent
-------------------	------------	--	----------------------	----------------------

	phi			
ξ, θ, η	xi, theta, eta	Indicates coordinate or differentiation	context dependent	context dependent
x, y	x, y	Indicates coordinate or differentiation	context dependent	context dependent
0	zero	Initial	NA	NA

Super
script

$\hat{}$	carrot	Indicates unit vector	NA	NA
$\overrightarrow{}$	arrow	Indicates vector	NA	NA

Bold

a, A	boldface	Vector quantity	context dependent	context dependent

CHAPTER 1. INTRODUCTION

1.1 Summary of Chapters

I see one of the missions of the Institute of Research for Technology Development (IR4TD) at the University of Kentucky Toyota Paint Lab as harvesting scientific research [1-4], [5,6] and bringing this bounty to the factory floor where it contributes to continuous improvement. It is rooted in its founder's embrace of the Japanese terms *monozukuri* and *hitozukuri*. Monozukuri translates to a superlative practice of a craft, hitozukuri translates to the education and training required to become excellent at, and improve, that craft [7].

This dissertation topic was selected based on a lifelong interest in anything related to automotive technology. Automotive painting [8-14], [15] does not conjure up the excitement of roaring engines; however, after years of experience at the hobby level, producing a showroom level finish is probably as or more, challenging than many of the mechanical arts.

At the individual vehicle level, automotive painting is accomplished with an air pressure sprayer. At the industrial level, painting is the work of the rotary bell atomizer. It is a rapidly spinning device, essentially conical shaped, for viscously diffusing kinetic energy into fluid film formed on its inner surface that is fed by a central source. This kinetic energy is ultimately spent on droplet formation. As the fluid film is flung off the periphery of the bell, it is shredded by aerodynamic forces. On the other hand, surface tension forces act to minimize surface areas and atomize these drops into spheres. The process of forming a mist of droplets earns the device its moniker, a rotary bell atomizer [16], [17], [18].

The desired outcomes of this dissertation were not known at the start; however, opportunities for contributions to the body of knowledge became apparent after many hours of immersion in the literature. It is believed that one of the most general contributions is leaving behind a trail of learning in rotational fluid mechanics as applied to rotary bells. This trail is embedded in a sequence of topics herein, beginning with the Navier-Stokes equations and having increasingly sophisticated mathematical expressions that eventually enables insight into and an understanding of advanced literature in the field.

A novel outcome is within approximated fluid film properties consisting of thickness and velocity profiles on the inner wetted surface of a rotary bell. Moreover, this approximation works for an arbitrary profile that has reasonable similarity to bells used in the art. An important similarity, or constraint, is that the radius of curvature at any point on the bell profile is much greater than the film thickness; otherwise, the approximation is invalid. The analytical limits of the approximation were not investigated. The approximation can predict a fluid film that thickens, which is a condition that cannot be generalized with a low order model and simple boundary conditions. On the other hand, it did predict film thickness, including film thickening immediately adjacent to the bell periphery, for a very specific bell profile found in the literature.

Another outcome, that was the published, explained the underlying mathematics in a solution exploiting the rotational symmetry of roots in the complex plane. In the case of coupled differential equations, that included centrifugal and Coriolis terms, the velocity profiles were obtainable by direct substitution that led to a fourth order differential equation. Another more elegant solution consisted of multiplying one of the equations by i , an operation that is effectively rotation within the complex plane. This enables exploiting

a complex function that eventually yields velocity profiles in both direction as the solution to a differential equation reduced to second order.

A minor outcome of the dissertation research was a MatLab solution to one of the Von Karman swirling flow problems. The solution used a numerical solver, the output of which was used to create a graphical interpretation of the solution. Although similar graphical solutions are available online, the content in this dissertation provides a systematic, documented development of the equations and programmed solution. Although this problem is different from the high-speed rotary bell problem in that it is semi-infinite, it developed a vocabulary with working knowledge of rotational flow caused by a rotating boundary.

Another outcome was comparing the development of rotational terms in the Navier-Stokes equations within two formulations, depending on how these effects were included. The first formulation is referred to as the Greenspan formulation; it is essentially an application of the Coriolis Theorem in which, at point in space, consists of the cross product of angular velocity and a fluid velocity vector, and angular velocity crossed twice with a position vector. The other formulation is based on a kinematic substitution for absolute rotational velocity. It is the difference, at a point, between rotational surface speed of the bell at a radial position and local fluid velocity in the rotating frame, thereby leading to an absolute velocity in an inertial system. As it turns out, the difference between these two formulations is relatively minor and is caused by an assumed direction of rotational fluid velocity in the rotating frame, which in reality, lags the bell surface velocity.

Chapter 2 is a brief review of patent literature that is not meant to be exhaustive; rather it provides a glimpse into the wide scale and varying use of rotary atomizers. The obvious

commonality is in using a moving boundary surface to diffuse kinetic energy into a fluid film where it becomes the energy source needed for creating additional surface area. As the fluid is flung off the spinner at its periphery, surface tension attempts to “hold the fluid together” while dominant aerodynamics forces “shred” the fluid. As the parcels of fluid minimize their surface areas, spherical drops are eventually formed. In general, higher kinetic energy creates smaller drops. However, different regimes of atomization exist in which some seem very orderly with regularly spaced hair-like filaments of fluid exiting the periphery that break into droplets, and others seem random or chaotic.

Chapter 3 is a review of scientific and industrial publications related to fluid film formation inside a rotating surface of revolution and fluid atomization that occurs immediately beyond the periphery of the spinner. These two topics are related since atomization modeling often has film thickness at the periphery as an input. The term “rotary bell” seems to be a colloquialism of the automotive manufacturing industry. On the other hand, automotive repair businesses, or in the vernacular, body shops, use air pressure as the source of energy for atomization.

In this dissertation, the terms rotary bell, bell, cup, and spinner, are synonymous and their usage usually depends on the context of the publication. For example, academic publications often use “cup”, agricultural publications use “spinner”, and manufacturing publications use “bell”. Spinning refers to rotation about an axis that passes through an object, whereas rotation indicates the axis is external. However, common usage blurs this difference.

Chapters 4 through 9 are a progression of the mathematical formulations found while researching rotational fluid mechanics. The focus of this dissertation, thin fluid films on

high-speed rotary bells, is a unique subtopic within this field. As it turns out, the high-speed case coupled with no slip and no shear boundary conditions, limited to centrifugal and viscous forces, is the most reduced case and has analytical solutions. Inclusion of Coriolis terms creates a coupled set of differential equations that also have an analytical solution on certain domains.

Introduction of pressure and kinematic boundary conditions in combination with lower angular velocity leaves more surviving terms in the Navier-Stokes and, often, solutions are obtained numerically. However, as transient behavior and flow that is more complex enters the problem, more features such as surface wave regimes are revealed. These topics are not included in this dissertation.

Chapter 4 covers two main topics. First is the inclusion of centrifugal and Coriolis forces, both pseudo forces, that explain motion observed in a non-inertial rotating frame. Second is an intuitive method that substantiates neglecting terms of the Navier-Stokes equations; the case is made for neglecting fluid velocity normal to the surface of the bell. This method is related to the lubrication assumption found in the analyses of hydrodynamic bearings.

Chapter 5 covers a classic Von Karman swirling flow problem consisting of a semi-infinite body of fluid with a rotating boundary condition. This problem is a seemingly unrelated problem, almost opposite in a sense, to a thin film of fluid on a spinning bell. As it turns out, the ratio of angular velocity of the fluid and its kinematic viscosity always crops up in rotational fluid mechanics. It is related to the Ekman number and the thickness of the boundary layer in the Von Karman problem. This ratio characterizes a distance where the effects of the rotating boundary are present in the semi-infinite fluid. The Von Karman problem is solved numerically using MatLab, and codes were written to visualize the

decaying effects of the rotating boundary as a function of angular velocity to viscosity ratio. The significant outcomes of this chapter are the introduction to typical non-dimensional velocity forms found in rotational fluid mechanics, an inclusion of other terms of the Navier-Stokes equations, and additional vocabulary.

Chapter 6 uses several examples of rotating flows found in nature. First is an example of geostrophic flow that circulates around a mound of ocean water. At an equilibrium between Coriolis forces and pressure forces, the flow will be normal to these equal and opposite forces. In a more mathematical example, the Ekman spiral occurs because wind that is flowing over water induces a velocity in the water; however, the Coriolis force causes the resultant surface current to flow at an angle with respect to the wind. The surface current then induces a current below it. Again, the Coriolis force causes the deeper flow to be at an angle with respect to the surface current. This effect exponentially decays and spirals with depth, while the speed of the spiraling current decreases due to viscosity. Surviving terms from the Navier-Stokes equations, shown here without derivation, lead to a system of differential equations that form an exponential spiral of ocean current. Although this dissertation is not meant to be a study of oceanography; however, chapters five and six introduce and then serve to visualize the physical significance of the Ekman number.

Chapter 7 covers the Greenspan formulation of the Navier-Stokes equations. Two methods are presented for including the effects of rotation on observations in rotating coordinate systems. Greenspan opens his book with the explicit cross products that create centrifugal and Coriolis pseudo forces and explain motion seen by the non-inertial observer. Almost all other literature accomplishes the same with a simple kinematic substitution for fluid

velocity observed in the rotating frame. A thorough, almost pedantic, explanation of cross product methods in spherical coordinate systems concludes the chapter.

Chapter 8 is a detailed review of the thin film formulations where the bell geometry is bound by the coordinate axes. The cases of disk, conical and partial spherical bells include development of the equations of motion and calculations of film thickness. In this chapter, the similarities are generalized within a non-dimensional paradigm. The pattern of similarities yields an approximation for thin film properties on a bell that is not confined to profiles that are bounded by axes in the more common constant curvature curvilinear coordinate systems. Cylindrical and spherical coordinate systems, though curvilinear, have the remarkably simplifying property of constant curvature. The remainder of the chapter covers a coupled system of differential equations that include Coriolis and centrifugal terms and can be considered the “next step” in mathematical sophistication of a thin film analysis. A common solution method is analyzed and subtle symmetry in the complex plane is shown to be the mechanism for reducing the order in a solution method.

Chapter 9 is a turning point in this dissertation where a complex publication that casts the Navier-Stokes equation into a rotating curvilinear coordinate system is deciphered. The word “decipher” is used because a hurdle in mathematical learning had to be overcome, for understanding the results contained in this publication. In it, the coordinate system was defined by the arc length along the bell profile, an angle around the axis of rotation and a normal to the bell surface profile. This coordinate system is natural for working with a bell of reasonable arbitrary profile. The word “arbitrary” must be qualified to mean a smooth blend of conical and concave profile elements, as opposed to a randomly scribbled profile.

The simplest analytical constraint on a bell profile is that the radius of curvature anywhere on the profile must be much greater than the film thickness. The common cylindrical and spherical curvilinear systems have associated vector operators published so ubiquitously that there seemed to be no need to reference them. On the other hand, less common systems could require constructing these vector operators. The vector formulations of conservation equations in other coordinate systems depend on knowledge of the metric tensor, derivatives of unit vectors, and vector operators. In fact, the tedious derivation of the underlying mathematics leads to learning, as opposed to thoughtless copy and substitution. Moreover, understanding the Navier-Stokes equations, as cast into this coordinate system, enabled seeing that the most reduced form is equivalent to the approximation obtained from patterns in the equations that were cast in the simpler cylindrical and spherical coordinate systems. As it turns out, in the reduced equation which only includes centrifugal and viscous forces and the approximation can predict an increasing film thickness. This may sound like a simple effect, the analyses of thickening films on a rotating device could be protracted into multiple dissertations on the topics of fluid mechanics, numerical methods, and stability.

Chapter 10 explains the equivalence of the thin approximation and the most reduced form of the surface following Navier-Stokes equations. The resulting equation is compared to an example found in the literature of the field and yields perfect agreement. Stated as succinctly as possible, this novel result is essentially the equivalence of the cosine of the angle between centrifugal force and a tangent to the bell surface profile, though described in two different coordinate systems. One is a Cartesian system, and the other is a variable curvature curvilinear system. In the case of a variable curvature bell profile, the

approximated solution is a terminal result; however, the reduced Navier-Stokes equation can always be backpedaled to its full rigorous form.

Chapter 11 contains the abstracts of three published articles related to the field of rotary bell atomizers and in the context of automotive painting. The first publication was a detailed description of the evolution of metal pretreatment and concluded with evidence about the design, materials, and environmental factors that will influence the development of next generation of metal pretreatments. The second publication was on an underlying symmetry in the complex plane that enabled a reduction of order in a solution of thin film velocity profiles on a high-speed bell. The third publication included a coauthored section on the modeling of thin films on a rotary bell.

This dissertation develops an approximation for film properties on a rotary bell. It states this as a theory, which raises the question, is it a “good” theory [19], [20]. Williams states there are three elements of a good theory [19]. First, “Theory Needn’t be Right to be Good”, second, “Theory Needn’t be Mathematical to be Right”, and third, “Theory Needn’t be Incomprehensible to be Mathematical”.

Following William’s criteria in order, first, this approximation for film properties on a rotary bell with an “arbitrary” profile is based on a pattern that became apparent in solutions for conical and spherical bell profiles. The term “arbitrary” in this case does not mean any scribbled profile shape. The profile is considered confined to a smooth concave curve, but is not coincident with an axis in a common (Cartesian, cylindrical, spherical) coordinate system. This approximation does predict properties that are found in other published works that will be referenced later, however, this approximation does not reveal when it becomes invalid, or “not right”. Moreover, knowing this approximation was possibly “not right”

was the motivation for researching a formulation of the Navier-Stokes equations in a coordinate system conducive to analyzing “arbitrary” bell profiles. Such a publication was found, however, deciphering it required additional mathematics in the area of vector operators.

Second, although this theory for approximating film properties is ultimately in the form of an equation, initially, this pattern was non-mathematically stated “verbally” as follows:

$$[\text{centrifugal term}] \times [\text{cosine term}] = [\text{approximate curvature of the velocity field}]$$

The key to unifying other formulations of the centrifugal/viscous force balance was simply expressing them using the cosine term. The argument of the cosine term is the angle between the centrifugal force and the local surface tangent.

Finally and third, when the approximation is put into a mathematical form it is a comprehensible geometric relationship. However, showing that a projection of the Navier-Stokes equations into a surface following coordinate system degenerates into an equivalent form of the approximation at high speed did require considerable mathematical learning and this path of learning is documented in detail herein.

In the eyes of a physicist, this dissertation proved the obvious, that the laws of physics are independent of the chosen coordinate system. The mathematics learned by proving this with essentially brute force was worth every bit of that effort.

1.2 Map of Dissertation

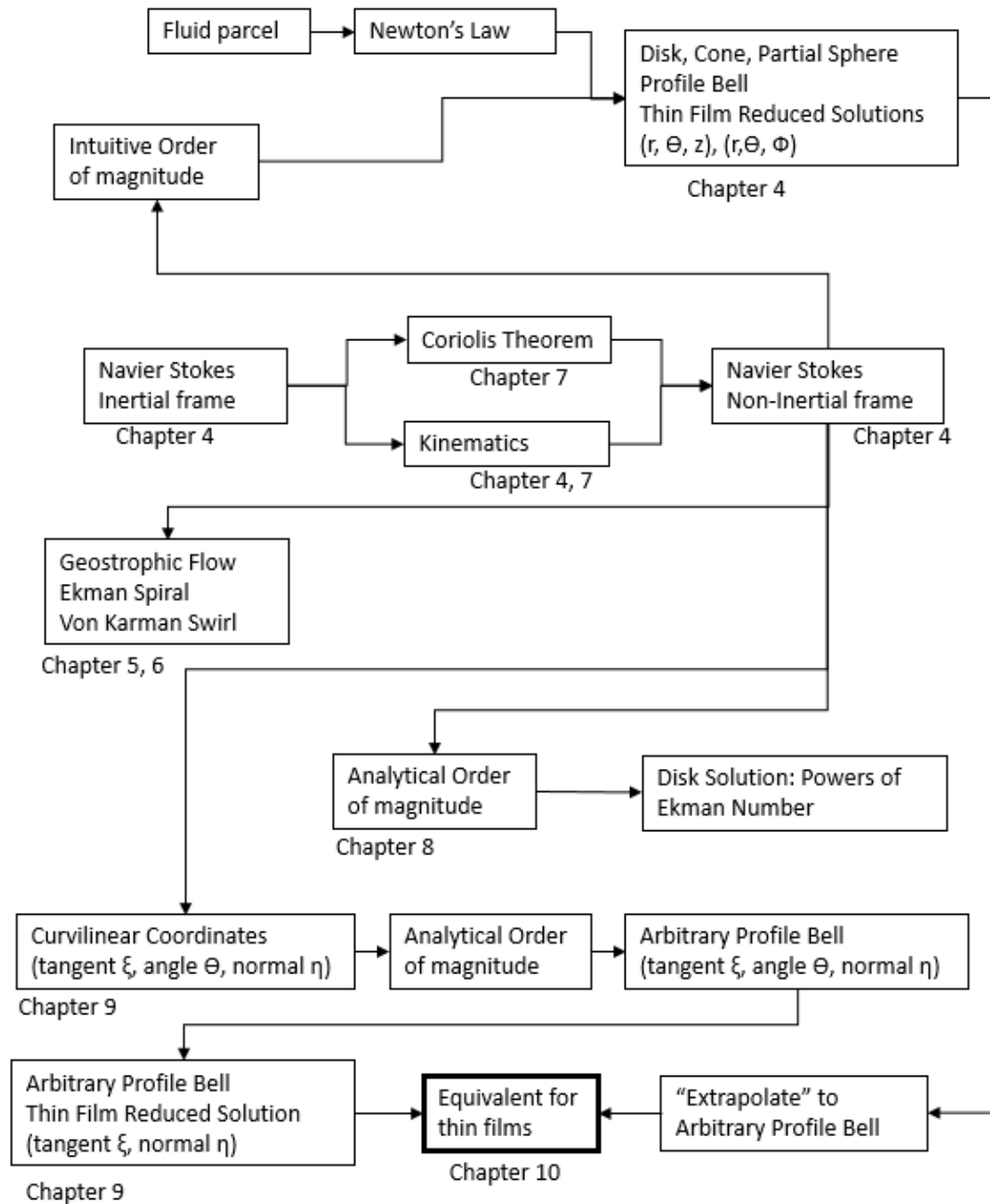


Figure 1.2-1 Map of Dissertation

Figure 1.2-1 illustrates the evolution of this dissertation. It starts from analyses of bell profiles confined by the coordinate axes in cylindrical and spherical systems, which leads to an approximation for arbitrary bell profiles defined in familiar Cartesian coordinates.

A collection of articles from the Lomonosov Moscow State University includes one of the most dispositive works on fluid films on rotating curvilinear surface, and it becomes a pivotal influence on this dissertation. The Lomonosov work is extraordinary because the bell profile is defined by an axisymmetric surface of revolution formed from a plane curve that contains two of the coordinate axes. The remaining coordinate is the azimuthal angle, similar to a cylindrical coordinate system. This is a significant paradigm shift; in the Lomonosov work, the coordinate axes conform to the bell profile, as compared to a bell profiles that conforms to the coordinate axes.

Chapter 10.1 of this dissertation reveals the equivalency between the Cartesian approximation and the most reduced case, with only inertial and viscous forces, of the Navier-Stokes equations in the coordinate described by the Lomonosov research. The mathematics leading to this result were tedious, and included working with the metric tensor, derivatives of directional unit vectors with respect to coordinates and defining vector operators specific to the coordinate system of the analysis. A curve of x and $y=f(x)$ in a Cartesian system and the same curve defined parametrically, $(R(\xi), Z(\xi))$, from the respective axes as a function of arc length, ξ , as it turns out, are trivially related, as seen within the following equation 1.2-1. However, from the perspective of fluid mechanics, the mathematics required to reach this conclusion were not trivial while the author of this dissertation considered himself on an ascending side of the learning curve.

$$\cos(\tan^{-1}(f'(x))) = R_{\xi} \quad R(\xi) = x \quad 1.2-1$$

This relationship validated the approximation; however, it also limited the approximation. While the reduced form of the Navier-Stokes equations, with only centrifugal and viscous

forces, in the “Lomonosov” coordinates can revert into a their full form, the Cartesian approximation is limited to thin films where the geometry at any point in the film is defined by the geometry of the bell surface profile.

The value of this approximation is revealed in latter chapters of this dissertation in which its applicability targets the industrial production process engineers whose brand revolves around optimized rotary bell operations for automotive industries. It puts a production engineer on a firmer ground, especially when working with suppliers of rotary bell painting equipment, because it removes a bit of the mystery, without advanced mathematics, about film properties inside the bell.

The work in this dissertation is humbled by those who formulated of the Navier-Stokes equations in surface following coordinates. Multiple dissertations could be generated if pressure and kinematic boundary conditions replaced the simple no-shear condition at the free surface, along with inclusion of initial velocity conditions and transients.

Shamelessly plagiarizing and stealing the wisdom of Thomas Edison, this dissertation was “99% education and 1% contribution”. In the coordinate system “free for all” of variable curvature curvilinear coordinates, it was a rewarding first step...

CHAPTER 2. PATENT HISTORY

2.1 Introduction

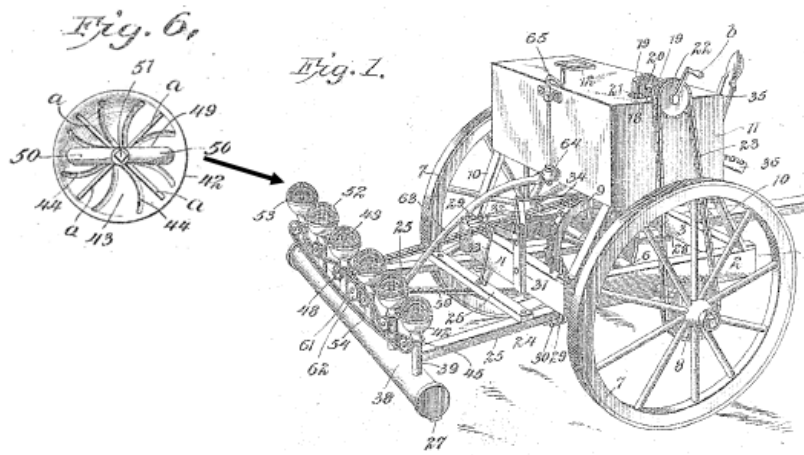
In this chapter, a brief history of the art of rotary atomization was drawn from the US Patent office. When put on paper, it self-narrates atomizer development in which a starting point of around 1900 was arbitrarily chosen; no effort was made to establish first use. Moreover, the patent search was not exhaustive; selections were those that illustrated disparate use, although the principles of operation remain common and timeless.

This collection of patents covered the atomization of insecticide, fuel oil for combustion, early automotive coating, pharmaceutical drying, food preparation, metal powders and tar coating of ingot molds. The applications and materials are limitless.

2.2 US Patent Database

On August 28, 1900, Charles Moore was issued patent 656,774 [21] for the “Insect Destroyer” illustrated in Figure 2.2-1. The invention was a drawn cart that had a rear-mounted array of rotary atomizers distributing a trailing plume of agricultural insecticide.

The atomizers received their angular velocity from a system of wheel-driven chains and sprockets.



The insecticide was from an aqueous-based solution of Paris green or London Blue stored in a tank, with the fluid fed via gravity flow to the rear

Figure 2.2-1 Disk Rotary Atomizer Insecticide Spray Bar [21]

mounted rotary atomizer array. The atomizers, or spraying devices, as they are referred to in the patent, revolve at a “comparatively high rate of speed” and the insecticide, “which is fed to the volute grooved” sprayers, “will be thrown therefrom centrifugally in the form of a fine spray”. The volutes could include a series of “radial frets” for additional control of spray. Frets may be considered to be similar to optional serrations that are found on the periphery of modern rotary atomizers.

Sydney Crosbie, a subject of the King of Great Britain, was issued US patent 1,149,810 on August 10, 1915 for a device that centrifugally atomized oil for producing a combustible

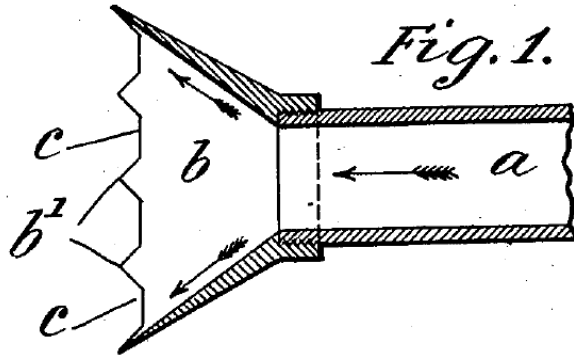


Figure 2.2-2 Conical Rotary Atomizer, 1915 [22]

fuel and air mixture [22]. This rotating device was substantially conical, as shown in Figure 2.2-2, taking on the shape of a spinning funnel. The fluid flow was reversed from a conventional funnel flow direction, and instead was fed from center, spreading out to the

periphery by centrifugal force. The periphery of this device has a periodic saw tooth pattern that further atomized the fluid with impact and slicing action, pulverizing the departing droplets.

Patent 1,861,475 was issued to Hopkins et al on June 7, 1932 [23]. The central theme of the patent was the inherent advantages of rotary, or centrifugal, atomization over the method of so-called spray guns. The spray gun employed compressed air as the source of atomization energy, however, the violent mixing of air and solvent-based organic coating caused eventual surface finish defects. On the other hand, centrifugally atomized fluid combined with an airflow that provided direction, but not atomization, was found to minimize surface finish defects. Their atomizer was a rotating cone with a centrally located fluid port. The “directing air” had its source behind the cone and its direction was towards

the surface receiving the organic coating. Current terminology refers to the “directing air” as “shaping air”.

Hadley received a patent on March 21, 1939 on a rotary atomizing device for applying a tar coating to the inside of steel ingot molds [24]. The purpose of the tar was to provide an insulator between the 2600°F steel and the 140°F mold because direct contact between molten steel and the mold caused undesirable surfaces conditions on the steel that damaged the mold surface. Prior methods of tar coating involved dipping, however, the amount of material deposited with not well controlled. On the other hand, spray coating “permits positive control of the quantity of tar applied to the inside walls, thus eliminating the difficulties from too heavy a coating”.

Salsas-Serra received patent 2,166,772 on July 18, 1939 for a rotary atomizer that contained several disks inside a bell-shaped body [25]. The disks were designed to throw droplets against the inside of the body where they were carried away by air currents, or the droplets were reflected off the inner surface of the body into a shredding aperture of the subsequent disks.

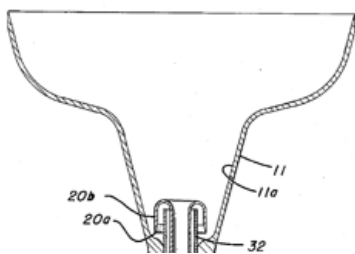


Figure 2.2-3 Fluid supply [26]

W. L. Smart was issued patent 2,728,607 in December 1955 for a method of supplying fluid through a non-rotating central tube [26]. This design enabled atomization of materials that would otherwise damage seals and bearings. Figure 2.2-3 illustrates the stationary U-turn feed path supplying the rotating bell-

shaped atomizer. This design was limited to upward feeding in order to isolate fluid from bearings.

Patent 3,000,574 [27], issued on September 19, 1961, was a unique device that used a

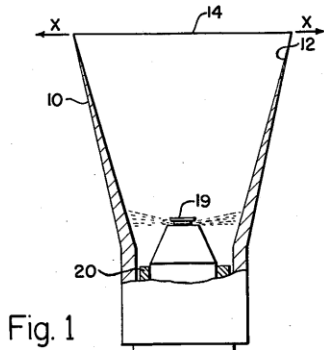


Fig. 1

Figure 2.2-4 Atomizer [27]

a circular compressed air atomizer within a spinning conical atomizer to direct atomized material onto the inner surface of the cone for further atomization by centrifugal force. Figure 2.2-4 illustrates the internal circular sprayer (19) depositing material onto the inner surface (12) of the rotating cone (10). Material that exited the edge of the cone was directed by air onto a

surface receiving the coating. The stream of material formed a hollow ring on the surface to be coated, and uniform coverage was achieved by advancing the atomizer at a fixed velocity and maintaining a constant distance from the surface. Although not in the claims section of the text, the inventor insinuated this dual atomization device deposited fluid on target with increased uniformity of the pattern.

Patent 4,458,844, issued to Ransburg Japan Ltd. on July 10, 1984 [28], contained a significant amount of teachable material with respect to rotary atomization, especially

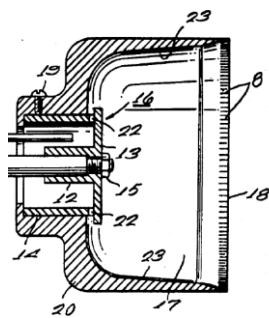


Figure 2.2-5 Cup with serrations [28]

related to serrations at the periphery of the spinning cup. Figure 2.2-5 illustrates these serrations as number (8). As solvent content of paint is reduced, the viscosity tends to increase, thus, requiring higher rotational speed for atomization. The

degree of atomization was inversely proportional to the fluid film thickness at the periphery; on the other hand, the volume of the fluid atomized was proportional to the film thickness. At higher rotational speeds and high volumetric flows, the fluid tended to form a sheet that extended over the edge of the periphery. As this sheet disintegrates due to aerodynamic shredding, the fluid droplets entrained air and led to a foam like coverage of the target and with a poor surface finish. The remedy disclosed in the patent was serrations along the periphery of the cup, or bell. These serrations maintained a ligament form of atomization. Considerable art was disclosed on the topic of serration design such as their depth, length, and pitch.

Patent 4,518,119 issued on May 21, 1985 [29], claimed that a crosshatch serration pattern

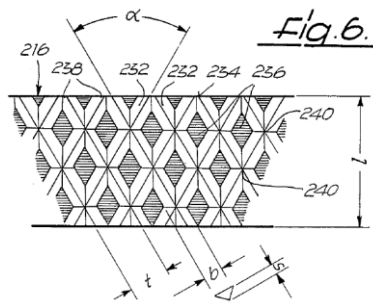


Figure 2.2-6 Cross Hatch Serrations [29]

at the periphery of a cup enhanced the mixing of two part paints. The pattern was a slightly raised lip at the edge of the bell and consisted of three and one half rows of raised rhombus patterns with each row is offset by half the pitch.

The patent contained two embodiments of the pattern that differ mostly by the number of rows. Figure 2.2-6 illustrates the inventor’s serration design.

Ford Global Technologies received patent 6,409,104 for a “Silicon Doped Amorphous Carbon Coating for Paint Bell Atomizers” in June 2002. Paint bells typically use materials like aluminum or titanium, which wear quickly when used with abrasive paints containing metal or mica flakes. Titanium bells last longer under such conditions but their cost is

several multiples over that of other less expensive materials. This patent claimed its surface treatment enabled less expensive bell materials could attain the same lifetime as the bells fabricated from much more expensive bulk material.

Metcalf et al patented “The production of powdered metals”, number 4,207,040 in June of 1980 [30]. Figure 2.2-7 illustrates the invention for producing powdered metals in a rotary

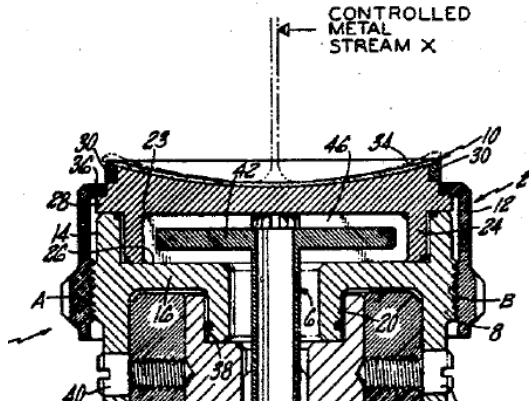


Figure 2.2-7 Powdered Metal [30]

atomization process. The fundamental process during rotary atomization is increasing surface area. Since energy is expended in creating a surface, a source of energy must be provided. Kinetic energy is transferred to the fluid by means of the no slip condition at the bell fluid interface.

The variation of designs and applications found in the patent office literature introduces the spectrum of industrial processes that exploit this seemingly simple process. However, simplicity to a casual observer belies a hidden world of analytical beauty.

CHAPTER 3. LITERATURE REVIEW

3.1 Introduction

The modes of centrally supplied rotary atomizer are historically classified as direct drop generation, ligament formation and sheet formation [31]. During the direct drop generation mode, drops emerge from the rim of the atomizer. In the ligament formation mode, ligaments emerge from the rim and these ligaments subsequently disintegrate into drops. Finally, in sheet mode, a film extends over the edge and disintegration can best be described as aerodynamic shredding of the film. The extent of film overhang is critical. If overhang is the same order of magnitude as the film thickness, researchers typically model this regime as if it has the characteristics of a flat jet [32].

The term spinning and rotating are used interchangeably in the literature, however, spinning usually means the axis of rotation is within the object whereas rotation implies the axis of rotation is outside the object. For example, the earth spins on its axis while rotating around the sun.

Rotary atomization depends on the characteristics of the fluid film near the rim, or periphery, of the spinning device. The spinner can be thought of as a surface of revolution formed by a planar curve. However, shapes taking advantage of natural boundaries of coordinate systems result in simpler solutions. Examples of shapes that lead to less complex solutions are disks, cones and partial spheres. The majority of published analyses rely on spherical or cylindrical coordinate systems.

Imagine a boundary, on one side of which is continuous fluid and on other side is fluid being shredded by aerodynamic forces; this image describes the environment around the

edge of a spinning device. It is for this reason that the literature search was centered on prior research within this physical region. Some articles analyzed the fluid film within, and up to the edge of the spinning device, while others covered stability of the fluid/air boundary at the edge; finally, some covered the balance of forces of fluid as it exited the device.

The literature on rotary atomization often inextricably links fluid film properties on the spinning device and atomization that occurs immediately beyond the periphery. Indeed, the fluid film properties near the periphery, mainly its thickness, are inputs to atomization analyses. Seeing this connection justifies the need for further learning and focusing on the film properties, i.e. the subject of this dissertation.

3.2 Literature Review

Walton and Prewett [33] in their 1949 article approximated rotary disk atomized drop diameters as an empirical function of surface tension, diameter, angular velocity and liquid density. Experiments included a range of rotational speeds and liquids as diverse as mercury. Outcomes included the spatial and dimensional distributions of main drops and satellites, plus evidence that drop size was independent of supply flow under certain conditions.

Hinze and Milbourn [34] derived an equation for the fluid radial velocity inside a rotating cone using spherical coordinates. The solution was based on a thin film approximation within the Navier-Stokes equations. Further derivations yielded an equation for film thickness as a function of radial position, and thickness of the fluid film at the rim of the cone was an input for a subsequent wave equation analyses. Although the wave equation formulation was not solved, it yielded an inequality, based on physical parameters that defined the threshold of disturbance growth on the immiscible surface. Dimensional analyses and experimental work have evolved into relationships for calculating the number of ligaments around the spinner edge. An intuitive analysis, substantiated by experimental data, described the transition from ligament regime to sheet (or film) regime.

Dixon *et al* [35] investigated the sheet regime of fluids exiting rotating and stationary disks. The peripheral velocity was an order of magnitude lower than the peripheral velocity of a production automotive paint bell. Though not strictly concerned with atomization, this work observed effects such as fluid slip on the rotating disk and the radius of fluid extension (to the point of breakup) past the disk as a function of angular velocity.

Fraser *et al* [36] investigated the effect of fluid feed disturbances inside the cup (bell) and how they propagated to the rim and affected breakup. This article was not focused on atomization; however, the uniformity of the film inside the cup, though a separately researched topic, was shown to influence rim atomization.

Dombrowski and Johns [37] [38] studied the aerodynamic instability of liquid sheets ejected from a fan spray nozzle. Although fan spray nozzles are not a form of rotary atomization, however, Sun *et al* [32] made an assumption (50 years later) that the film of fluid extending over the edge of a spinner (bell, cup, or disk) behaved similar to a sheet as described by Dombrowski. Since the radius of the spinning device is usually much larger than the critical wavelength of fluid disintegration, the curved wave is approximated as a straight wave in a Cartesian framework. Dombrowski and Johns developed an aerodynamic forcing term based on an assumed sinusoidal shape of the fluid sheet. A freebody diagram of a parcel of fluid in the sheet overhanging the bell rim includes this aerodynamic term, surface tension terms, viscous terms, and an inertial term. In their model, Dombrowski *et al* model used the thickness of the fluid at the edge of the bell as an input to their atomization theory, hence, the important connection to this dissertation. The outcome of the freebody analysis yields a wave equation with terms for sheets that have changing thickness. An assumption in Sun *et al* [32] considers the simpler case of a film of constant thickness. Dombrowski and Johns conclude with analysis of ligaments and drops produced by disintegration and a comparison to measurements. About 40 years after Dombrowski, Chuech [39] published an analysis similar to Dombrowski and Johns; a key differentiating item was the inclusion of spatial analyses along with temporal analyses.

Kimiya and Kayano [40] investigated the correlation between ligament thicknesses and drop diameters while operating at ligament producing conditions. In another paper, they experimentally investigated [41] a relationship between maximum drop sizes and two parameters; including the film thicknesses on the periphery of a spinning device and the extent of fluid sheet overhang. Their paper includes measurements from over 40 test points and compiles the data in charts consisting of dimensional and non-dimensional axes.

Using energy methods, Kimiya [42] derived an equation for determining for wavelength of maximum growth on an immiscible fluid/air surface at the edge of a spinning disk. The energy source was centrifugal force acting through a displacement, and energy was transferred to kinetic and surface energy, or dissipated by viscous flow.

Rauscher *et al* [43] analyzed thin film flows on a rotating disk with a very sophisticated approach that included higher order terms of an asymptotic solution. Fortunately, this and other similar research showed that these higher order effects became less significant at typical high RPM operating conditions of rotary atomizers used in the automotive industry. They derived an equation for the lowest order film thickness and as expected, obtained the same equation as other low order analyses.

Matsumoto *et al* [31] described the transition between atomization modes. Starting at a relatively low flow rate, individual drops were generated around the periphery and then as the flow rate was increased, the number of drops per second, or frequency, increased until a critical value. At this critical value of flow, the mode changed suddenly to ligament formation and the location of drop formation moved from the bell edge to the end of the ligaments; in other words, drops were formed as the “far end” of the ligaments destabilized. Finally, with further increases in the flow a fluid film extended over the edge of the bell.

In addition, empirical data were presented on the mode transitions but the accompanying analyses were an interpretative explanation of otherwise quantitative analyses.

Dombrowski and Lloyd [44] defined two regimes, including aerodynamic and turbulent, within the sheet mode of atomization. Within plots of flowrate versus rotational speed, they established an apparent boundary between these regimes. An observation presented was that the fluid sheet clung to the outer surface of the spinning cup where it was effected by vortex flow when the fluid passed over a sharp edge, i.e. surface tension was implicated. However, when the cups were polished with silicon-based wax, most likely changing the surface energy, the sheet did not cling and climb the outer edge of the cup, but instead departed at the edge. Also, if the spinning device was operating in a ligament mode with higher viscosity fluids, longer and thinner ligaments with a large drop at the end of the ligaments were produced. The ligament mode also tended to produce a bimodal drop distribution with main and satellite drops. Overall, the majority of their paper was on the correlation between measured and calculated D_{32} drop sizes and they closed with a plot of calculated drop sizes versus flowrates that encompassed various atomization modes. Although their plot showed abrupt changes in the calculated drop size, the observations do not show this abruptness. Large drops were generated in a direct mode over a narrow range of low flows; upon entering the ligament mode, the drop size fell and then increased as the flow was increased.

Dombrowski and Boize [45] analyzed a low volume rotary atomizer for pesticides using a spinning device with serrations. It is known that the theoretical number of ligaments can vary greatly and be less or more than the number of serrations; in this publication, the actual ligament count was below the number of serrations. This work summarized trends in the

data, including that the number of satellites increased with flow rate due to a delay in the disintegration of filaments connecting the main drop to the edge of the spinner. In addition, ligament lengths tended to correlate with viscosity and their drop size equations for the drop and filament modes were compared to those from other research.

Frost [46] published an article in 1981 that was referenced by Li et al in 2018 [47], demonstrating the longevity of reference to this work. In the Li article, the modes of droplet formation, direct, ligament, and sheet were bounded with non-dimensional groups and compared to other works [48]. Liquid properties such as density, viscosity, and surface tension were modified with glycerol and a proprietary wetting agent. They observed, but did not elaborate on, the effect of an off-center fluid feed. The spark photography, which was excellent, showed on real-time the periphery of a spinning disk subject to uneven flow caused by off-center feeding, resulting in simultaneous direct, ligament and sheet atomization. They also covered ligament spacing, disintegration frequency, and drop size; all of this work was experimental.

Kawase and De [49] published experimental results for shear thinning fluid on a rotating disk and its effect on the number of ligaments. Two working fluids were used, including an aqueous solution of carboxymethyl cellulose and another of hydroxyethyl cellulose. The rates of viscosity versus shear were obtained from a power law mode; an example of a shear rate model is the Cross Model [50]. Empirical equations based on Reynolds and Weber numbers were calibrated and an experimental study of shear thinning was performed in the same manner as Newtonian fluids; then, these data were numerically adjusted by a percent of shear thinning additive.

Dunskii et al experimented with fluids on a spinning disk that contained a surface having poor wetting properties, or in the case of aqueous solutions, has a hydrophobic surface [51]. Their work demonstrated incomplete coverage of the spinning disk led to polydispersity atomization at low flow rates. In contrast, atomization was uniform after the entire disk was covered at high fluid flow rates.

Alcock and Froelich studied conical atomizers used for dispensing agricultural pesticide [52]. Their method for calculating the exit velocities of drops leaving the atomizer periphery used the Bernoulli principle because the cone exit velocity was approximately proportional to ωr and concentrated on investigating the power usage of atomizers and its connection to the physical process. Although a prediction for efficiency was not obtained, they were able to measure the zones of effectiveness of the atomizers under investigation.

Yanagisawa investigated a different configuration of fluid on a spinning disk [53]. Instead of a continuous supply of center-fed fluid, the disk had an initial quantity of liquid and the fluid had initial surface height profile. This application is common in the semi-conductor industry for wafer lithography. The article's two main points were to investigate slippage of the fluid at the fluid/surface interface and the development of equations that described time evolution of the fluid surface. The key to understanding the second point was in deriving the conservation of mass equation for a volume of liquid with a decreasing surface level, which in cylindrical coordinates was determined to be as $\frac{dh}{dt} r d\theta dr$, where h was the height of the fluid and the flux through the control volume was written as a flow-per-unit length. This flow-per-unit length was obtained from the film thickness equation, without the factor of $2\pi r$.

Sisoev et al formulated the problem of a thin fluid film on a spinning disk in terms of powers of δ , where $\delta = H_0\sqrt{\omega/\nu}$ [54]. This quantity is the square root of the reciprocal of the Ekman number, $Ek = \frac{1}{L^2} \frac{\nu}{\omega}$. In the cylindrical coordinate system, three dimensionless velocities and two changes of variables formed a set of Navier-Stokes equations with the clearest sense of “order of magnitude” of the equation components. Their formulation grouped Navier-Stokes terms by δ^0 , δ^2 and δ^4 .

Sisoev and Shkadov followed their previous article with an analysis of flow stability of a thin fluid film on a rotating disk, with the inclusion of dimensionless pressure and time variables within in a transient analysis [55]. Herein this dissertation, the results of Sisoev et al developed within a cylindrical system are applied to the Navier-Stokes equation formulated in the spherical coordinate system, or other mutually orthogonal systems.

Middleman [56] studied the effect of rotationally induced air flow over a spinning fluid film while equating the shear stress caused by this flow as the surface boundary condition as an alternative to the simple zero shear boundary condition. Although this work described flow from an initial finite volume of fluid, as used in the semi-conductor industry, nevertheless, it elucidated the fact that boundary condition shear stress will exceed centrifugal force in inducing radial flow of the film for relatively large radii and thin films.

Sato [57] described and acquired data from a round nozzle, closed rotary atomizer that was distinctly different from the typical open conical rotary atomization, the nozzle also incorporated an electrical field that contributed to drop formation. At high rotary speeds, the high momentum forces were much greater than the electrical forces; consequently, drop

disintegration was caused mostly by momentum rather than electrical forces. At this high speed, the electric field works only to charges the drops.

Makarytchev et al [58] made updates to an earlier publication by Bruin [59] that analyzed a fluid film inside of a spinning cone in which it was pointed out that the Ekman thickness in the Bruin publication should have been stated as $\delta = \sqrt{\nu/\omega \sin \beta}$; the sine term had not been included by Bruin. Both publications covered film thickness and velocity profiles in a spinning cup, or bell, over low to very high rotation rates. At high rotation rates, the film equations simply degenerated to those of Hinze and Milborn [34]. This agreement in form was a consequence of Hinze and Milborn simplifying their equation of motion in a priori approach as the rotation rate was increased whereas Bruin and others solved the problem in a manner where elements of the solution could be neglected as the rotation rate was increased.

Bruin's article [59] has a method for solving a system of ordinary differential equations that is based on the change of variables $\Psi = U - Wi$, where U and W represent dimensionless velocities in the radial and tangential directions respectively. As it turns out, solving a fourth order equation for one yielded the other after two derivative operations. On the other hand, if the two simplified momentum equations were summed with one multiplied by i , or $\sqrt{-1}$, the change of variables enabled both velocity profiles to be obtained from Ψ ; moreover, the equation was reduced from fourth order to second order. The underlying mechanism for this reduction of order is explained in further detail in the chapter 11.1.

Birnie and Manley studied film formation of a fixed dosage of fluid on a spinning wafer in a semi-conductor lithography application [60]. Although this dissertation is on continuous flow, their work included evaporation and correlated spinning evaporation rates with room temperature vapor pressure of several solvents. The entire analysis was based on the equation of Hinze and Milborn [34].

Momoniat and Mason [61] also investigated the initial volume of fluid, or non-continuous flow, problem encountered in and around semi-conductor lithography processes. Their analysis included the Coriolis terms, thereby, deriving equations similar to those found in Bruin and Makarytchev et al. As in prior works, an initial fluid profile was capable of forming a breaking wave. Their solution method included multiplying one of the equations in the system of equations by $\sqrt{-1}$, and then summing the equations. A change of variables created a complex function that included both velocity terms. Although they combined coefficients of the roots, they did not include details of the underlying symmetry as is shown in chapter 11.1 of this dissertation.

Lenewit et al studied spiral flow patterns and surface instabilities on slowly rotating disks [62] to investigate surface flow instabilities; they also were able to connect instabilities on inclined planes to those in a rotating disk geometry that inspired the thought to connect inclined plane analyses beyond spinning disks to spinning cones.

Wang studied flow over periodic parallel grooves, perpendicular to and in the direction of the grooves [63]. The purpose was to calculate theoretically the fluid slip at a solid boundary where the no-slip condition is usually applied.

Domnick et al performed a Design of Experiments (DOE) with 32 conditions [64] to investigate film thickness profiles for a stationary bell position and a bell that contained different configurations of edges and angles. Their testing indicated that the drop disintegration processes were completed within a few millimeters off the bell edge.

Another article by Domnick et al investigated the macro environment from a rotary bell to the target substrate, with a goal of predicting film thicknesses on the target [65]. A “near bell” effect mentioned included a “trapped vortex ring” about three bell diameters in the axial direction from the bell that was a zone of recirculation; such recirculation can lead to long travel times to a target, and hence more evaporation time. Their measurements at different radial positions showed a strong separation of drops sizes, with larger drops reaching larger radial distances.

A third article by Domnick et al was similar to their previous articles but also included a method for charging the droplets [66]. Charging methods that transfer charge to droplets include direct charging which places a potential on the bell, and indirect charging which uses corona discharge from electrodes to create a field of free ions.

Matar and Lawrence studied the effect of insoluble surfactant on the suppression of interfacial wave formation and the stabilizing effects of Marangoni stresses on film dynamics [67].

Chuech studied instability of liquid sheets similar to Dombrowski and Johns [37] but also included temporal and spatial analyses [68]. The author declared a weakness in temporal theory because it was noted that disturbances are assumed to grow temporally everywhere,

whereas most fluid oscillations show amplitudes as constant in time and growth only in spatial directions.

Domnick et al used a CRAY cluster computer for CFD simulation of flow through a conical atomizer with overall elapsed times as much as 500 hours. Their findings included mention of the normal component of the centrifugal force having a stabilizing effect on the film inside a spinning cone without dewetting. Film stability was seen as important because it prevents air mixing with paint that could result in air bubbles being trapped in the paint as it deposits on a surface. They also observed the disintegration region just after the edge of the bell and characterized it as neither jet nor sheet disintegration; this designation is potentially similar to the mechanism proposed by Sun et al [32]. A plot of volume fraction verses drop diameters had a bimodal distribution, with imperfections in the serration geometry considered to be the suspected cause.

Ogasawara et al conducted extensive photographic and empirical analysis of flow in a spinning cup and subsequent atomization [69] and mapped flow regimes into a two dimensional space bounded by flow rates and RPM. In this log-log space, two diagonal lines split the area into dropwise breakup, ligament breakup and fine ligament breakup. In addition to classifying atomization, they classified flow patterns and waves on the bell surface in the same two-dimensional space and stated that the wave patterns inside the bell influenced breakup patterns, although this statement was not based on rigorous cause and effect analysis. A comparison of bells with and without grooves or serrations was also presented in which the serrated bell was dissolved to produce a narrower distribution of drop diameters; narrow distributions are usually preferable in automotive painting.

Fukuta et al solved a bell design problem for applying metallic paints with the same level of satisfactory appearance as nonmetallic paints [70]. Their findings included a maximum bell periphery speed of 50 meters per second, a minimum drop on target velocity of 12 meters per second, and a shaping air vented through angled passages that introduced a swirling flow to cause paint to be applied in an annular pattern rather than a Gaussian-like centrally heavy pattern.

Mogilevskii and Shkadov projected the Navier-Stokes equations into a curvilinear coordinate system [71] in which a curve defined in a (\hat{r}, \hat{z}) plane of a three dimensional cylindrical coordinate system that has its \hat{z} axis coincident with the axis of rotation that would sweep out a solid surface of rotation. This surface is the impenetrable boundary of a spinning device that contains the fluid. The Del, material and Laplacian operators are formed using Lamé constants consistent with the coordinates and these operators are applied to the Navier-Stokes equations thereby providing the continuity and momentum equations expressed in curvilinear coordinates. The basis vectors in the curvilinear system are (ξ, θ, η) ; along the surface, the coordinate is ξ , and η is perpendicular to the surface. The boundary conditions for the free surface included kinematic and pressure constraints that enabled flow stability analysis. In terms of relevancy to high-speed rotary bells, their formulation degenerates to the Hinze and Milborn [34] formulation, however, instead of the solid surface boundary being a coordinate axis, it can be “any reasonable” curve. What constitutes “reasonableness” would be that of a high degree of visual similarity of the profile as compared to current industrial bells.

Kim and Kim discussed an analysis of thin fluid film on a rotating disk from a continuous supply [72], beginning an analysis using the Navier-Stokes equations and free surface

boundary conditions. As an alternative to the parabolic or second order solutions, the unique components of their analysis were quartic, fourth order, polynomials describing velocity profiles. Although the full Navier-Stokes solution was necessary to capture the structure of the instabilities found within certain angular velocity ranges, the high-speed rotary bell case reduced to a zeroth order case similar to Hinze and Milborn.

Sisoev et al studied wave formation in the film of a spinning disk [73] in which lower flow rates produced a smooth film and high flow rates caused waves to form. These waves were initially circumferential and appeared to travel from the center to the periphery, with further increases in flow, nonaxisymmetric waves appeared. In addition, stationary spiral waves were observed that unwound in the direction of rotation, having been triggered by nonaxisymmetric fluid supply feeding onto the disk. Their approach can be considered as classical, in which the formulation was in nondimensional Navier-Stokes equations coupled with kinematic and pressure boundary conditions at the free surface. The numerical solutions were based on assumed nondimensionalized velocity profiles in the radial and azimuthal directions. The polynomial terms generated were identical to the profiles obtained with no slip, no shear boundary conditions. This work, like others, analyzed surface wave structure at relatively low RPM's as compared to those used in rotary bell applicators for paint application. Nevertheless, the outcomes of this extremely were valuable in further understanding of the Navier-Stokes equations.

Ogasawara et al [74], in an article similar to their conference paper [69], studied the effects of multiple port liquid feed holes. At higher RPM's, the fluid film consisted of "streaks" of varying thickness that eventually transitioned into a smooth film. Bells with and without

serrations were used in these breakup pattern experiments with the serrated bell operated in a “fine ligament region” at RPM’s higher than for unserrated bell.

Ahmed and Youssef [75] compared their experimental data with that of several researchers and concluded these studies were inconsistent, mainly due to the range of the variables used for each correlation. This seemingly innocuous statement came from assessing the many papers were supposed to be essentially the same experiment but produced divergent results. Nevertheless, despite the different locations in “experimental space”, the trends in the data were actually consistent.

Liu et al [76] looked at the differences in spinning disk atomization versus spinning cup atomization and concluded that a focus on cups provided uniqueness to their work. This article heavily referenced the work of Kimiya [42] in calculations that described the transitions from direct drop formation, to ligament formations, and finally to sheet formation.

Tirumkudulu and Paramati [77] researched two opposing fluid jets to create an approximately round sheet of fluid with diminishing thickness as a function of radius. Although this work was not on spinning fluid sheets, the fundamental fluid dynamics equations are the same as the spinning case and provide insight into the sheet regime of drop formation.

Ahmed and Youssef [78] experimentally compared different spinner configurations and discussed at length that the various configurations of spinners that can be reasonably estimated with a simple flat disc. The flat spinner that was modeled with cylindrical coordinates was deemed the least complex mathematical framework; it was also significant

when considering its application to other analytical work. For example, an order of magnitude analysis in a cylindrical coordinate system is reasonably applicable in another coordinate system, such as spherical or other curvilinear.

Bizjan et al [79] studied atomization caused by a spinning wheel; although the configuration is significantly different from a rotary cup atomizer, the fundamental fluid mechanics and instabilities are similar. Wheel atomizers can have multiple planes of atomization, depending on the operating parameters, and the source is not rotationally uniform. These characteristics combine to create very complex boundary conditions. The atomization mechanism for cups, disks and wheels start with a fluid flowing onto a moving surface that is influenced into motion by viscous and surface adhesion forces. Initial periodic interface disturbances are consistent with Kelvin-Helmholtz instabilities caused by the differential velocity between the fluid and the surrounding air. Then the growing wave stage is initiated, consistent with a Rayleigh-Taylor instabilities caused by a higher density fluid is pushed by a body force into a lower density fluid; the waves have a continuous spectrum and their growth rates are a function of the wave number. Therefore, the “seemingly single” that is wavelength present in certain flow regimes is actually the wavelength of the maximum growth rate relative to the rest of the spectrum. As their paper progressed from theoretical analyses to experimental analyses, the non-dimensional groups of Weber Number, Reynolds Number, and Ohnesorge number were drawn into the discussion.

A unique characteristic of wheel atomization is the depletion of fluid as it is ejected from the surface. This depletion along the circumference causes a varying film thickness and hence, varying atomization, as the film progresses from the source point to the point where

the film is too thin to atomize. Wheels can also have a fluid supply that extends along the axial direction, leading to fluid/air interface surface instabilities in the circumferential and axial directions.

Sun et al [32] proposed the concept of a thin film of fluid overhanging the spinning cup/disk that behaves similar to the flat jet instability mechanism developed by Dombrowski [37]. Sun's application was for oil atomization in a turbine engine. The analysis of Dombrowski et al had a temporal/spatial dependency where the periodic wave amplitude depended on the distance from the flat jet orifice. In contrast, the Sun analysis assumed the entire circumferential wave had the same spatial characteristics associated with each value of a continuous distribution of an exponential growth factor. Continuity, in a theoretical sense, would dictate that only integer values of waves could exist around the exact periphery of the disk/cup. However, as it turns out, the wavelengths were relatively small, and were treated as being continuously distributed. In addition, the underlying principle in Dombrowski was a "second order system" in the fluid film, with mass, restoring force, surface tension and damping due to viscosity. The driving force was also assumed to be a sinusoidal pressure distribution caused by the differential velocity at the air fluid and interface that acted on the film to reinforce temporal wave growth; moreover, the growth rate itself was a function of the film parameters and the wavenumber, which is related to wavelength. Application of Newton's second law to a parcel of overhanging fluid, along with an assumption of a periodic response, yielded a differential equation in time and space. This differential equation led to a characteristic equation that related the growth rates to the wavenumber. The curve of growth rate as a function of wavenumber did indeed have

a maximum, and that associated wavelength was to be related to the spacing of ligaments that formed around the periphery of the spinning cup.

Yang et al [80] studied the application of a thin Newtonian film of photoresist on a concave spherical substrate. In general, photoresist applications have differences from paint applications for the reason photoresist is supplied mostly as a dose rather than as a continuous supply. This fluid remains on the spinning surface thereby enabling evaporation, heat transfer, and viscosity to become significant factors affecting fluidic behavior. On the other hand, in the case of a paint atomizer, the resident time of the material on the spinning surface can be orders of magnitude less than the resident time (100 seconds) for a photoresist. Their analyses start with a differential equation representing a force balance of centrifugal, gravity and viscous forces as shown in equation 3.2-1.

$$-\eta \frac{\partial^2 u}{\partial n^2} = \rho \omega^2 r \cos \theta - \rho g \cos \theta \quad 3.2-1$$

Since the angular velocity of a photoresist application can be an order, or two, lower than the angular velocity found in paint atomization, gravity forces were included in their analysis. When a fluidic “body force vs. viscous force” balance problem was formulated on a curved surface, as compared to a disk, or cone of constant angle, an inflection point developed that was dependent on the local slope, where the fluid film becomes thicker with advancement in the direction of flow. The remainder of their work included fluid slippage and solvent evaporation. This analysis, along with the analyses of Hinze and Milborn [34], and Sun et al [32] all exploited the natural boundaries in spherical or cylindrical coordinate systems. However, the curved surface can have local minimum film thickness in a radial domain of interest, whereas, for cones and disks a minimum thickness occurs at the

maximum value of radial position at the periphery. In other words, the fluid film thickness decreased as the radius increased. However, the concept of a disk of infinite radius is theoretical boundary condition.

Symons and Bizard [81] studied a novel method of measuring film thickness inside spinning cones by projecting a scale onto the surface of an opaque fluid to make comparative displacement measurements that were proportional to the thickness. Their experiments were at relatively low RPM where gravitational acceleration is on the same order as centripetal acceleration; they also referenced the work of Bruin [59] and Makarytchev et al [58].

Constantin and Johnson [82] studied the problem of an ocean on a rotating sphere. In their article, the connection to a rotating cup, or bell, was the derivation of cross product terms that led to Coriolis and normal acceleration terms. This work was accomplished in a spherical coordinate system.

The work of Shen et al [83] was based on a numerical study with a grid domain that spanned from fluid entering the cup, spreading across the cup surface, and finally to the periphery where fluid disintegration extended a few millimeters beyond the edge. They used the FLUENT commercial code and a volume of fluid (VOF) Reynolds stress model for a bell having an axisymmetric conical region that blended into a curve. Although the article emphasized camera-verified differences in flows as fluid progressed along its path, a graph in their work showed the fluid film thickness increasing as direction of flow changed direction due to surface curvature can be considered a connection to this dissertation.

The number of articles on the subject of film properties inside rotary bells and atomization far exceeds those included here; however, the references provided are considered to be more than ample material for substantiating the outcome of this dissertation. In addition, the references included in this literature review were obtained solely through the University of Kentucky online library search tool. No articles were purchased or obtained from sources that were not known to protect fully the rights of authors.

CHAPTER 4. PRELIMINARIES

4.1 Introduction

This chapter introduces non-inertial rotating reference frames and the “thin film approximation”. The Navier-Stokes equations, usually accompanied by the continuity equation, most often appear as a system of partial differential equations in an inertial coordinate system. The most common coordinate system is Cartesian because of the simplicity of working with the unit vectors that are constant. Cylindrical and Spherical coordinate systems are also common; however, they have the additional burden of unit vectors that change with position.

A thin film approximation is a method of simplifying problems by taking advantage of a high aspect ratio between length scales. In the case of rotary bells, fluid entering the bell around the center of rotation spreads out in a radially wide but thin layer. The width dimension is several orders of magnitude greater than the film thickness dimension. A thin film approximation enables neglecting fluid velocities normal to the bell surface.

Section 4.2 derives rotational terms in cylindrical coordinates; section 4.3 develops a cylindrical thin film approximation. Section 4.4 derives rotational terms in spherical coordinates; section 4.5 develops a spherical thin film approximation.

4.2 Non-Inertial Rotating Frame - Cylindrical Coordinate System

Equation 4.2-1 describes the derivative of an arbitrary vector (\vec{A}) in an inertial frame indicated by the subscript i on the left hand side and an equivalent representation in the non-inertial rotating frame of the right hand side as indicated by the subscript r .

$$\left(\frac{d}{dt}(\vec{A})\right)_i = \left(\frac{d}{dt}(\vec{A})\right)_r + \vec{\omega} \times (\vec{A}) \quad 4.2-1$$

Equation 4.2-2, or the second derivative of an arbitrary vector, is obtained by a single recursive application of the derivative equation, 4.2-1. In the case of a position vector, the right hand side includes centrifugal and the Coriolis terms. These fictitious terms, or forces when proportioned by mass, explain the apparent motion as seen by a non-inertial observer in the rotating frame.

$$\begin{aligned} \left(\frac{d}{dt}\left(\frac{d}{dt}(\vec{A})\right)\right)_i &= \left(\frac{d}{dt}\left(\left(\frac{d}{dt}(\vec{A})\right)_r + \vec{\omega} \times \vec{A}\right)\right)_r + \vec{\omega} \\ &\quad \times \left(\left(\frac{d}{dt}(\vec{A})\right)_r + \vec{\omega} \times \vec{A}\right) \end{aligned} \quad 4.2-2$$

To visualize these principles in a cylindrical frame, imagine throwing a ball to an opposing rider while on a playground merry-go-round. The observers on the ride see the ball curve away as if guided by unknown forces. On the other hand, the stationary observer, in the inertial frame, sees the ball traveling in a straight line. Newton's second law must be applied in inertial frames. Equation (4.2-2) is reduced to the equation (4.2-3) after vector operations.

$$\vec{\ddot{A}}_i = \vec{\ddot{A}}_r + 2\omega \times \vec{\dot{A}}_r + \omega \times (\omega \times \vec{A}) \quad 4.2-3$$

Figure 4.2-1 illustrates the components in a cylindrical coordinate that aid in visualizing the cross product operations and the relationship of the angular velocity vector and the unit vectors.

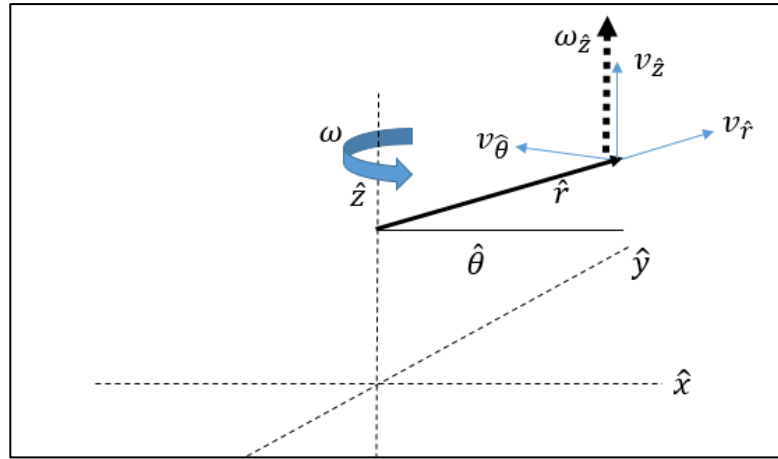


Figure 4.2-1 Cylindrical Coordinate System

Equations (4.2-4 a-c) are the cylindrical cross product relationships.

$$\hat{r} \times \hat{z} = -\hat{\theta} \quad (a) \quad 4.2-4$$

$$\hat{\theta} \times \hat{z} = \hat{r} \quad (b)$$

$$\hat{r} \times \hat{\theta} = \hat{z} \quad (c)$$

The cross product relationships are substituted into the second and third term on the right hand side of equation (4.2-3). Equation (4.2-5) includes the assumption of constant angular velocity and angular velocity constrained to \hat{z} .

$$\vec{\ddot{A}}_i = \vec{\ddot{A}}_r + 2\omega_{\hat{z}} \times (v_{\hat{r}} + v_{\hat{\theta}} + v_{\hat{z}}) + \omega_{\hat{z}} \times (\omega_{\hat{z}} \times r_{\hat{r}}) \quad 4.2-5$$

After completing vector operations in equation (4.2-5), the Coriolis term and the centrifugal terms are shown in equation (4.2-6).

$$\vec{A}_i = \vec{A}_r - 2\omega V_r \hat{\theta} + 2\omega V_\theta \hat{r} + \omega^2 A_r \hat{r} \quad 4.2-6$$

The Coriolis terms are the second and third terms on the right hand side of equation 4.2-6. The centrifugal term is the fourth term on the right hand side. The radial and tangential terms are usually added to the Navier-Stokes Equation as a body forces. The Coriolis term depends on the rotation rate and the fluid velocity at \hat{r} . The centrifugal term depends on \hat{r} and the rotation rate squared.

4.3 Thin Film Approximation – Cylindrical Coordinate System

The continuity equation in cylindrical coordinates

$$\frac{\partial \rho}{\partial t} + \frac{1}{r} \frac{\partial(\rho r v_r)}{\partial r} + \frac{1}{r} \frac{\partial(\rho v_\theta)}{\partial \theta} + \frac{\partial \rho v_z}{\partial z} = 0 \quad 4.3-1$$

For steady, incompressible, and axisymmetric flow conditions, equation 4.3-1 simplifies to equation 4.3-2.

$$\frac{1}{r} \frac{\partial(r v_r)}{\partial r} + \frac{\partial v_z}{\partial z} = \frac{\partial v_r}{\partial r} + \frac{v_r}{r} + \frac{\partial v_z}{\partial z} = 0 \quad 4.3-2$$

The continuity equation is non-dimensionalized with the following parameters.

$$r = L r' \quad z = H z' \quad v_r = U v_r' \quad v_z = (?) v_z' \quad 4.3-3$$

Since the equation for continuity must still be true after substitution of the dimensionless parameters shown in 4.2-3, the scale factor to be determined of v'_z must be $\left(\frac{UH}{L}\right)$.

$$\frac{U}{L} \frac{\partial v_r'}{\partial r'} + \frac{U}{L} \frac{v_r'}{r'} + \frac{1}{H} \left(\frac{UH}{L}\right) \frac{\partial v_z'}{\partial z'} = 0 \quad 4.3-4$$

Since the length scale in the radial direction (L) is much greater than the length scale in the \hat{z} direction (H), the result is the velocity in \hat{z} is much less than the radial velocity in \hat{r} , thus substantiating its neglect.

4.4 Non-Inertial Rotating Frame - Spherical Coordinate System

Restating equation 4.2-3 and focusing on the second and third terms on the right hand side, equation 4.4-1 leads to centrifugal and Coriolis terms in a spherical coordinate system.

$$\ddot{\vec{A}}_i = \ddot{\vec{A}}_r + 2 \omega \times \dot{\vec{A}}_r + \omega \times (\omega \times \vec{A}) \quad 4.4-1$$

The angular velocity vector ω shown in Figure 4.4-1 is vertical in the sense of a Cartesian or cylindrical system, however, since it is not parallel to any unit vectors in the spherical system; it is resolved into radial \hat{r} and polar angle $\hat{\theta}$ components.

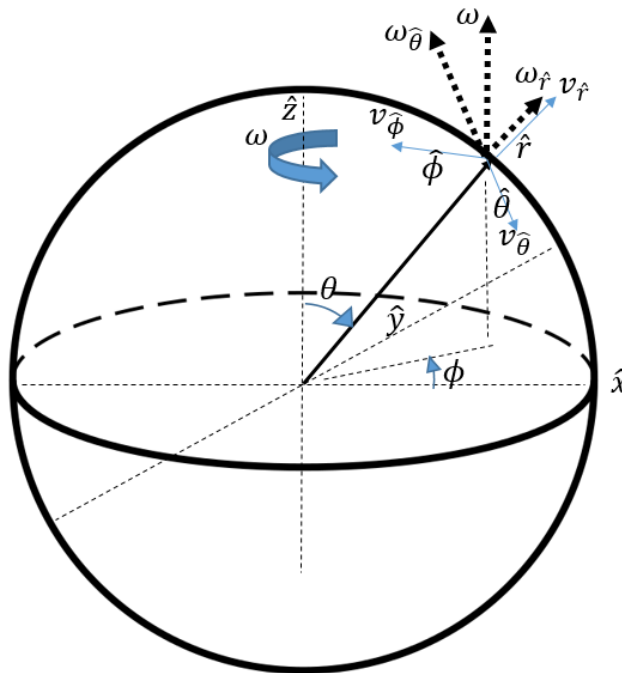


Figure 4.4-1 Spherical Coordinate System

Equations 4.2-4 a-c are the spherical unit vector cross product relationships.

$$\hat{r} \times \hat{\theta} = \hat{\phi} \quad (a) \quad 4.4-2$$

$$\hat{\theta} \times \hat{\phi} = \hat{r} \quad (b)$$

$$\hat{\phi} \times \hat{r} = \hat{\theta} \quad (c)$$

Equations 4.4-2 (a-c) are substituted into equation 4.4-1 along with a resolution of the angular velocity vector into the appropriate spherical unit vectors, yielding equation 4.4-3.

$$\begin{aligned} \ddot{A}_i = \ddot{A}_r + 2(\omega \cos \theta \hat{r} - \omega \sin \theta \hat{\theta}) \times (v_{\hat{r}} + v_{\hat{\theta}} + v_{\hat{\phi}}) + \\ (\omega \cos \theta \hat{r} - \omega \sin \theta \hat{\theta}) \times ((\omega \cos \theta \hat{r} - \omega \sin \theta \hat{\theta}) \times r_{\hat{r}}) \end{aligned} \quad 4.4-3$$

Equation 4.4-4 is obtained after completing vector operation shown in equation 4.4-3.

$$\begin{aligned} \ddot{A}_i = \ddot{A}_r + 2\omega(-v_{\hat{\phi}} \sin \theta \hat{r} - v_{\hat{\phi}} \cos \theta \hat{\theta} + (v_{\hat{\theta}} \cos \theta + v_{\hat{r}} \sin \theta) \hat{\phi}) + \\ r\omega^2(-\sin^2 \theta \hat{r} - \cos \theta \sin \theta \hat{\theta}) \end{aligned} \quad 4.4-4$$

Grouping like terms in equation (4.4-4) enables restating it as equation (4.4-5) [84].

$$\begin{aligned} \ddot{A}_i = \ddot{A}_r + \\ -(2\omega v_{\hat{\phi}} \sin \theta + r\omega^2 \sin^2 \theta) \hat{r} - (2\omega v_{\hat{\phi}} \cos \theta + r\omega^2 \cos \theta \sin \theta) \hat{\theta} \\ + (2\omega v_{\hat{r}} \sin \theta + 2\omega v_{\hat{\theta}} \cos \theta) \hat{\phi} \end{aligned} \quad 4.4-5$$

In equation (4.4-5), centrifugal terms are multiplied by $r\omega^2$, and Coriolis terms are multiplied by 2ω . These terms are entered into the spherical Navier-Stokes equations as body forces. The relationships shown in equation (4.4-2) are only valid under very strict conditions, namely, the angular velocity is resolved into the variable directions at the point of interest. The general cross product operation in spherical coordinates is not a simple extension of the Cartesian formula. This is because the unit vectors change with position.

If the angular velocity was written as $\{\omega_r, 0_\theta, 0_\phi\}$, and that was “crossed”, using the Cartesian determinant, with the velocity $\{v_{\hat{r}}, v_{\hat{\theta}}, v_{\hat{\phi}}\}$, an incorrect answer would be obtained.

4.5 Thin Film Approximation – Spherical Coordinate System

Equation 4.5-1 is the continuity equation in spherical coordinates.

$$\frac{1}{r^2} \frac{\partial}{\partial r} (r^2 v_r) + \frac{1}{r \sin(\theta)} \frac{\partial}{\partial \theta} (v_\theta \sin(\theta)) + \frac{1}{r \sin(\theta)} \frac{\partial v_\phi}{\partial \phi} = 0 \quad 4.5-1$$

Two assumptions simplify equation 4.5-1. First, the flow is axisymmetric and derivatives with respect to azimuthal angles are neglected. Second, since the fluid film is thin, the range of the polar angle θ around the nominal value is small and validates the assumption that $\sin(\theta)$ is virtually a constant. These assumptions, along with the derivative of the first terms in parenthesis, lead to equation 4.5-2.

$$\frac{1}{r^2} \left(r^2 \frac{\partial}{\partial r} v_r + 2r v_r \right) + \frac{1}{r} \frac{\partial}{\partial \theta} (v_\theta) = 0 \quad 4.5-2$$

Equation 4.5-2 is further simplified to equation 4.5-3.

$$\frac{\partial v_r}{\partial r} + \frac{2v_r}{r} + \frac{1}{r} \frac{\partial v_\theta}{\partial \theta} = 0 \quad 4.5-3$$

Equation (4.5-3) is non-dimensionalized with the substitutions from equations (4.5-4) a-d. L is a characteristic length such as bell radius or diameter. U is a characteristic velocity such as the peripheral speed of bell. Theta is a characteristic angle such as the range of the polar angle through the thin film of fluid.

$$r = Lr' \quad v_r = Uv_r' \quad \theta = \Theta\theta' \quad v_\theta = (?)v_\theta' \quad 4.5-4$$

In equation 4.5-5, $L\theta$ corresponds to the term H in the previous cylindrical case. Since both are the thickness of the film, both are assumed much smaller than the characteristic length, L . Since continuity must hold, the unknown scale factor in the theta direction is $UL\theta/L$, which can be simplified to $U\theta$.

$$\frac{U\partial v'_r}{L\partial r'} + \frac{U2v'_r}{Lr'} + \frac{1}{L\theta r'} \left(\frac{UL\theta}{L} \right) \frac{\partial v'_\theta}{\partial \theta'} = 0 \quad 4.5-5$$

Equation 4.5-5 is applicable in the case of a bell modeled by a constant polar angle, yielding a conical bell. Since the length scale in the radial direction (L) is much greater than the length scale in the $\hat{\theta}$ direction ($L\theta$), the result is the velocity in $\hat{\theta}$ is much less than the radial velocity in \hat{r} , thus substantiating its neglect. A conical bell is a common profile and some of the earliest publications on high-speed rotating thin films are derived in this configuration.

A bell could also be modeled as rotating partial sphere in a spherical coordinate system. In that case, v'_r is the velocity that is normal to the bell surface, hence, it becomes the neglected velocity.

This chapter concludes with sections 4.6 and 4.7. They are similar to the commonly published Navier-Stokes equations in cylindrical and spherical coordinate systems; however, they include the centrifugal and Coriolis terms as derived in this chapter.

4.6 Cylindrical Navier-Stokes – Rotating System

The radial, tangential, and azimuthal Navier-Stokes equations for rotating non-inertial frames are shown in equations (4.6-1), (4.6-2), and (4.6-3).

$$\begin{aligned} \rho \left(\frac{\partial v_r}{\partial t} + v_r \frac{\partial v_r}{\partial r} + \frac{v_\theta}{r} \frac{\partial v_r}{\partial \theta} - \frac{v_\theta^2}{r} + v_z \frac{\partial v_r}{\partial z} \right) & \quad 4.6-1 \\ & = -\frac{\partial P}{\partial r} + \mu \left(\frac{\partial}{\partial r} \left(\frac{1}{r} \frac{\partial (r v_r)}{\partial r} \right) + \frac{1}{r^2} \frac{\partial^2 v_r}{\partial \theta^2} - \frac{2}{r^2} \frac{\partial v_\theta}{\partial \theta} + \frac{\partial^2 v_r}{\partial z^2} \right) \\ & \quad + \rho g_r + \rho 2\omega v_\theta + \rho r \omega^2 \end{aligned}$$

$$\begin{aligned} \rho \left(\frac{\partial v_\theta}{\partial t} + v_r \frac{\partial v_\theta}{\partial r} + \frac{v_\theta}{r} \frac{\partial v_\theta}{\partial \theta} + \frac{v_r v_\theta}{r} + v_z \frac{\partial v_\theta}{\partial z} \right) & \quad 4.6-2 \\ & = -\frac{1}{r} \frac{\partial P}{\partial \theta} + \mu \left(\frac{\partial}{\partial r} \left(\frac{1}{r} \frac{\partial (r v_\theta)}{\partial r} \right) + \frac{1}{r^2} \frac{\partial^2 v_\theta}{\partial \theta^2} + \frac{2}{r^2} \frac{\partial v_r}{\partial \theta} + \frac{\partial^2 v_\theta}{\partial z^2} \right) \\ & \quad + \rho g_\theta - \rho 2\omega v_r \end{aligned}$$

$$\begin{aligned} \rho \left(\frac{\partial v_z}{\partial t} + v_r \frac{\partial v_z}{\partial r} + \frac{v_\theta}{r} \frac{\partial v_z}{\partial \theta} + v_z \frac{\partial v_z}{\partial z} \right) & \quad 4.6-3 \\ & = -\frac{\partial P}{\partial z} + \mu \left(\frac{1}{r} \frac{\partial}{\partial r} \left(r \frac{\partial v_z}{\partial r} \right) + \frac{1}{r^2} \frac{\partial^2 v_z}{\partial \theta^2} + \frac{\partial^2 v_z}{\partial z^2} \right) + \rho g_z \end{aligned}$$

These equations assume a constant “vertical” angular velocity and an incompressible fluid.

4.7 Spherical Navier-Stokes – Rotating System

The spherical Navier-Stokes equations are shown as equations (4.7-1), (4.7-2), and (4.7-3). These equations assume an angular velocity that is constant, with a polar angle equal to zero, and an incompressible fluid

$$\begin{aligned}
 & \rho \left(\frac{\partial v_r}{\partial t} + v_r \frac{\partial v_r}{\partial r} + \frac{v_\theta}{r} \frac{\partial v_r}{\partial \theta} + \frac{v_\phi}{r \sin(\theta)} \frac{\partial v_r}{\partial \phi} - \frac{v_\theta^2 + v_\phi^2}{r} \right) = & 4.7-1 \\
 & - \frac{\partial P}{\partial r} + \mu \left(\frac{\partial}{\partial r} \left(\frac{1}{r^2} \frac{\partial}{\partial r} (r^2 v_r) \right) + \frac{1}{r^2 \sin(\theta)} \frac{\partial}{\partial \theta} \left(\sin(\theta) \frac{\partial v_r}{\partial \theta} \right) \right. \\
 & \left. + \frac{1}{r^2 \sin^2(\theta)} \frac{\partial^2 v_r}{\partial \phi^2} - \frac{2}{r^2 \sin(\theta)} \frac{\partial}{\partial \theta} (v_\theta \sin(\theta)) - \frac{2}{r^2 \sin(\theta)} \frac{\partial v_\phi}{\partial \phi} \right) + \rho a_r \\
 & + \rho 2\omega v_\phi \sin \theta + \rho r \omega^2 \sin^2 \theta
 \end{aligned}$$

$$\begin{aligned}
 & \rho \left(\frac{\partial v_\theta}{\partial t} + v_r \frac{\partial v_\theta}{\partial r} + \frac{v_\theta}{r} \frac{\partial v_\theta}{\partial \theta} + \frac{v_\phi}{r \sin(\theta)} \frac{\partial v_\theta}{\partial \phi} + \frac{v_r v_\theta}{r} - \frac{v_\phi^2 \cot(\theta)}{r} \right) = & 4.7-2 \\
 & - \frac{1}{r} \frac{\partial P}{\partial \theta} + \mu \left(\frac{1}{r^2} \frac{\partial}{\partial r} \left(r^2 \frac{\partial v_\theta}{\partial r} \right) + \frac{1}{r^2} \frac{\partial}{\partial \theta} \left(\frac{1}{\sin(\theta)} \frac{\partial}{\partial \theta} (v_\theta \sin(\theta)) \right) \right. \\
 & \left. + \frac{1}{r^2 \sin^2(\theta)} \frac{\partial^2 v_\theta}{\partial \phi^2} + \frac{2}{r^2} \frac{\partial v_r}{\partial \theta} - \frac{2 \cot(\theta)}{r^2 \sin(\theta)} \frac{\partial v_\phi}{\partial \phi} \right) + \rho a_\theta \\
 & + \rho 2\omega v_\phi \cos \theta + \rho r \omega^2 \cos \theta \sin \theta
 \end{aligned}$$

$$\begin{aligned}
 & \rho \left(\frac{\partial v_\phi}{\partial t} + v_r \frac{\partial v_\phi}{\partial r} + \frac{v_\theta}{r} \frac{\partial v_\phi}{\partial \theta} + \frac{v_\phi}{r \sin(\theta)} \frac{\partial v_\phi}{\partial \phi} + \frac{v_r v_\phi}{r} + \frac{v_\theta v_\phi \cot(\theta)}{r} \right) = & 4.7-3 \\
 & - \frac{1}{r \sin(\theta)} \frac{\partial P}{\partial \phi} + \mu \left(\frac{1}{r^2} \frac{\partial}{\partial r} \left(r^2 \frac{\partial v_\phi}{\partial r} \right) + \frac{1}{r^2} \frac{\partial}{\partial \theta} \left(\frac{1}{\sin(\theta)} \frac{\partial}{\partial \theta} (v_\phi \sin(\theta)) \right) \right. \\
 & \left. + \frac{1}{r^2 \sin^2(\theta)} \frac{\partial^2 v_\phi}{\partial \phi^2} + \frac{2}{r^2 \sin(\theta)} \frac{\partial v_r}{\partial \phi} + \frac{2 \cot(\theta)}{r^2 \sin(\theta)} \frac{\partial v_\theta}{\partial \phi} \right) + \rho a_\phi \\
 & - \rho 2\omega v_r \sin \theta - \rho 2\omega v_\theta \cos \theta
 \end{aligned}$$

CHAPTER 5. VON KARMAN MODEL

5.1 Introduction

Rotating flow is a classical problem in analytic fluid mechanics. The Von Karman swirling flow problems are a group of classic problems with known solutions. The path to a solution in rotating flow begins with setting non-dimensional velocities equal to functions of a non-dimensional variable as shown in equations 5.1-1 a-c.

The demonstration problem is a semi-infinite stationary fluid, in a cylindrical coordinate system with a lower bound that is an infinite rotating disk. The velocity profiles at any radial position “ r ” are scaled versions of reference profiles F , G , and H . It is important to note that in this particular problem, the semi-infinite fluid “container” is not rotating; the angular velocity ω term applies to the boundary. The boundary at $z = 0$ is rotating. There is no “rotating observer”; hence, the Coriolis and centrifugal body force terms do not explicitly appear in the Navier-Stokes equations.

$$\frac{v_r}{r\omega} = F(\eta) \quad (a) \quad 5.1-1$$

$$\frac{v_\theta}{r\omega} = G(\eta) \quad (b)$$

$$\frac{v_z}{\sqrt{\nu\omega}} = H(\eta) \quad (c)$$

The non-dimensional functions are of a single non-dimensional variable η . It is a scaled length in the vertical direction as shown in equation 5.1-2.

$$\eta = z\sqrt{\frac{\omega}{\nu}} \quad 5.1-2$$

Equations 5.1-3 are equations 5.1-1 restated in a more convenient form for substitution into the Navier-Stokes Equations.

$$v_r = r\omega F(\eta) \quad (a) \quad 5.1-3$$

$$v_\theta = r\omega G(\eta) \quad (b)$$

$$v_z = \sqrt{\nu\omega} H(\eta) \quad (c)$$

The purpose this problem is introducing the scaled variable $z\sqrt{(\omega/\nu)}$. It appears in rotational fluid mechanics problems and is one of several published forms of the Ekman number. However, in thin film problems, its physical significance is not seen as readily as in this problem of semi-infinite depth.

5.2 Continuity Equation of Infinite Fluid on Spinning Boundary

The cylindrical continuity equation, 4.3-2 for the case of steady state and axisymmetric flow is restated as equation 5.2-1.

$$\frac{1}{r} \frac{\partial (rv_r)}{\partial r} + \frac{\partial v_z}{\partial z} = 0 \quad 5.2-1$$

Equations 5.1-3 a-c are substituted into the continuity equation 5.2-1

$$\frac{1}{r} \frac{\partial (r r \omega F(\eta))}{\partial r} + \frac{\partial \sqrt{v\omega} H(\eta)}{\partial z} = 0 \quad 5.2-2$$

Equations 5.2-3 through equation 5.2-5 show some of the steps that lead to the result in equation 5.2-6.

$$2\omega F(\eta) + \sqrt{v\omega} \frac{dH}{d\eta} \frac{d\eta}{dz} = 0 \quad 5.2-3$$

$$2\omega F(\eta) + \sqrt{v\omega} \frac{dH}{d\eta} \sqrt{\frac{\omega}{v}} = 0 \quad 5.2-4$$

$$2\omega F + \omega H_\eta = 0 \quad 5.2-5$$

$$2F + H_\eta = 0 \quad 5.2-6$$

5.3 Radial Navier-Stokes Equation of Infinite Fluid on Spinning Boundary

Equation (4.6-1), the momentum equation for the radial direction in a cylindrical coordinate system, is restated here as equation (5.3-1) for the purpose of a starting point. Notice “body force” terms of gravity, Coriolis, and centrifugal are not included.

$$\rho \left(\frac{\partial v_r}{\partial t} + v_r \frac{\partial v_r}{\partial r} + \frac{v_\theta}{r} \frac{\partial v_r}{\partial \theta} - \frac{v_\theta^2}{r} + v_z \frac{\partial v_r}{\partial z} \right) = \quad 5.3-1$$

$$-\frac{\partial P}{\partial r} + \mu \left(\frac{\partial}{\partial r} \left(\frac{1}{r} \frac{\partial (r v_r)}{\partial r} \right) + \frac{1}{r^2} \frac{\partial^2 v_r}{\partial \theta^2} - \frac{2}{r^2} \frac{\partial v_\theta}{\partial \theta} + \frac{\partial^2 v_r}{\partial z^2} \right)$$

If the analysis is limited to steady state axisymmetric flow, terms with derivatives of time and derivatives of theta drop out. Since there is no fluid rotation at large values of z, the pressure is not a function of radial position, and is a function of z only, therefore, the pressure term drops out. The second term on the right hand side also drops out, however, that is not apparent until equation 5.1-3 (a) is substituted into equation 5.3-1. The result is shown in equation 5.3-2.

$$v_r \frac{\partial v_r}{\partial r} - \frac{v_\theta^2}{r} + v_z \frac{\partial v_r}{\partial z} = \nu \frac{\partial^2 v_r}{\partial z^2} \quad 5.3-2$$

Substitution of equations 5.1-3 (a-c) into equation 5.3-2 yields equation 5.3-3.

$$r \omega F \omega F - \frac{r^2 \omega^2 G^2}{r} + \sqrt{\nu \omega} H r \omega \frac{dF}{d\eta} \sqrt{\frac{\omega}{\nu}} = \nu r \omega F'' \frac{\omega}{\nu} \quad 5.3-3$$

Equation 5.3-3 is simplified and this leads to equation 5.3-4. Notice that derivatives of eta include the scale factor of the square root of angular velocity divided by kinematic viscosity.

$$F^2 - G^2 + HF_\eta = F_{\eta\eta} \quad 5.3-4$$

5.4 Tangential Navier-Stokes Equation of Infinite Fluid on Spinning Boundary

Equation 4.6-2, the momentum equation for the tangential direction in a cylindrical coordinate system, is restated here as equation 5.4-1 for the purpose of a starting point. Notice the body force and Coriolis terms are not included.

$$\begin{aligned} \rho \left(\frac{\partial v_\theta}{\partial t} + v_r \frac{\partial v_\theta}{\partial r} + \frac{v_\theta}{r} \frac{\partial v_\theta}{\partial \theta} + \frac{v_r v_\theta}{r} + v_z \frac{\partial v_\theta}{\partial z} \right) \\ = -\frac{1}{r} \frac{\partial P}{\partial \theta} + \mu \left(\frac{\partial}{\partial r} \left(\frac{1}{r} \frac{\partial (r v_\theta)}{\partial r} \right) + \frac{1}{r^2} \frac{\partial^2 v_\theta}{\partial \theta^2} + \frac{2}{r^2} \frac{\partial v_r}{\partial \theta} + \frac{\partial^2 v_\theta}{\partial z^2} \right) \end{aligned} \quad 5.4-1$$

If the analysis is limited to steady state axisymmetric flow, terms with derivative of time and derivative of theta drop out. The second term on the right hand side also drops out, however, that is not apparent until equation 5.1-3 (b) is substituted into equation 5.4-1. The result is shown in equation 5.4-2.

$$v_r \frac{\partial v_\theta}{\partial r} + \frac{v_r v_\theta}{r} + v_z \frac{\partial v_\theta}{\partial z} = \nu \frac{\partial^2 v_\theta}{\partial z^2} \quad 5.4-2$$

Substitution of equations 5.1-3 (a-c) into equation 5.4-2 yields equation 5.4-3.

$$r\omega F \omega G + \frac{r\omega F r\omega G}{r} + \sqrt{v\omega} H r\omega G_\eta \sqrt{\frac{\omega}{\nu}} = \nu r\omega G_{\eta\eta} \frac{\omega}{\nu} \quad 5.4-3$$

After simplification of equation 5.4-3, equation 5.4-4 is the result.

$$2FG + HG_\eta = G_{\eta\eta} \quad 5.4-4$$

5.5 Solution to the System of Ordinary Differential Equations

Equations 5.2-6, 5.3-4, and 5.4-4 form a system of ordinary differential equations 5.5-1 in the scaled variable η .

$$\begin{aligned}2F + H_{\eta} &= 0 \quad (a) & 5.5-1 \\F^2 - G^2 + HF_{\eta} &= F_{\eta\eta} \quad (b) \\2FG + HG_{\eta} &= G_{\eta\eta} \quad (c)\end{aligned}$$

The accompanying boundary conditions are equations 5.5-2 a-b.

$$\begin{aligned}F = 0 \quad G = 1 \quad H = 0 \quad \text{at } \eta = 0 & \quad (a) & 5.5-2 \\F = 0 \quad G = 0 \quad \text{for } \eta \rightarrow \infty & \quad (b)\end{aligned}$$

The boundary condition at eta equal to zero consists of no slip in the radial direction and F is equal to zero with no slip in the tangential direction; therefore, G is equal to one. When G is equal to one, the tangential velocity at the surface of the rotating disk is equal to the radius times the angular velocity, as required for no-slip. The value of H is equal to zero because the disk is impervious. At infinity, the radial and tangential velocities are both equal to zero.

The solution to the system of equations (5.5-2) is obtained from a succinct program in MatLab using the “bvp4c” built in function. The function is shown in Figure 5.5-1.

```

function [x, y] = vkns
solinit = bvpinit(linspace(0,10,101),[0 0 1 0 0]);
options = bvpset('Stats','on','RelTol',1e-5);
sol = bvp4c(@vknsodes,@vknsbcs,solinit,options);
x = sol.x;% nu values at x(j)
y = sol.y;% F(i=1),F',G(i=3),G',H(i=5)at y(i,j)
% System of Equations
function soe = vknsodes(~,y)%replace x with ~
soe = [y(2)
       y(1)^2-y(3)^2+y(5)*y(2)
       y(4)
       2*y(1)*y(3)+y(5)*y(4)
       -2*y(1)];
end
% Boundary Conditions - y(n)-bc = 0
function bc = vknsbcs(ya,yb)
bc = [ya(1)-0
      ya(3)-1
      ya(5)-0
      yb(1)-0
      yb(3)-0];
end
end

```

Figure 5.5-1 Matlab Function solves system of ODE's

For a MatLab solution, the system of ODE's 5.5-1 must be represented in a state space formulation as shown in equation 5.5-3. Once the state space representation is established, the declaration of “y” terms in the function is apparent. They correspond to the F, G, and H terms and their derivatives in equation 5.5-3. The boundary conditions at eta equal to zero are declared as array $ya(i)$, and at the other limit of the domain, they are declared as array $yb(i)$.

$$\frac{d}{d\eta} \begin{bmatrix} F \\ F_\eta \\ G \\ G_\eta \\ H \end{bmatrix} = f(\eta) = \begin{bmatrix} F_\eta \\ F^2 - G^2 + HF_\eta \\ G_\eta \\ 2FG + HG_\eta \\ -2F \end{bmatrix} \quad 5.5-3$$

The boundary condition at infinity is approximated as being beyond the point where the functions F, G, and H reach their final values.

The solution to the system of equations 5.5-3 is shown in Figure 5.5-2.

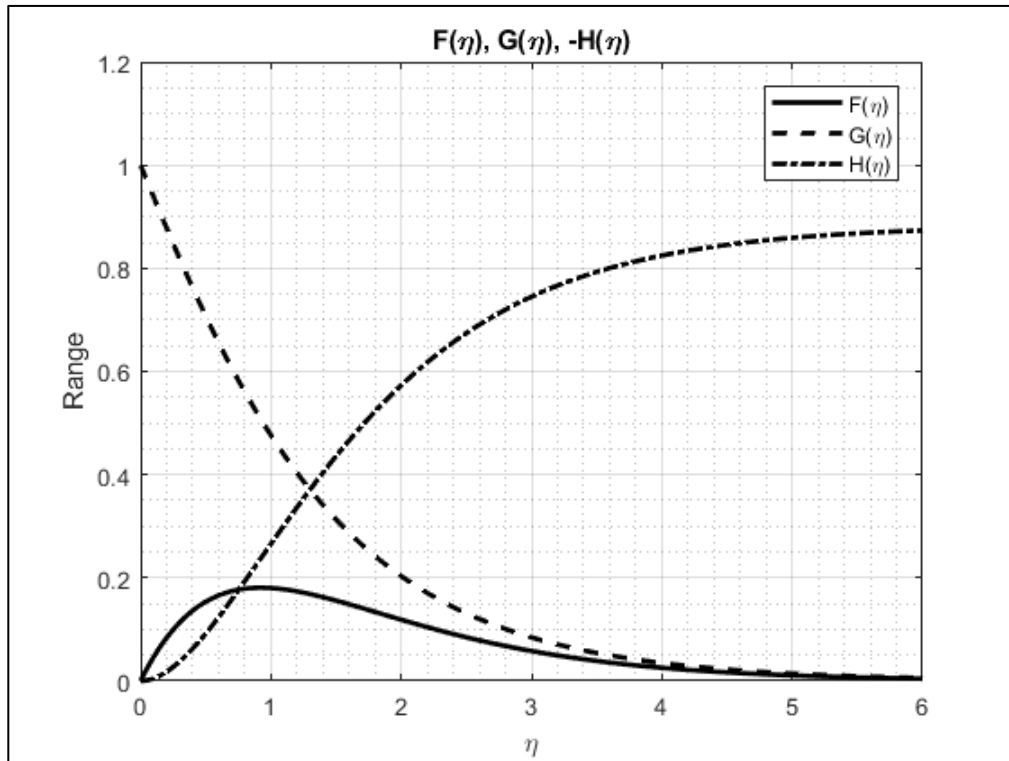


Figure 5.5-2 Solution to System of ODE's

A more intuitive picture of a three dimensional flow field is shown in Figure 5.5-3. As vorticity diffuses into the fluid from the spinning disk at η equal to zero, it is balanced by velocity in the z direction towards the spinning boundary condition. At a value of eta approximately equal to six, the radial and tangential flow fields have decayed to zero.

The functions F and G are essentially the Rossby numbers for radial and tangential velocity. The Rossby number, equation 5.5-4, is defined as a velocity divided by a frequency, and then divided by a length. The Rossby number is a ratio of inertia forces to Coriolis forces, or the ratio of distance traced by velocity per radian of rotation compared to a reference length.

$$Ro = \left(\frac{U}{\omega}\right) \frac{1}{L} = \frac{U}{L\omega}$$

5.5-4

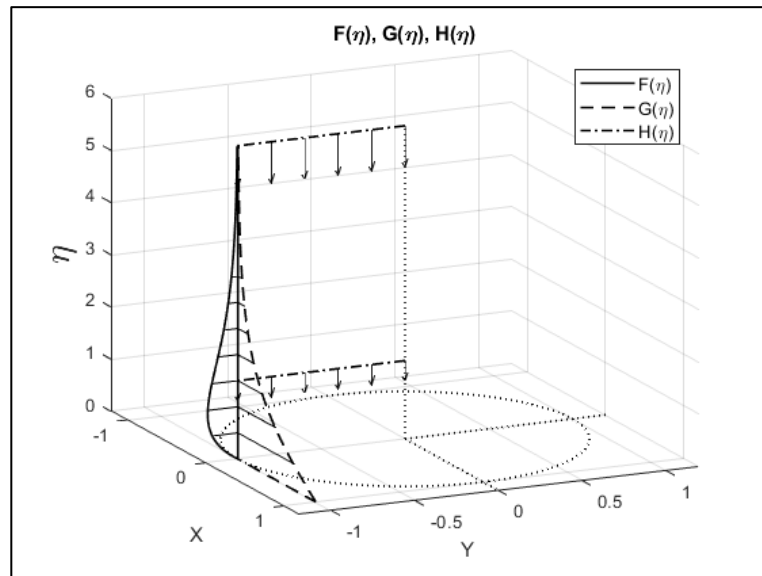


Figure 5.5-3 Three dimensional flow field

Figure 5.5-2 and Figure 5.5-3 illustrate the significance of $\eta = z\sqrt{(\omega/\nu)}$ in a fluid of semi-infinite depth, which is generally not as apparent in a thin film analysis. As can be seen in Figure 5.5-3, the radial and rotational velocity fields go to zero after several multiples of η .

CHAPTER 6. THE EKMAN NUMBER

6.1 Introduction

The purpose of this chapter is to assess the importance and ubiquitous presence of the Ekman number in rotational fluid mechanics. Initially, a discussion of ocean currents in this thin film centric dissertation seems out of place since flows present in oceans are orders of magnitude larger and slower than a thin fluid film on a high RPM rotary bell. However, a dimensionless quantity called the Ekman number appears in the analysis of both cases. For flows on a high-speed bell, the Ekman number characterizes the order of magnitude of the terms in the Navier-Stokes equation. In oceanographic, and other large-scale flows, in addition to characterizing the order of magnitude of terms, the Ekman number also characterizes the extent of the boundary layer.

Rotational fluid mechanics are an important tool for analyzing oceanographic and atmospheric flow. In the case of the semi-infinite Von Karman flow of the previous chapter, it was shown that the quantity $z\sqrt{(\omega/\nu)}$ characterizes the distance into a fluid where effects from the rotating boundary are present and ultimately decay. On the other hand, in a thin film of rotating fluid, this same quantity is algebraically present; however, its physical significance is less obvious, although its value indicates that thin film flow is in within the viscous boundary layer. The Ekman number is a ratio of viscous and Coriolis forces and defined as $\nu/(\Omega L^2)$. The quantity $z\sqrt{(\omega/\nu)}$ is of the form of a square root of the reciprocal of the Ekman number.

In the case of geostrophic oceanic flow, the observer on a rotating earth sees a current of water circulating around a heightened mound of ocean water. As the mound of water “tries to flatten” under the effect of gravity, a radially outward flow emerges from the mound. However, the Coriolis “force” is continuously nudging the flow at a right angle to its velocity, creating a spiral flow that eventually forms a loop current at some distance from the mound. Thereby a, circulating loop current is formed when Coriolis forces and pressure forces are balanced.

The combination of Von Karman swirling flow and Atmospheric/Oceanographic flows introduce vocabulary, non-dimensional variables, and analyses that form pathways to further understanding of rotating fluid mechanics.

The eponymous Ekman Spiral is one of the most interesting observations in nature. It is a more dependent on mathematical analysis than the preceding example of geostrophic flow that can be present around a mound of water. The Ekman spiral is a function of the viscous forces generated by vertical gradients of horizontal ocean current velocities and Coriolis forces. In general, oceanic behavior can be analyzed under an assumption that the earth is locally, flat and it success justifies using the familiar Cartesian coordinate system as the analytical framework.

Coriolis forces, or apparent forces in an accelerating frame, are obtained from the second term on the right hand side (RHS) of equation 4.2-3, or the fourth term on the left hand side (LHS) of equation 7.1-1. They are as shown by equation 6.1-1, where Ω is the rotation of the earth and \mathbf{q} is a velocity vector.

$$\mathbf{F}_{Cor} = 2\Omega \times \mathbf{q} \quad 6.1-1$$

If Cartesian velocities $v_{x,y,z}$ are substituted into equation 6.1-1, and the cross product is expanded, equation 6.1-2 is obtained.

$$\begin{aligned} \mathbf{F}_{Cor} &= 2 \begin{bmatrix} \hat{i} & \hat{j} & \hat{k} \\ 0 & \Omega \cos \theta & \Omega \sin \theta \\ v_x & v_y & 0 \end{bmatrix} \\ &= 2 \left((-\Omega \sin \theta v_y) \hat{i} - (-\Omega \sin \theta v_x) \hat{j} + (-\Omega \cos \theta v_x) \hat{k} \right) \end{aligned} \quad 6.1-2$$

In the equations of motion, the components from equation 6.1-2 appear on the LHS; however, when moved to the RHS, the \hat{i}, \hat{j} terms change sign. The viscous forces are characterized by the second derivative of horizontal velocities with respect to depth. The familiar molecular viscosity coefficient μ is replaced with an eddy viscosity [85] term A_z . The Coriolis terms and the eddy viscosity terms yield a coupled set of differential equations for horizontal current velocity as a function of depth. The coupled system is shown as equations 6.1-3 and 6.1-4. In these equations, f is equal to $2\Omega \sin \theta$ and represents the local vertical component of the earth's rotation as a function of latitude.

$$fv + A_z \frac{\partial^2 u}{\partial z^2} = 0 \quad 6.1-3$$

$$-fu + A_z \frac{\partial^2 v}{\partial z^2} = 0 \quad 6.1-4$$

This system of equations has a solution consisting of horizontal u and v velocities listed as equations 6.1-5 and 6.1-6. In these equations, z is the ocean depth, and “ a ” is equal to the quantity $\sqrt{f/(2A_z)}$.

$$u = V_0 e^{az} \cos\left(\frac{\pi}{4} + az\right) \quad 6.1-5$$

$$v = V_0 e^{az} \sin\left(\frac{\pi}{4} + az\right) \quad 6.1-6$$

Figure 6.1-1 illustrates an Ekman spiral where a wind, indicated by the top arrow that is parallel to an axis, is blowing across the ocean surface, and the water is responding by moving at an angle to the wind. Each subsequent “layer” of water induces motion in the “layer” below it, however, the Coriolis force nudges velocity at a right angle to its direction, and eddy viscosity is causing an exponential decrease of current velocity as ocean depth increases. The net result is a spiral of magnitude and direction that eventually decays.

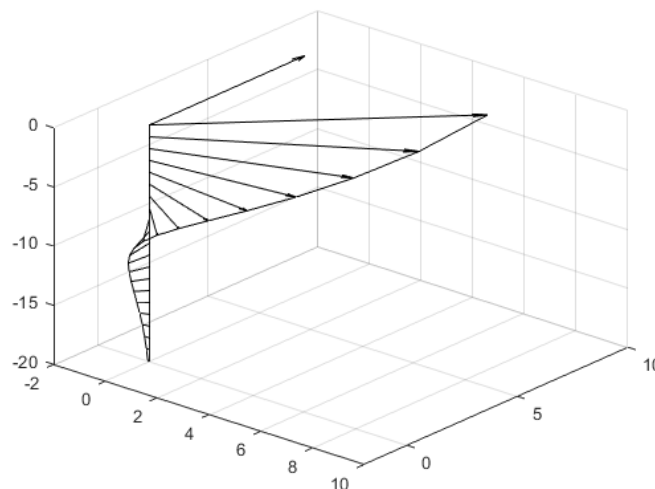


Figure 6.1-1 Ekman spiral (axes scaled for illustration)

In equations 6.1-5 and 6.1-6, the form of the constant coefficient in the exponential and sinusoidal terms is $\sqrt{f/(2A_z)}$. The combination of this constant coefficient and the depth is in the form of a reciprocal Ekman number.

CHAPTER 7. GREENSPAN FORMULATION

7.1 Introduction

In the field of rotational fluid mechanics, H. P. Greenspan is widely recognized for his text, *The Theory of Rotating Fluids* [86]. The first equations in the text are shown here as equations 7.1-1 (a-b), they are the conservation of mass and conservation of momentum, where \mathbf{q} is the velocity vector, Ω is the coordinate system rotation, and \mathbf{r} is a position.

$$\nabla \cdot \mathbf{q} = 0 \quad (\text{a}) \tag{7.1-1}$$

$$\begin{aligned} \frac{\partial \mathbf{q}}{\partial t} + \frac{1}{2}(\mathbf{q} \cdot \nabla) \mathbf{q} + (\nabla \times \mathbf{q}) \times \mathbf{q} + 2\Omega \times \mathbf{q} + \Omega \times (\Omega \times \mathbf{r}) = \\ -\frac{1}{\rho} \nabla P + \mathcal{F} - \nu \nabla \times (\nabla \times \mathbf{q}) \quad (\text{b}) \end{aligned}$$

The fourth and fifth terms on the left hand side of equation 7.1-1 (b) are the same as those found in equation 4.2-3. These are the Coriolis force and the centrifugal force respectively.

Further reading in Greenspan reveals a path for relating velocities in the inertial and rotating systems as shown by equation 7.1-2.

$$\mathbf{q}_{inert} = \Omega \times \mathbf{r} + \mathbf{q}_{rot} \tag{7.1-2}$$

Greenspan introduced equations of motion, shown in equation 7.2-1, in a rotating system where \mathbf{q} was velocity measured in the rotating system, and a pathway, as defined in equation 7.1-2, to an inertial system. These equations are perfectly valid, although somewhat opposite to conventional progression. The mathematical migration is usually

from stationary system where inertial properties are established by nature, to rotating system where inertial properties are established by calculation.

A subtle, but critically important point that was not covered in section 4.2 is that the cross product operation in spherical coordinates is not as simple as the Cartesian determinant operation. This difference is because in spherical or cylindrical systems the unit vectors depend on position, whereas in Cartesian systems they are fixed. For cylindrical and spherical systems, the vectors of interest, namely, angular velocity, linear velocity, and position, all at the same point, were resolved into components along the appropriate unit vectors at that location. This restrictive condition permits the spherical cross product to have the same form as the Cartesian cross product. The correct answer was obtained because all quantities were expressed in terms of components multiplied by unit vectors that form a local mutually orthogonal system. An alternative, but less efficient, method for spherical cross products is to transform the spherical vectors into a Cartesian system, perform the cross product operation, and then transform to spherical vectors. Most of this chapter demonstrates such an alternative path. Other than the merit of proving an alternative, this section arrives at the same result as section 4.4.

Virtually all the publications referenced in this dissertation use a simplified kinematic substitution applied in a mutually orthogonal coordinate system to achieve essentially the same result as the more tedious vector mechanics approach summarized here. It was limited to polar rotations, meaning the axis of rotation runs north to south. This kinematic substitution accounts for the rotational surface velocity of the spinning object as a reference for the observer “on” the spinning object, transforming the equations of motion into an inertial frame.

Additionally, and as an alternative to manual calculations, this chapter demonstrates use of a symbolic processor for obtaining expanded terms of some of the cross products in equation 7.2-1.

7.2 Coriolis Terms – Spherical Vector Cross Product

The Coriolis terms are derived in this section. The angular velocity vector in spherical coordinates for spin along the polar axis is shown in equation 7.2-1.

$$\boldsymbol{\omega} = (\omega_{\hat{r}}, 0\hat{\theta}, 0\hat{\phi})_{Spherical} \quad 7.2-1$$

The map from Cartesian unit vectors to spherical unit vectors is shown in equation 7.2-2.

$$\begin{bmatrix} \cos \phi \sin \theta & \sin \phi \sin \theta & \cos \theta \\ \cos \phi \cos \theta & \cos \theta \sin \phi & -\sin \theta \\ -\sin \phi & \cos \phi & 0 \end{bmatrix}_{C \rightarrow S} \begin{pmatrix} \hat{x} \\ \hat{y} \\ \hat{z} \end{pmatrix} = \begin{pmatrix} \hat{r} \\ \hat{\theta} \\ \hat{\phi} \end{pmatrix} \quad 7.2-2$$

The map from spherical unit vectors to Cartesian unit vectors is shown in equation 7.2-3.

$$\begin{bmatrix} \cos \phi \sin \theta & \cos \phi \cos \theta & -\sin \phi \\ \sin \phi \sin \theta & \cos \theta \sin \phi & \cos \phi \\ \cos \theta & -\sin \theta & 0 \end{bmatrix}_{S \rightarrow C} \begin{pmatrix} \hat{r} \\ \hat{\theta} \\ \hat{\phi} \end{pmatrix} = \begin{pmatrix} \hat{x} \\ \hat{y} \\ \hat{z} \end{pmatrix} \quad 7.2-3$$

If the map 7.2-3, with θ and ϕ set equal to zero, operates on the vector 7.2-1, the spherical angular velocity unit vector is transformed into a Cartesian vector, and as expected, it is in the \hat{z} direction. In that coordinate transformation, the spherical radial magnitude is implicitly a function of the two angles. The angles appear in the transformation matrix.

$$\begin{bmatrix} 0 & 1 & 0 \\ 0 & 0 & 1 \\ 1 & 0 & 0 \end{bmatrix}_{S \rightarrow C} \begin{pmatrix} \omega_{\hat{r}} \\ 0 \\ 0 \end{pmatrix} = \begin{pmatrix} 0 \\ 0 \\ \omega_{\hat{z}} \end{pmatrix} \quad 7.2-4$$

Next, a “generic” velocity vector expressed in terms of spherical unit vectors is transformed into Cartesian coordinates.

$$\begin{aligned} & \begin{bmatrix} \cos \phi \sin \theta & \cos \phi \cos \theta & -\sin \phi \\ \sin \phi \sin \theta & \cos \theta \sin \phi & \cos \phi \\ \cos \theta & -\sin \theta & 0 \end{bmatrix}_{S \rightarrow C} \begin{pmatrix} V_{\hat{r}} \\ V_{\hat{\theta}} \\ V_{\hat{\phi}} \end{pmatrix} = & 7.2-5 \\ & \begin{bmatrix} V_{\hat{\theta}} \cos \phi \cos \theta - V_{\hat{\phi}} \sin \phi + V_{\hat{r}} \cos \phi \sin \theta \\ V_{\hat{\phi}} \cos \phi + V_{\hat{\theta}} \cos \theta \sin \phi + V_{\hat{r}} \sin \phi \sin \theta \\ V_{\hat{r}} \cos \theta - V_{\hat{\theta}} \sin \theta \end{bmatrix}_C = \begin{pmatrix} V_{\hat{x}} \\ V_{\hat{y}} \\ V_{\hat{z}} \end{pmatrix} \end{aligned}$$

If the right hand side of 7.2-4 is crossed with the right hand side of 7.2-5, the result is in Cartesian coordinates on the right hand side of equation 7.2-6.

$$\begin{aligned} & 2 \begin{pmatrix} 0 \\ 0 \\ \omega_{\hat{z}} \end{pmatrix}_C \times \begin{pmatrix} V_{\hat{\theta}} \cos \phi \cos \theta - V_{\hat{\phi}} \sin \phi + V_{\hat{r}} \cos \phi \sin \theta \\ V_{\hat{\phi}} \cos \phi + V_{\hat{\theta}} \cos \theta \sin \phi + V_{\hat{r}} \sin \phi \sin \theta \\ V_{\hat{r}} \cos \theta - V_{\hat{\theta}} \sin \theta \end{pmatrix}_C & 7.2-6 \\ & = 2 \omega \begin{pmatrix} -V_{\hat{\phi}} \cos \phi - V_{\hat{\theta}} \cos \theta \sin \phi - V_{\hat{r}} \sin \theta \sin \phi \\ V_{\hat{\theta}} \cos \theta \cos \phi + V_{\hat{r}} \cos \phi \sin \theta - V_{\hat{\phi}} \sin \phi \\ 0 \end{pmatrix}_C \end{aligned}$$

Finally, using map 7.2-2, the right hand side of equation 7.2-6 is transformed into spherical unit vectors as shown in expression 7.2-7. The Coriolis components of equation (4.4-5) are shown again as equation 7.2-8.

$$2 \omega \begin{pmatrix} -V_{\hat{\phi}} \sin \theta \\ -V_{\hat{\phi}} \cos \theta \\ V_{\hat{\theta}} \cos \theta + V_{\hat{\theta}} \sin \theta \end{pmatrix} \quad 7.2-7$$

$$\begin{pmatrix} a_{\hat{r}} \\ a_{\hat{\theta}} \\ a_{\hat{\phi}} \end{pmatrix} = 2 \omega \begin{pmatrix} -v_{\hat{\phi}} \sin \theta \\ -v_{\hat{\phi}} \cos \theta \\ v_{\hat{r}} \sin \theta + v_{\hat{\theta}} \cos \theta \end{pmatrix} \quad 7.2-8$$

Figure 7.2-1 shows output from a symbolic processor that was used to verify the results of equation 7.2-8.

```

cs[θ_, φ_] := {{Sin[θ] * Cos[φ], Sin[θ] * Sin[φ], Cos[θ]},
  {Cos[θ] * Cos[φ], Cos[θ] * Sin[φ], -Sin[θ]}, {-Sin[φ], Cos[φ], 0}}

MatrixForm[cs[θ, φ]]

$$\begin{pmatrix} \cos[\phi] \sin[\theta] & \sin[\theta] \sin[\phi] & \cos[\theta] \\ \cos[\theta] \cos[\phi] & \cos[\theta] \sin[\phi] & -\sin[\theta] \\ -\sin[\phi] & \cos[\phi] & 0 \end{pmatrix}$$


sc[θ_, φ_] := {{Sin[θ] * Cos[φ], Cos[θ] * Cos[φ], -Sin[φ]},
  {Sin[θ] * Sin[φ], Cos[θ] * Sin[φ], Cos[φ]}, {Cos[θ], -Sin[θ], 0}}

MatrixForm[sc[θ, φ]]

$$\begin{pmatrix} \cos[\phi] \sin[\theta] & \cos[\theta] \cos[\phi] & -\sin[\phi] \\ \sin[\theta] \sin[\phi] & \cos[\theta] \sin[\phi] & \cos[\phi] \\ \cos[\theta] & -\sin[\theta] & 0 \end{pmatrix}$$


lvs := {{Vr}, {Vθ}, {Vφ}}

sc[0, 0].{ω, 0, 0}
{0, 0, ω}

sc[θ, φ].lvs
{{Vθ Cos[θ] Cos[φ] + Vr Cos[φ] Sin[θ] - Vφ Sin[φ]},
 {Vφ Cos[φ] + Vθ Cos[θ] Sin[φ] + Vr Sin[θ] Sin[φ]}, {Vr Cos[θ] - Vθ Sin[θ]}}

MatrixForm[
cp = Cross[{0, 0, ω}, {Vθ Cos[θ] Cos[φ] + Vr Cos[φ] Sin[θ] - Vφ Sin[φ],
  Vφ Cos[φ] + Vθ Cos[θ] Sin[φ] + Vr Sin[θ] Sin[φ], Vr Cos[θ] - Vθ Sin[θ]}]]

$$\begin{pmatrix} -V\phi \omega \cos[\phi] - V\theta \omega \cos[\theta] \sin[\phi] - Vr \omega \sin[\theta] \sin[\phi] \\ V\theta \omega \cos[\theta] \cos[\phi] + Vr \omega \cos[\phi] \sin[\theta] - V\phi \omega \sin[\phi] \\ 0 \end{pmatrix}$$


MatrixForm[Simplify[cs[θ, φ].cp]]

$$\begin{pmatrix} -V\phi \omega \sin[\theta] \\ -V\phi \omega \cos[\theta] \\ \omega (V\theta \cos[\theta] + Vr \sin[\theta]) \end{pmatrix}$$


```

Figure 7.2-1 Symbolic Processor Calculation - Coriolis Terms

7.3 Centrifugal Terms – Spherical Vector Cross Product

The centrifugal terms are derived in this section, with a starting point again the polar angular velocity in spherical coordinates, equation 7.3-1. Its transformation, using the same mapping as the previous section is equation 7.3-2.

$$\boldsymbol{\omega} = (\omega\hat{r}, 0\hat{\theta}, 0\hat{\phi})_{\text{spherical}} \quad 7.3-1$$

$$\boldsymbol{\omega} = \{\omega_{\hat{x}}, \omega_{\hat{y}}, \omega_{\hat{z}}\}_{\text{Cartesian}} \quad 7.3-2$$

The first term on the LHS of 7.3-3 is crossed with the Cartesian position vector that was written in terms of trigonometric functions of the spherical coordinates. This position vector is second term on the LHS of equation 7.3-3. The result of equation 7.3-3 is crossed again with the angular velocity vector and shown as equation 7.3-4. This result, still in Cartesian coordinates, is finally stated in terms of spherical unit vectors as shown as expression 7.3-5.

$$\begin{aligned} \omega\{0_{\hat{x}}, 0_{\hat{y}}, 1_{\hat{z}}\}_C \times r\{\sin\theta\cos\phi, \sin\theta\sin\phi, \cos\theta\}_C = & \quad 7.3-3 \\ r\omega(-\sin\theta\sin\phi, \cos\phi\sin\theta, 0) \end{aligned}$$

$$\begin{aligned} \omega\{0_{\hat{x}}, 0_{\hat{y}}, 1_{\hat{z}}\}_C \times r\omega\{-\sin\theta\sin\phi, \cos\phi\sin\theta, 0\} = & \quad 7.3-4 \\ -r\omega^2(\cos\phi\sin\theta, \sin\theta\sin\phi, 0) \end{aligned}$$

$$(-r\omega^2\sin^2\theta, -r\omega^2\cos\theta\sin\theta, 0) \quad 7.3-5$$

```

cs[θ_, φ_] := {{Sin[θ] * Cos[φ], Sin[θ] * Sin[φ], Cos[θ]},
  {Cos[θ] * Cos[φ], Cos[θ] * Sin[φ], -Sin[θ]}, {-Sin[φ], Cos[φ], 0}}

MatrixForm[cs[θ, φ]]

$$\begin{pmatrix} \text{Cos}[\phi] \text{Sin}[\theta] & \text{Sin}[\theta] \text{Sin}[\phi] & \text{Cos}[\theta] \\ \text{Cos}[\theta] \text{Cos}[\phi] & \text{Cos}[\theta] \text{Sin}[\phi] & -\text{Sin}[\theta] \\ -\text{Sin}[\phi] & \text{Cos}[\phi] & 0 \end{pmatrix}$$


sc[θ_, φ_] := {{Sin[θ] * Cos[φ], Cos[θ] * Cos[φ], -Sin[φ]},
  {Sin[θ] * Sin[φ], Cos[θ] * Sin[φ], Cos[φ]}, {Cos[θ], -Sin[θ], 0}}

MatrixForm[sc[θ, φ]]

$$\begin{pmatrix} \text{Cos}[\phi] \text{Sin}[\theta] & \text{Cos}[\theta] \text{Cos}[\phi] & -\text{Sin}[\phi] \\ \text{Sin}[\theta] \text{Sin}[\phi] & \text{Cos}[\theta] \text{Sin}[\phi] & \text{Cos}[\phi] \\ \text{Cos}[\theta] & -\text{Sin}[\theta] & 0 \end{pmatrix}$$


cp1 = Cross[ω {0, 0, 1}, r { Sin[θ] Cos[φ], Sin[θ] Sin[φ], Cos[θ]}]
{-r ω Sin[θ] Sin[φ], r ω Cos[φ] Sin[θ], 0}

cp2 = r ω^2 Cross[{0, 0, 1}, {-Sin[θ] Sin[φ], Cos[φ] Sin[θ], 0}]
{-r ω^2 Cos[φ] Sin[θ], -r ω^2 Sin[θ] Sin[φ], 0}

cs[θ, φ].cp2 // Simplify
{-r ω^2 Sin[θ]^2, -r ω^2 Cos[θ] Sin[θ], 0}

```

Figure 7.3-1 Symbolic Processor Calculation - Centrifugal Terms

Spherical coordinates, consisting of length, polar angle, and azimuthal angle, cannot be crossed using the determinant method of Cartesian coordinates. However, spherical quantities expressed in terms of unit vectors at a common origin with a Cartesian system, when mapped to Cartesian quantities, crossed, and then returned to spherical quantities, yield the correct result.

In section 4.4 the angular velocity in a Cartesian system was transformed into an angular velocity in the spherical system and cross products were computed. In this chapter, the

opposite approach was taken. Angular velocity in a spherical system was transformed into a Cartesian system, the cross products were computed and then transformed back to spherical coordinates; as expected, the outcomes were the same.

Ultimately, the vector mechanics approach of kinematics is more general. However, if the problem at hand were limited to spinning around a polar axis, then the simplified kinematic approach would be more algebraically efficient.

CHAPTER 8. THIN FILM MODEL

8.1 Introduction

Thin film models are the default method for analyzing fluid flow on a high-speed rotary bell. The starting point in its analyses is usually a “simple force balance” statement of centrifugal and viscous forces acting on a parcel of fluid that leads to an equation of motion. A more rigorous method is starting with the formalism of the Navier-Stokes equations and obtaining the same simplified equations through valid elimination of inconsequential forces. Elimination of inconsequential forces can be based on intuitive assumption, or more rigorously on an order of magnitude analysis. The typical assumptions include steady state, flow normal to the film is zero, axisymmetric flow, constant rotation rate and direction and fully developed flow. The benefit for starting with the formalism of the Navier-Stokes equations is for analyses to be the result of the processes using vocabulary and methods of developed science rather than experience. It is believed that engineering analyses should be as process driven as possible, although there are usually multiple methods of obtaining a solution. Each step has substantiation requirements that others may not have seen but may be easily learn.

8.2 Disk Model of Rotary Bell

The model of fluid flow on a disk, where the source is an infinite line coincident with the axis of rotation, and the flow on the disk extends to infinity, is best analyzed in a cylindrical coordinate system. This application can also be modeled in a spherical coordinate system with the polar angle set to pi, however, for this particular configuration, a cylindrical system seems natural.

In section (4.2), the terms that inertially described acceleration as observed in a rotating frame were developed. In section (4.3), the thin film approximation was derived. Equation (8.2-1) is the Navier-Stokes equation in the radial direction that includes terms that enable inertially correct observations in a rotating frame. It is a restatement of equation (4.6-1).

$$\begin{aligned} \rho \left(\frac{\partial v_r}{\partial t} + v_r \frac{\partial v_r}{\partial r} + \frac{v_\theta}{r} \frac{\partial v_r}{\partial \theta} - \frac{v_\theta^2}{r} + v_z \frac{\partial v_r}{\partial z} \right) & \quad 8.2-1 \\ = -\frac{\partial P}{\partial r} + \mu \left(\frac{\partial}{\partial r} \left(\frac{1}{r} \frac{\partial (rv_r)}{\partial r} \right) + \frac{1}{r^2} \frac{\partial^2 v_r}{\partial \theta^2} - \frac{2}{r^2} \frac{\partial v_\theta}{\partial \theta} + \frac{\partial^2 v_r}{\partial z^2} \right) \\ + \rho g_r + \rho 2\omega v_\theta + \rho r \omega^2 \end{aligned}$$

In the case of a high-speed rotary bell, the following assumptions simplify equation 8.2-1.

- Steady State
- Centrifugal force is \gg Coriolis force
- Gravity is neglected
- Pressure is constant ambient in the thin film
- Axisymmetric flow
- Fluid velocity normal to the disk is zero
- Flow is fully developed in the radial direction sufficiently far from origin

With these assumptions, equation 8.2-1 is reduced to a constant coefficient second order differential equation in z as shown in equation 8.2-2.

$$0 = \mu \left(\frac{\partial^2 v_r}{\partial z^2} \right) + \rho r \omega^2 \quad 8.2-2$$

Equation 8.2-2 is rewritten as equation 8.2-3 and has three constraints in the form of two boundary conditions and the volumetric flow, which is designated as Q . Equation 8.2-3 is the same equation derived by Sun et al [32].

$$\frac{\partial^2 v_r}{\partial z^2} = - \frac{\rho r \omega^2}{\mu} \quad 8.2-3$$

The boundary conditions and flow constraint are shown as equations 8.2-4 a-c. The boundary conditions are (a) no shear at the fluid air interface and (b) no slip of fluid on the disk surface. The flow constraint (c) requires the integrated radial fluid velocity over the height of the film at any radial position must be equal to Q .

$$\begin{aligned} \frac{\partial v_r}{\partial z} &= 0 \quad z = h \quad (a) \\ v_r &= 0 \quad z = 0 \quad (b) \\ Q &= \int_0^h 2\pi r v_r dz \quad r > 0 \quad (c) \end{aligned} \quad 8.2-4$$

If equation 8.2-3 is integrated twice and the two boundary conditions are applied, the result is equation 8.2-5. The film height “ h ” remains unknown.

$$v_r = \frac{\rho r \omega^2}{\mu} \left(hz - \frac{z^2}{2} \right) \quad 8.2-5$$

The film height is obtained by integrating the radial velocity over the height of the film at any radial position and setting the result equal to Q cubic meters per second, as shown in equation 8.2-6.

$$Q = \int_0^h 2\pi r \left(\frac{\rho r \omega^2}{\mu} \left(hz - \frac{z^2}{2} \right) \right) dz \quad 8.2-6$$

The result of integrating equation 8.2-6 is equation 8.2-7. It is the height of the film at any location on the disk greater than zero.

$$h = \sqrt[3]{\frac{Q3\mu}{2\pi\rho r^2\omega^2}} \quad 8.2-7$$

The tangential velocity is obtained from the tangential Navier-Stokes equation. Equation 4.6-2 is restated as equation 8.2-8.

$$\begin{aligned} \rho \left(\frac{\partial v_\theta}{\partial t} + v_r \frac{\partial v_\theta}{\partial r} + \frac{v_\theta}{r} \frac{\partial v_\theta}{\partial \theta} + \frac{v_r v_\theta}{r} + v_z \frac{\partial v_\theta}{\partial z} \right) & \quad 8.2-8 \\ = -\frac{1}{r} \frac{\partial P}{\partial \theta} + \mu \left(\frac{\partial}{\partial r} \left(\frac{1}{r} \frac{\partial (r v_\theta)}{\partial r} \right) + \frac{1}{r^2} \frac{\partial^2 v_\theta}{\partial \theta^2} + \frac{2}{r^2} \frac{\partial v_r}{\partial \theta} + \frac{\partial^2 v_\theta}{\partial z^2} \right) \\ + \rho g_\theta - \rho 2\omega v_r \end{aligned}$$

The following assumptions simplify equation 8.2-8. Often it is referred to as conservation of momentum in the tangential direction, or Navier-Stokes equation in the tangential direction.

- Steady State
- Gravity is neglected
- Pressure is constant ambient due to thin film
- Axisymmetric
- Velocity normal to the disk is zero
- Flow is fully developed in the radial direction sufficiently far from origin

With these assumptions, equation 8.2-8 can be reduced to a constant coefficient second order differential equation in z as shown in equation 8.2-9. This is the same equation obtained by Sun et al [32] using the method of freebody diagram.

$$0 = \mu \frac{\partial^2 v_\theta}{\partial z^2} - \rho 2\omega v_r \quad 8.2-9$$

Equation 8.2-9 is integrated twice with the no slip and no shear boundary conditions yielding equation 8.2-10 as the tangential velocity profile of the film on the disk.

$$v_\theta = \frac{\rho^2 r \omega^3}{12\mu^2} (4hz^3 - z^4 - 8h^3z) \quad 8.2-10$$

Equations 8.2-5, 8.2-7, and 8.2-10 define radial velocity, film thickness and tangential velocity on a high-speed rotary bell. Calculation of these quantities has importance since they lead to understanding fluid behavior. However, that importance extends further because at the periphery of the rotary bell, they are the “initial conditions” in an analysis of atomization.

8.3 Conical Model of Rotary Bell

An early publication by Hinze and Milborn [34] used a spherical coordinate system constrained to a constant polar angle as one of the simplifying assumptions. Their analysis was based on further simplifications of including only centrifugal and viscous forces. An alternative is starting with the Navier-Stokes equations and removing terms based on similar assumptions, or more rigorously, an order of magnitude analysis. In either case, results are the same; however, one path leaves a more detailed trail of teachable material. Equation 4.7-1 is restated here as equation 8.3-1, the radial momentum equation in spherical coordinates.

$$\begin{aligned}
 & \rho \left(\frac{\partial v_r}{\partial t} + v_r \frac{\partial v_r}{\partial r} + \frac{v_\theta}{r} \frac{\partial v_r}{\partial \theta} + \frac{v_\phi}{r \sin(\theta)} \frac{\partial v_r}{\partial \phi} - \frac{v_\theta^2 + v_\phi^2}{r} \right) = & 8.3-1 \\
 & - \frac{\partial P}{\partial r} + \mu \left(\frac{\partial}{\partial r} \left(\frac{1}{r^2} \frac{\partial}{\partial r} (r^2 v_r) \right) + \frac{1}{r^2 \sin(\theta)} \frac{\partial}{\partial \theta} \left(\sin(\theta) \frac{\partial v_r}{\partial \theta} \right) \right. \\
 & \left. + \frac{1}{r^2 \sin^2(\theta)} \frac{\partial^2 v_r}{\partial \phi^2} - \frac{2}{r^2 \sin(\theta)} \frac{\partial}{\partial \theta} (v_\theta \sin(\theta)) - \frac{2}{r^2 \sin(\theta)} \frac{\partial v_\phi}{\partial \phi} \right) + \rho \vec{a}_r \\
 & + \rho 2\omega v_\phi \sin \theta + \rho r \omega^2 \sin^2 \theta
 \end{aligned}$$

The following assumptions simplify equation 8.3-1, also known as the equation of conservation of momentum in the radial direction, or Navier-Stokes equation in the radial direction.

- Steady State
- Centrifugal force is \gg Coriolis force
- Gravity is neglected
- Pressure is constant ambient due to thin film
- Axisymmetric – all derivative with respect to azimuth angle are zero
- Velocity normal to the cone surface is zero
- Flow is fully developed in the radial direction sufficiently far from origin

- The sine of the polar angle to a point in the film is approximated as constant
- The radius from polar angle = 0 to a point in the film is approximated as constant
- Constant polar angle of β

With these assumptions, equation 8.3-1 reduced to a constant coefficient second order differential equation in z as shown in equation 8.3-2. This is the same equation obtained by Hinze and Milborn [34].

$$\frac{\partial^2 v_r}{r^2 \partial \theta^2} = -\frac{\rho r \omega^2}{\mu} \sin^2 \beta \quad 8.3-2$$

Equation 8.3-2 is integrated twice to obtain the radial velocity. However, unlike the case of the cylindrical coordinate disk, the film thickness normal to the cone is specified by two coordinates, whereas, in the case of a disk the only required dimension is in the z direction. The film thickness is specified by the product $r_s \theta_s$, where the subscript “s” refers to the air/fluid surface inside the cone. The boundary conditions used during integration of equation (8.3-2) are listed below; they include the no-slip at the cone surface and the no-shear at the air/fluid interface.

- $v_r|_{\theta_\Delta} = 0$
- $\frac{dv_r}{dz}|_{\theta_s r_s} = h$

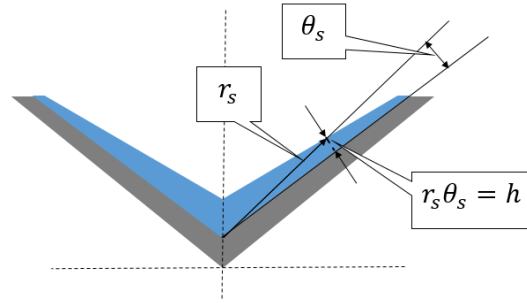


Figure 8.3-1 Air/Fluid Boundary Condition Location

Figure 8.3-1 shows the boundary location on the air-to-fluid surface where the shear is zero. This location is now the product of two dimensions since the thickness of the fluid cannot be written in the form of a single dimension, such as “z” in the cylindrical coordinate system.

Integration of equation 8.3-2 using the boundary conditions yields equation 8.3-3 for radial velocity of the flow inside the spinning cone.

$$v_r = \frac{\rho\omega^2 \sin^2 \beta}{\mu} \left(r_s^3 \theta_s \theta - r^3 \frac{\theta^2}{2} \right) \quad 8.3-3$$

If equation 8.3-3 is integrated over the height of the film and that result is set equal to Q, the actual film thickness, equation 8.3-4, can be obtained. It is assumed that the normal distance term, $r \sin \beta$, is constant over the film thickness

$$Q = \int_0^{\theta_s} 2\pi r \sin \beta \frac{\rho\omega^2 \sin^2 \beta}{\mu} \left(r_s^3 \theta_s \theta - r^3 \frac{\theta^2}{2} \right) r d\theta \quad 8.3-4$$

After integration, equation 8.3-4 yields equation 8.3-5. This equation is the film thickness at any point inside the spinning cone.

$$h = \sqrt[3]{\frac{Q3\mu}{2\pi\rho R^2\omega^2 \sin \beta}}$$

8.3-5

While arriving at equation 8.3-5, the following two relationships are used.

- $r_s^3 \theta_s^3 = h^3$
- $r \sin \beta = R$

In these relationships, “r” is in the direction of the coordinate “r”; however, “R” is normal to the axis of rotation and is the product of coordinate “r” and the sine of the cone half-angle β .

The disk solution and conical solutions merge when the spherical model has a polar angle of 90 degrees. In Hinze and Milborn’s article, the tangential velocity was not calculated; on the other hand, Sun et al did calculate the tangential velocity from the Coriolis force. However, Sun et al decoupled the equations although that is not necessary for an analytical solution.

8.4 Spherical Model of Rotary Bell

Rotary bell atomizers are usually conical but some have a curved region usually near the periphery. Closed form solutions of the Navier-Stokes equations tend to be simpler if the boundaries follow coordinate axes. For example, a spinning disk has a surface where z equals zero, or in spherical coordinates, a polar angle equal to 90 degrees. A conical bell has a constant polar angle, typically around 60 degrees. Published analyses of cones and disk are common, likely due to their presence in many industrial processes. Yang et al published an article on spinning a photoresist onto concave mirrors [80]. In which, the boundary followed a constant radius in a spherical coordinate system. In fact, rotary bells with profiles that seem to be described by a “function” rather than a coordinate axis are common; however, not as much literature exists on them as compared to simpler conical and disk geometries. Nomenclature introduced in this chapter is defined in Figure 8.4-1.

In this section, a spherical coordinate system continues to be the framework of the analysis. The difference in this case is that the radius will be held constant and equations similar to the disk and cone will be developed. Unlike the disk and cone where the analysis can extend infinitely in the direction of the radial coordinate, extending a constant radius forms a circular path. Moreover, if the angle of the bell surface is at 90 degrees, or the surface normal is perpendicular to the axis of rotation a singularity would exist. Therefore, the modeled spherical surface should not extend near this limit, or the results will be erroneous.

Another unique consequence of a spherical bell is the establishment of a minimum film thickness point. This point is found from the location where the derivative of the film thickness with respect to the polar angle is zero. Fluid entering the bell from the center proceeds towards the periphery while the film thickness decreases until it attains a location

of the minimum. After this minimum, the film thickness increases until the flow arrives at the periphery of the bell.

Previously, the radial Navier-Stokes equation was used for deriving an equation for fluid velocity in the radial direction, where the radial direction is defined as flow from the center of the bell to the periphery. In the case of a spherical bell, the polar angle would also be in the “radial direction”, i.e. direction of flow is from center to periphery. The Navier-Stokes equation for the polar direction is restated here as equation 8.4-1 and was previously introduced as equation 4.7-2.

$$\rho \left(\frac{\partial v_\theta}{\partial t} + v_r \frac{\partial v_\theta}{\partial r} + \frac{v_\theta}{r} \frac{\partial v_\theta}{\partial \theta} + \frac{v_\phi}{r \sin(\theta)} \frac{\partial v_\theta}{\partial \phi} + \frac{v_r v_\theta}{r} - \frac{v_\phi^2 \cot(\theta)}{r} \right) = \quad 8.4-1$$

$$- \frac{1}{r} \frac{\partial P}{\partial \theta} + \mu \left(\frac{1}{r^2} \frac{\partial}{\partial r} \left(r^2 \frac{\partial v_\theta}{\partial r} \right) + \frac{1}{r^2} \frac{\partial}{\partial \theta} \left(\frac{1}{\sin(\theta)} \frac{\partial}{\partial \theta} (v_\theta \sin(\theta)) \right) \right)$$

$$+ \frac{1}{r^2 \sin^2(\theta)} \frac{\partial^2 v_\theta}{\partial \phi^2} + \frac{2}{r^2} \frac{\partial v_r}{\partial \theta} - \frac{2 \cot(\theta)}{r^2 \sin(\theta)} \frac{\partial v_\phi}{\partial \phi} \Big) + \rho \vec{a}_\theta$$

$$+ \rho 2\omega v_\phi \cos \theta + \rho r \omega^2 \cos \theta \sin \theta$$

The following assumptions simplify equation 8.4-1. It is the equation for conservation of momentum in the polar direction, or Navier-Stokes equation in the polar direction.

- Steady State
- Centrifugal force is \gg Coriolis force
- Gravity is neglected
- Pressure is constant ambient due to thin film
- Axisymmetric – all derivative with respect to azimuth angle are zero
- Velocity normal to the cone (v_r) surface is zero
- Flow is fully developed in the polar (radial) direction sufficiently far from origin
- The radius from the origin to a point in the film is approximated as constant
- The radius from axis of rotation to a point in the film is approximated as constant
- Constant bell radius \mathcal{R}

The simplified equation for conservation of momentum in the polar angle direction is equation 8.4-2.

$$-\frac{\rho r \omega^2}{\mu} \cos \theta \sin \theta = \frac{\partial^2 v_\theta}{\partial r^2} \quad 8.4-2$$

In equation 8.4-2, the angle used to resolve the centrifugal force vector into components that are parallel to the fluid flow and normal to the surface of the bell varies with the position. This is a departure from previous bell analyses where the centrifugal force vector varied in magnitude, though not direction. In the case of a constant radius analysis, the magnitude and direction vary. In Figure 8.4-1, the centrifugal component of the left hand side of equation 8.4-2 depends on the perpendicular distance, R , from the spin axis as shown by equation 8.4-3. The perpendicular distance from the axis of spin, R , is the common location that enables single variable analysis of the various thin film geometries.

$$\frac{\rho r \omega^2}{\mu} \cos \theta \sin \theta = R \frac{\rho \omega^2}{\mu} \cos \theta \quad 8.4-3$$

Furthermore, the cosine term can be removed from equation (8.4-3) since the cosine of the polar angle can be expressed as the adjacent side divided by the hypotenuse \mathcal{R} .

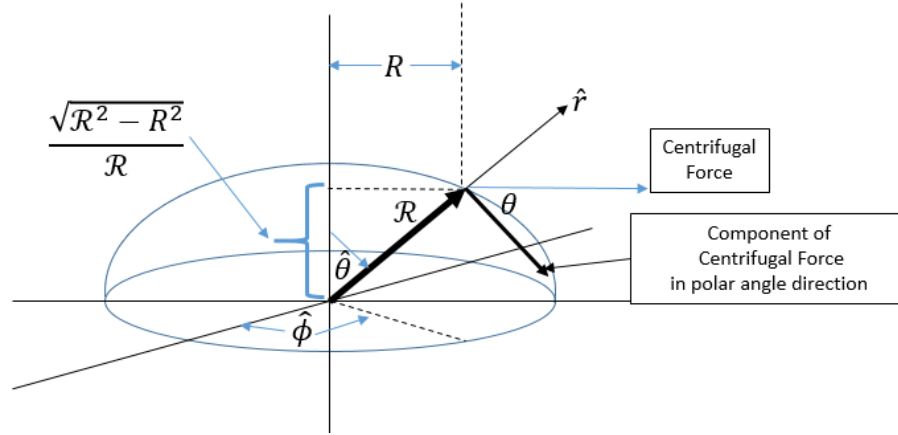


Figure 8.4-1 Spherical bell analysis

The cosine term from equation 8.4-3 was replaced with an expression that is a function of the distance from the axis of rotation and the radius of the bell. This result is substituted into equation 8.4-2, the final form of which is equation 8.4-4.

$$-\frac{\rho}{\mu}\omega^2 R \frac{(\mathcal{R}^2 - R^2)^{1/2}}{\mathcal{R}} = \frac{\partial^2 v_\theta}{\partial r^2} \quad 8.4-4$$

After integrating equation 8.4-4 and applying the no slip condition at the bell surface and the no shear condition at the fluid air interface, equation 8.4-5 for the velocity in the polar angle direction is obtained.

$$v_r = \frac{\rho \mathcal{R} \omega^2 (\mathcal{R}^2 - R^2)^{1/2}}{\mu \mathcal{R}} \left(hr - \frac{r^2}{2} \right) \quad 8.4-5$$

Equation 8.4-5 is similar to other equations for fluid velocity in the direction parallel to the bell surface. In the spherical case, the radial dimension is normal to the surface of the bell.

However, the fluid flows “radially” outward from the theoretical line source at the center of spin towards the periphery of the bell

8.5 Non-Dimensional Forms

Equations 8.2-3, 8.4-4, and 8.3-2 are restated together as equations 8.5-1 through 8.5-3 for establishing physical similarity, they were derived in the cylindrical and spherical coordinate systems. Equation 8.5-1 was derived in a cylindrical coordinate system and represents conservation of momentum in the radial direction. Equation 8.5-2 was derived in a spherical system and also represents conservation of momentum in the radial direction, but in this case, the radial dimension is at a constant polar angle other than 90 degrees. In

$$\frac{\partial^2 v_r}{\partial z^2} = -\frac{\rho\omega^2}{\mu} r \quad 8.5-1$$

$$\frac{\partial^2 v_r}{r^2 \partial \theta^2} = -\frac{\rho\omega^2}{\mu} r \sin^2 \beta \quad 8.5-2$$

$$\frac{\partial^2 v_\theta}{\partial r^2} = -\frac{\rho\omega^2}{\mu} R \frac{(\mathcal{R}^2 - R^2)^{1/2}}{\mathcal{R}} \quad 8.5-3$$

the spherical system, a polar angle of 90 degrees is equivalent to a cylindrical coordinate system. Finally, equation 8.5-3 is also in a spherical coordinates, but it has a constant radius instead of a constant polar angle. A constant radius surface has not been as present in the literature as often as the other configurations, possibly due to not providing any “industrial advantage” over the disk or cone implementation of processes that exploit

$$\left(\begin{array}{c} \text{Approximate} \\ \text{Curvature of} \\ \text{Rossby Number} \end{array} \right) = - \left(\begin{array}{c} \text{Reynolds} \\ \text{Number} \end{array} \right) \times \left(\begin{array}{c} \text{Geometric} \\ \text{Factor} \end{array} \right) \quad 8.5-4$$

spinning thin film properties. Equation 8.5-4 shows a generic non-dimensional form of the equation for fluid velocity in a direction from the centerline source to the periphery of a spinning bell.

To apply the principle of equation 8.5-4 to equation 8.5-1, multiply both side of 8.5-1 by $\mathcal{R}^2/\mathcal{R}\omega$, as shown in equation 8.5-5. In this case, script “R”, \mathcal{R} , is the perpendicular distance from the rotation axis to the periphery.

$$\frac{\partial^2 \frac{v_r}{\mathcal{R}\omega}}{\partial \left(\frac{z}{\mathcal{R}}\right)^2} = \frac{\partial^2 Ro}{\partial z'^2} = -Re = -\frac{\rho (\mathcal{R}\omega) r}{\mu} = -\frac{\rho \omega^2}{\mu} r \frac{\mathcal{R}^2}{\mathcal{R}\omega} \quad 8.5-5$$

Equation 8.5-5 can be simplified by removing of terms that were included to illustrate the sequential derivation. The variable “r” is the radial dimension of a cylindrical coordinate system and is also perpendicular to the rotation axis. It is also equal to “R”, or the perpendicular distance from the rotation axis to a point in the fluid film in any coordinate system.

$$\frac{\partial^2 Ro}{\partial z'^2} = -Re \quad 8.5-6$$

The same non-dimensional transformation is applied to equation 8.5-2. In this case, there is the presence of the half angle of the conical geometry, $\sin^2(\beta)$. A significant difference from the cylindrical case is that the variable “r” is no longer perpendicular to the rotation axis; however, the quantity, $R = r \sin \beta$, is perpendicular. Equations 8.5-7, 8.5-8, and 8.5-9 show a result similar to equation (8.5-6), but with geometry factor that accounts for the conical profile.

$$\frac{\partial^2 \frac{v_r}{\mathcal{R}\omega}}{\partial \left(\frac{r\theta}{\mathcal{R}}\right)^2} = \frac{\partial^2 Ro}{\partial \theta'^2} = -\frac{\rho (\mathcal{R}\omega) (r \sin \beta)}{\mu} \sin \beta \quad 8.5-7$$

$$\frac{\partial^2 Ro}{\partial \theta'^2} = -\frac{\rho (\mathcal{R}\omega) (r \sin \beta)}{\mu} \sin \beta \quad 8.5-8$$

$$\frac{\partial^2 Ro}{\partial \theta'^2} = -Re \sin \beta \quad 8.5-9$$

In a spherical coordinate system, a surface of revolution can be obtained by sweeping a line of constant polar angle, or a curve of constant radius. The profile generated by a

constant radius has the property of a changing tangent vector as a function of "R", which is the perpendicular distance from the axis of rotation. The procedure applied to equation (8.5-3) is shown in equation 8.5-10.

$$\frac{\partial^2 \frac{v_\theta}{R\omega}}{\partial \left(\frac{r}{R}\right)^2} = \frac{\partial^2 Ro}{\partial r'^2} = -\frac{\rho\omega^2 R}{\mu} \left(\frac{R}{\omega}\right) \frac{(\mathcal{R}^2 - R^2)^{1/2}}{\mathcal{R}} \quad 8.5-10$$

The terms on the right hand side of equation (8.5-11) form a Reynolds number and a geometric term that accounts for the changing tangent of the bell surface.

$$\frac{\partial^2 \frac{v_\theta}{R\omega}}{\partial \left(\frac{r}{R}\right)^2} = \frac{\partial^2 Ro}{\partial r'^2} = -\frac{\rho \mathcal{R}\omega R}{\mu} \frac{(\mathcal{R}^2 - R^2)^{1/2}}{\mathcal{R}} \quad 8.5-11$$

Equation (8.5-12) is the final form.

$$\frac{\partial^2 Ro}{\partial r'^2} = -Re \frac{(\mathcal{R}^2 - R^2)^{1/2}}{\mathcal{R}} \quad 8.5-12$$

All three cases follow the same pattern as proposed in equation 8.5-4. The second derivative, or approximate curvature, of the Rossby number is equal to a negative of a Reynolds number. The most compact form is equation 8.5-13 where Γ is a geometric factor that depends on the shape of the bell. It could have been included in a modified Reynolds number, however in this form the shape of the velocity profile becomes intuitive based on the approximation of negative curvature and the no slip, no shear, boundary conditions.

$$Ro'' = f(Re, \Gamma) \quad 8.5-13$$

8.6 Coupled Differential Equations – Conical Model of Rotary Bell

The prior analyses of thin film rotary bells were based on simplifying assumptions that reduced the Navier-Stokes equations to second order ordinary differential equations and decoupled the centrifugal and Coriolis terms. In this section, the differential equations include coupled centrifugal and Coriolis terms. The analysis is still limited to inertial forces and viscous forces, however, the inertial forces in the radial equation have centrifugal and Coriolis contributions.

The form of the Navier-Stokes equations that includes the coupled centrifugal and Coriolis forces can be obtained by at least two methods. Both methods establish an inertially correct application of conservation of momentum as seen by the observer in a rotating coordinate system. In the first method, equation 8.6-1 is substituted into the non-rotating spherical Navier Stokes equations [59], [58]. In the second, the terms previously derived in equation 4.2-3 are included in the Navier-Stokes equations [86]. In equation 8.6-1, v'_ϕ is the velocity seen in the rotating coordinates.

$$v'_\phi = -v_\phi + \omega r \sin \beta \quad 8.6-1$$

The Navier-Stokes equation for the radial and tangential directions in a rotating spherical coordinate system as derived by Makarytchev et al [58] are shown as equations 8.6-2 a, b. If the terms of the equations are divided by ω^2 , at large values of omega, only the centrifugal and viscous terms remain. It is the same of that of Heinz and Milborn [34],

however, if the Coriolis terms are allowed to remain, the system of equations has multiple solution techniques, including a solution based on reduction of order.

$$-\omega^2 r \sin^2 \beta + 2v'_\phi \omega \sin \beta = \frac{v}{r^2} \frac{\partial^2 v_r}{\partial \theta^2} \quad (a) \quad 8.6-2$$

$$2v_r \omega \sin \beta = -\frac{v}{r^2} \frac{\partial^2 v'_\phi}{\partial \theta^2} \quad (b)$$

At large values of omega, these equations degenerate into two separate ordinary differential equations with one for radial velocity and the other for tangential velocity. The “Greenspan” formulation of the same equations is shown as equations (8.6-3 a, b).

$$-r\omega^2 \sin^2 \beta - 2\omega v_\phi \sin \beta = \frac{v}{r^2} \frac{\partial^2 v_r}{\partial \theta^2} \quad (a) \quad 8.6-3$$

$$\rho 2\omega v_r \sin \beta = \frac{v}{r^2} \frac{\partial^2 v_\phi}{\partial \theta^2} \quad (b)$$

In equations 8.6-2 and 8.6-3, β , was the fixed half angle of the rotating cone. The dependent variables were velocity in the radial direction and velocity in the tangential direction. Although both equations were obtained from partial differential equations, the independent variable is the position in the film thickness that was defined as the product of radial position and angle.

Equations 8.6-2 and 8.6-3 can be non-dimensionalized by first dividing both equations by the centrifugal terms, which is the first term on the LHS of the (a) equations. Then the following substitutions, 8.6-4, 8.6-5, and 8.6-6, complete the non-dimensional process.

$$W = \frac{v'_\phi}{\omega r \sin(\beta)} \quad 8.6-4$$

$$U = \frac{v_r}{\omega r \sin(\beta)} \quad 8.6-5$$

$$\theta = -\frac{s}{r} \sqrt{\frac{v}{\omega r \sin(\beta)}} \quad 8.6-6$$

The non-dimensional forms of equations 8.6-2 and 8.6-3 are shown as equations 8.6-7 a, b and 8.6-8 a, b.

$$-1 + 2W = \frac{\partial^2 U}{\partial s^2} \quad (a) \quad 8.6-7$$

$$-2U = \frac{\partial^2 W}{\partial s^2} \quad (b)$$

$$-1 - 2W = \frac{\partial^2 U}{\partial s^2} \quad (a) \quad 8.6-8$$

$$2U = \frac{\partial^2 W}{\partial s^2} \quad (b)$$

The boundary conditions, no slip at the cone surface, and no shear at the air interface, are shown as equation 8.6-9 a, b.

$$U(s = 0) = W(s = 0) = 0 \quad (a) \quad 8.6-9$$

$$\left. \frac{dU}{ds} \right|_{s=s'} = \left. \frac{dW}{ds} \right|_{s=s'} = 0 \quad (b)$$

The subtle difference between equations 8.6-7 and 8.6-8 is the W term has an opposite sign. As it turns out, Makarytchev et al formulated the direction of the tangential velocity in the rotating frame as opposite in direction of the angular velocity. On the other hand, the

Greenspan formulation assumed all velocities are in the direction of positive unit vectors. The Greenspan formulation will result in a negative tangential velocity, thereby indicating the assumed direction was opposite of the actual direction. Both of these systems of equation are solvable by direct substitution. The second derivative of either equation readily accepts substitution of the other equation, the result of which is a fourth order ordinary differential equation and four boundary conditions.

Another solution method is found in Makarytchev et al [58]; Doerre and Nelson published details of this solution method [87]. First, multiply 8.6-7 b by $(-i)$ and add this to equation (8.6-7 a), yielding equation (8.6-10).

$$\frac{\partial^2 U}{\partial s^2} - i \frac{\partial^2 W}{\partial s^2} - i2U - 2W = -1 \quad 8.6-10$$

If the substitution $\Psi = U - iW$ is made in equation 8.6-10, it can be rewritten as equation (8.6-11), along with the no slip at s equal to zero, and no shear at the air interface, boundary conditions as shown by equations 8.6-12 a, b.

$$\frac{\partial^2 \Psi}{\partial s^2} - i2\Psi = -1 \quad 8.6-11$$

$$\Psi = (U + iW)|_{s=0} = 0 \quad (a) \quad 8.6-12$$

$$\frac{d\Psi}{ds} = \left(\frac{dU}{ds} + i \frac{dW}{ds} \right) \Big|_{s=s'} = 0 \quad (b)$$

Since the difference between the Makarytchev et al formulation and the Greenspan formulation is the assumed sign of the tangential velocity with the tangential velocity being

the imaginary component, intuitively, the complex conjugate could be a solution to the Greenspan formulation.

To prove this, first multiply equation 8.6-8 b by $+i$. Next, the “a” and “b” equations are added together, yielding equation 8.6-13.

$$\frac{\partial^2 U}{\partial s^2} + i \frac{\partial^2 W}{\partial s^2} - i2U + 2W = -1 \quad 8.6-13$$

Equation 8.6-13 can be simplified with substitution of $\Psi^* = U + iW$, which is the complex conjugate of the function substituted into the Makarytchev formulation. The boundary conditions in terms of U and W remain the same, though Ψ changes. The result is equation 8.6-14.

$$\frac{\partial^2 \Psi^*}{\partial s^2} - i2 \Psi^* = -1 \quad 8.6-14$$

The solutions of equation 8.6-11 and equation 8.6-14 have the same form; however, the tangential velocities are different. In the case of $\Psi = U - iW$, the velocities are found from equations 8.6-15 a, b.

$$v_r = \mathcal{R}e(\Psi) = \frac{\Psi + \bar{\Psi}}{2} = U \quad (a) \quad 8.6-15$$

$$v_\phi = \mathcal{I}m(\Psi) = \frac{\Psi - \bar{\Psi}}{2i} = -W \quad (b)$$

On the other hand, the velocities rendered by $\Psi^* = U + iW$, are shown as equations 8.6-16.

$$v_r = \mathcal{R}e(\Psi^*) = U \quad (a) \tag{8.6-16}$$

$$v_\phi = \mathcal{I}m(\Psi^*) = W \quad (b)$$

This proves that the complex conjugate of a solution to the Makarytchev formulation is a solution to the Greenspan formulation.

8.7 Discussion and Numerical Results

In this section, the simplified Navier-Stokes equations for rotating thin films are compared in three different configurations, including a disk, a cone and a partial hemisphere. The disk and cone configurations are common in the atomization literature. They are an approach for the theoretical study of fluid phenomena and include the real-world application in agricultural spraying. On the other hand, an example of rotating fluid in a partial hemispherical body was found in the coating of optical components[80]. The literature has many references to the study of fluid between nested rotating spheres.

Table 8.7-1 contains the equations of motion, radial velocity, and film thickness for spinning disks, cones, and partial hemispheres, all in vertical order. In order to build a degree of commonality among the configurations for film thickness, a nomenclature describing radial position was needed.

Table 8.7-1 Disk, Cone, and Hemisphere Film Characterization

Equation of Motion Radial	Radial Velocity	Film Thickness
$\mu \frac{\partial^2 v_r}{\partial z^2} = -\rho r \omega^2$	$v_r = \frac{\rho r \omega^2}{\mu} \left(h z - \frac{z^2}{2} \right)$	$h = \sqrt[3]{\frac{Q 3 \mu}{2 \pi \rho R^2 \omega^2}}$
$\frac{\partial^2 v_r}{r^2 \partial \theta^2} = \frac{-\rho r \omega^2}{\mu} \sin^2 \beta$	$v_r = \frac{\rho \omega^2 \sin^2 \beta}{\mu} \left(r_s^3 \theta_s \theta - r^3 \frac{\theta^2}{2} \right)$	$h = \sqrt[3]{\frac{Q 3 \mu}{2 \pi \rho R^2 \omega^2 \sin \beta}}$
$\frac{\partial^2 v_\theta}{\partial r^2} = -\frac{\rho}{\mu} \omega^2 R \frac{(\mathcal{R}^2 - R^2)^{1/2}}{\mathcal{R}}$	$v_r = \frac{\rho \mathcal{R} \omega^2 (\mathcal{R}^2 - R^2)^{1/2}}{\mu \mathcal{R}} \left(h \delta - \frac{\delta^2}{2} \right)$	$h = \sqrt[3]{\frac{Q 3 \mu \mathcal{R}}{2 \pi \rho R^2 \omega^2 (\mathcal{R}^2 - R^2)^{1/2}}}$

Table 8.7-1, column 3, contains three forms of “r”. The first is lower case “r” that signifies the radial coordinate in a cylindrical system, which is equal to a spherical coordinate system

with a 90° polar angle. The second is upper case “R” that signifies radial distance from the axis of rotation; in a spherical system with a polar angles less than 90° , this distance is $r \sin \beta$. The third form is an upper-case script “ \mathcal{R} ” that signifies the radius of the hemispherical bell. This brief explanation of nomenclature avoids confusion when working with papers from various authors.

Figure 8.7-1 is a plot of film thickness as a function of R. It is a typical operating point for

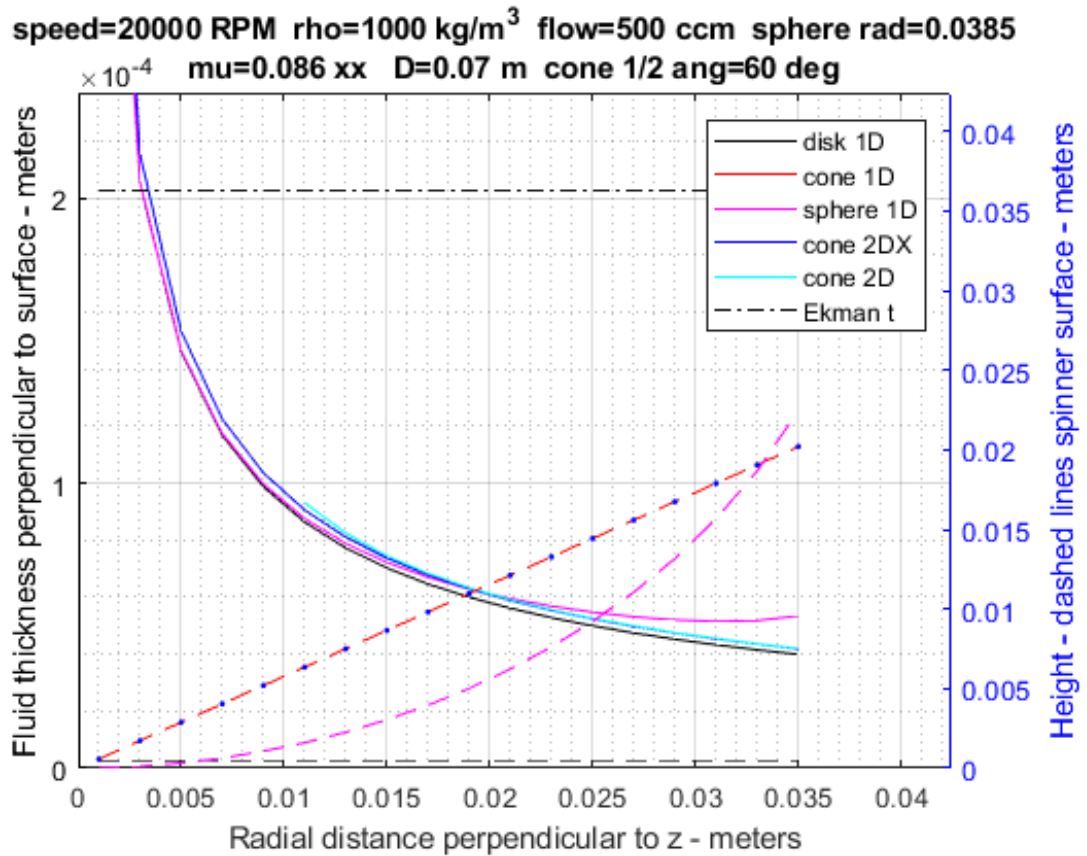


Figure 8.7-1 Film thickness vs R (distance from axis of rotation)

automotive painting and is for demonstration purposes only. The horizontal axis (abscissa) is the radial distance from the axis of rotation; the vertical axis is film thickness; all distances are in meters.

The dashed lines in the lower portion of the plot are the cross sections of the configuration, or the wetted surface of the bell. The black dashed line represents the disk; the red dashed line is the wetted surface of the cone; and the magenta dashed curved line is the wetted surface of the hemispherical bell.

The three closely spaced solid lines represent film thicknesses for different bells; however, at a certain distance the hemispherical bell indicates an increasing film thickness. This increase is because of the trigonometric relationship between viscous and centrifugal forces that changes as a function of position.

8.8 Reduction of order

The coupled Navier-Stokes equations that have been simplified to include only inertial and viscous forces have at least two solution methods. The first is a direct substitution of equations that yields a fourth order equation; the second method is a complex change of variables that enables a reduction from fourth order to second order. The connection between those solutions methods is covered in the remainder of this chapter.

Calculating a solution from either method is not difficult, however, the connection between the two is not immediately apparent and the papers that employ this solution method offered no apparent background on the derivation. As it turns out, the connection became relatively simple after sketching the roots of the characteristic equations in the complex plane and the observing the reflective property of two derivative operations.

Below are equations 8.6-7 and shown here as equations (8.8-1) for reference.

$$-1 + 2W = U'' \quad (a) \qquad 8.8-1$$

$$-2U = W'' \quad (b)$$

If either equation, both functions of s , is differentiated twice, then other equation can be used in a substitution for eliminating a dependent variable, either U or W . The result is shown as equations 8.8-2.

$$U'''' + 4U = 0 \quad (a) \qquad 8.8-2$$

$$W'''' + 4W = 2 \quad (b)$$

Equations 8.8-2 are constant coefficient ordinary differential equations that can be transformed into polynomial space with the substitution $e^{\alpha s}$ equal to $U(s)$ or $W(s)$. After

this substitution, the characteristic polynomial equation associated with either homogenous differential equation is equation 8.8-3.

$$\alpha^4 + 4 = 0 \quad 8.8-3$$

Figure 8.8-1 shows the roots of characteristic polynomial 8.8-3. The roots have a $\pm \pi/2$ rotational symmetry.

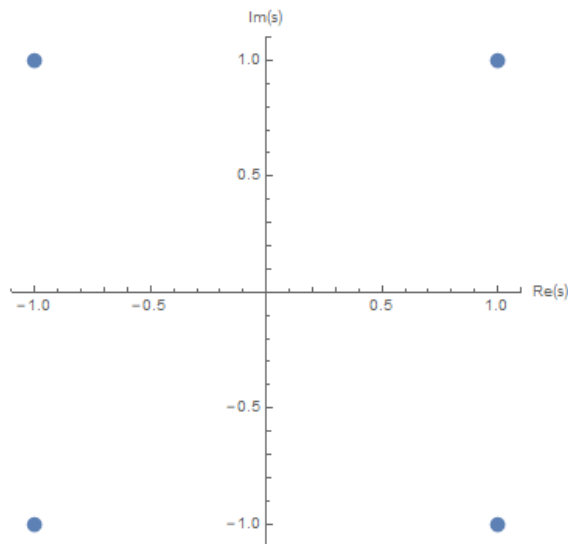


Figure 8.8-1 Complex Plane and roots of $\alpha^4 + 4 = 0$

The solution to the homogenous characteristic polynomial is equation 8.8-4.

$$U = Ae^{(1+i)s} + Be^{(1-i)s} + Ce^{(-1+i)s} + De^{(-1-i)s} \quad 8.8-4$$

Equation 8.8-1 (a) states that W is the second derivative of U , plus a constant term. The second derivative of equation 8.8-4, divided by 2, is shown as equation 8.8-5.

$$W = iAe^{(1+i)s} - iBe^{(1-i)s} - iCe^{(-1+i)s} + iDe^{(-1-i)s} + \frac{1}{2} \quad 8.8-5$$

When equation 8.8-5 is multiplied by i , then subtracted from U and the constants restated, the result is equation 8.8-6. Two of the roots are cancelled, indicating that the complex function $U - Wi$ is the solution of a second order equation.

$$U - Wi = C_1 e^{(1+i)s} + C_2 e^{(-1-i)s} - \frac{1}{2}i \quad 8.8-6$$

Indeed, if equation 8.8-6 is substituted into equation 8.6-11 and the operations are performed, it is verified as a solution. Differentiating equation 8.8-4 had the effect of multiplying the coefficients of the $\pm(1+i)$ roots by $\sqrt{2}e^{\frac{\pi}{4}i}$ and the $\pm(1-i)$ roots by $\sqrt{2}e^{-\frac{\pi}{4}i}$. A second differentiation had the effect of multiplying the coefficients of the $\pm(1+i)$ roots by $2e^{\frac{\pi}{2}i}$, or $2i$, and the $\pm(1-i)$ roots by $2e^{-\frac{\pi}{2}i}$, or $-2i$.

Visualizing these operations in terms of degrees, the A and D coefficients are scaled by $\sqrt{2}$ and rotated by plus 45° per differentiation, and the B and C coefficients are also scaled by $\sqrt{2}$ but rotated by minus 45° per differentiation. The factor of 2 is cancelled as shown in equation 8.8-5. Finally, when W is multiplied by i , or $e^{\frac{\pi}{2}i}$, the A and D coefficients are rotated to -1 , while the B and C coefficients are rotated back to their original value. Hence, A and D are preserved and B and C are cancelled after the subtraction operation.

In the system of equations 8.8-1, the radial velocity U or the tangential velocity W can be found by configuring a fourth order ordinary differential equation in terms of either, then differentiating that result to obtain the other. On the other hand, stating U and W as components of a complex function of s , a solution is obtained by solving a second order equation, i.e. a reduction of two orders.

8.9 Conclusion

Chapter 8 covered the mathematics of thin film flow and partial hemisphere spinners that have received sparse coverage in the literature. The “centrifugal only” radial momentum equation and “Coriolis only” momentum equation have very intuitive results obtained with non-dimensional numbers and predicting the correct curvature of the velocity profiles.

CHAPTER 9. CURVILINEAR MODEL

9.1 Introduction

This chapter is heavily influenced by works of researchers at the Lomonosov Moscow State University [55],[54],[71],[73] and builds mathematical tools needed to comprehend their elegant articles. Most vector mechanics problems encountered in the literature and academic education are framed in Cartesian, cylindrical or spherical coordinates. When a work deviates from these conventional references, an alternative is glossing over conclusions and foregoing the deeper understanding only found at the author's level of granularity. On the other hand, depending on the level of interest in an article and the level of expertise of a reader, a quick perusal is inadequate and a lengthy effort in learning is necessary. This chapter describes the latter.

The first article is an order of magnitude analysis applicable to fluid film on a spinning disk using a cylindrical coordinate system as the framework for analysis. The components of the Navier-Stokes equations were grouped by powers of $\delta = H_0\sqrt{\omega/\nu}$. The relative magnitudes of Navier-Stokes terms found in this example are assumed to scale with corresponding terms in other rotating orthogonal curvilinear coordinates systems. The assumption is considered applicable if the bell profile is a smooth blend of conical to concave profiles, however, the range of smoothness is not determined analytically but by visual similarity of hardware.

The second article by Mogilevskii and Shkadov [71] is one of the most definitive works on thin film formation in a concave spinning object. Unfortunately, for those that are new to this field and stumble upon it, the immediate observation is its Spartan wording and

seemingly cryptic formulation of the Navier-Stokes equations. As it turns out, the key to decrypting the mathematics is more mathematics. The three most important tools for comprehending their paper are, first, calculation of the metric tensor, second, calculating derivatives of unit vectors with respect to coordinate displacements, and third, and a most tedious task of constructing vector operators.

The next three sections of this chapter recreate the derivation of these three mathematical tools. The vector invariants are presented in two forms, first, as an operator, and second as an indicial notation equation. Although the indicial notation equations are easier to implement, they are also much more tedious to derive.

First, the continuity equation and several terms in the outward momentum equation found in Mogilevskii and Shkadov are derived. Once familiar with the methods, the paradigm shifts from exciting new learning to a procedural analysis that reveals the once seemingly cryptic formulation of the Navier-Stokes equations.

Finally, an approximation obtained from a pattern found in thin film modeling in more conventional coordinates is shown to be the most simplified case of the advanced formulation of Mogilevskii and Shkadov. This approximation is an excellent vehicle for understanding thin film formation on a rotary bell in a Production Engineering environment. On the other hand, the approximation is a shortcut and not extendable to more detailed analysis; moreover, it is further constrained to the simple boundary conditions of no slip and no shear. The article of Mogilevskii and Shkadov included pressure and kinematic boundary conditions of the free surface; this dissertation limits the boundary conditions to no slip and no shear. Furthermore, depending on location, a curved bell profile can yield a film that is increasing in thickness. Without going into the details,

increasing film thickness can most conveniently be described as a possible adverse condition. While this is an innocuous sounding statement, an analysis of transient fluid flow stability would displace and overshadow the subject matter found in this dissertation and spread into the discipline of numerical methods with dependencies on initial and boundary conditions, the subject of probably several dissertations and further research.

9.2 Order of Magnitude Analysis

This section contains a detailed recreation of work published by Sisoev et al [54]. Although it would be more convenient simply to cite the outcome of their work, it was felt that to appreciate the labor and contribution that went into the article and to learn new methods, the non-dimensional continuity equation and equations of motion had to be derived, thereby showing the many intermediate algebraic steps entailed in the analysis. Moreover, this dissertation may serve as a teaching guide for others that want to learn this material; tedious work and a few hints make the learning a bit more efficient and tolerable.

Equations describing fluid mechanics in rotating cylindrical and spherical coordinate systems have been developed in chapters four through eight using thin film, or lubrication theory, assumptions. In this section, an order of magnitude analysis analytically determines the relative influence of terms in the Navier-Stokes equations. The assumptions are an axisymmetric, body force free, steady state flow supplying a spinning disk. Two of these assumptions lead to neglect of derivatives of time and azimuthal angle.

This analysis is, in part, based on an article by Sisoev et al [54] that included nondimensional variables and changes of variables. However, the pressure term nondimensional variable was obtained from another article by Sisoev and Shkadov [55]. Although their analysis was in cylindrical coordinates on a spinning disk, as previously stated, the results are applicable to other bell profiles with similar geometry.

A ratio of variables integrated into other non-dimensional variables is defined by equation (9.2-1). This ratio, defined as δ , is dimensionless since H_0 has units of length and the combined terms under the root sign have units of $1/Length^2$.

$$\delta = H_0 \sqrt{\frac{\bar{\omega}}{\nu}} \quad 9.2-1$$

Three nondimensional velocities u, v, w are defined by equations 9.2-1 to 9.2-4. The LHS's of equations 9.2-2 through 9.2-4 have units of velocity, and the RHS's have a term of angular velocity multiplied by length, thus, creating non-dimensional variables.

$$u_r = \omega r \delta^2 u \quad 9.2-2$$

$$u_\theta = \omega r (1 + \delta^2 v) \quad 9.2-3$$

$$u_z = \omega H_0 \delta^2 w \quad 9.2-4$$

Equations 9.2-2 to 9.2-4 are in the directions of cylindrical coordinates as indicated by the subscripts. Using the kinematic substitution discussed in previous chapters, equation 9.2-3 accounts for observations in a rotating coordinate system. The pressure nondimensional variable is defined in equation 9.2-5.

$$p = p_n \rho \omega^2 H_0^2 \quad 9.2-5$$

Their article states the accuracy of the non-dimensional equations without consideration of boundary conditions; this accuracy is on the order $(H/r)^2$. However, where this information enters into the analysis is not obvious until the inclusion of a pressure term, which is also ultimately neglected. Combining elements of these two articles was the key to understanding the order of magnitude analysis.

Finally, the following changes of variables in r and z to nondimensional lengths are shown as equations 9.2-6 and 9.2-7.

$$x = \ln\left(\frac{r}{R}\right) \quad 9.2-6$$

$$y = \frac{z}{H_0} \quad 9.2-7$$

The cylindrical continuity equation from 4.3-1 is shown again as equation 9.2-8.

$$\frac{\partial \rho}{\partial t} + \frac{1}{r} \frac{\partial(\rho r v_r)}{\partial r} + \frac{1}{r} \frac{\partial(\rho v_\theta)}{\partial \theta} + \frac{\partial \rho v_z}{\partial z} = 0 \quad 9.2-8$$

If prior assumptions of axisymmetric, incompressible flow and steady state are applied, equation 9.2-8 reduces to equation 9.2-9.

$$\frac{1}{r} \frac{\partial}{\partial r} (r u_r) + \frac{\partial}{\partial z} (u_z) = 0 \quad 9.2-9$$

Several of the intermediate steps of substituting equations 9.2-1 to 9.2-4 into equation 9.2-9 are shown as equations 9.2-10 to 9.2-14. The intermediate steps are not accompanied with explanatory text and are shown to establish a chain of derivation common to the publications referenced in this chapter.

Equation 9.2-14 contains nondimensional velocities; however, r and z remain as

$$\frac{1}{r} \frac{\partial}{\partial r} (r \omega r \delta^2 u) + \frac{\partial}{\partial z} (\omega H_0 \delta^2 w) = 0 \quad 9.2-10$$

$$\omega \delta^2 \frac{1}{r} \frac{\partial}{\partial r} (r^2 u) + \omega H_0 \delta^2 \frac{\partial}{\partial z} (w) = 0 \quad 9.2-11$$

$$\omega \delta^2 \frac{1}{r} \frac{\partial}{\partial r} (r^2 u) + \omega H_0 \delta^2 \frac{\partial}{\partial z} (w) = 0 \quad 9.2-12$$

$$\frac{1}{r} \left(r^2 \frac{\partial u}{\partial r} + u 2r \right) + H_0 \frac{\partial w}{\partial z} = 0 \quad 9.2-13$$

$$r \frac{\partial u}{\partial r} + 2u + H_0 \frac{\partial w}{\partial z} = 0 \quad 9.2-14$$

dimensional numbers. They are transformed to nondimensional by substitution of forms

of equation 9.2-6 and 9.2-7. Equation 9.2-6 is differentiated with respect to r , yielding equation 9.2-15.

$$\frac{d}{dr}x = \frac{d}{dr}\ln(r) - \frac{d}{dr}\ln(R) \quad 9.2-15$$

The second term on the RHS of 9.2-15 is a constant; therefore, its derivative is equal to zero. Equation 9.2-16 shows the derivative operation completed.

$$\frac{dx}{dr} = \frac{1}{r} \quad 9.2-16$$

Equation 9.2-17 will be substituted into equation 9.2-14.

$$\frac{r}{dr} = \frac{1}{dx} \quad 9.2-17$$

Equation 9.2-18 is a differential form of equation 9.2-7. Its reciprocal is equation 9.2-19 and it will be substituted into equation 9.2-14 .

$$dy = \frac{dz}{H_0} \quad 9.2-18$$

$$\frac{1}{dy} = \frac{H_0}{dz} \quad 9.2-19$$

After equations 9.2-17 and 9.2-19 are substituted into equation 9.2-14, equation 9.2-20 is obtained; it is the continuity equation of Sisoiev et al defined by nondimensional velocities and lengths.

$$\frac{\partial u}{\partial x} + 2u + \frac{\partial w}{\partial y} = 0 \quad 9.2-20$$

As previously mentioned, the Navier-Stokes equations can be “inertially corrected” by the method used in deriving equations 4.6-1 to 4.6-3 and 4.7-1 to 4.7-3, or by a kinematic substitution into the azimuthal velocity that includes absolute angular velocity of the spinning bell and radial position perpendicular to the axis of rotation [87].

The radial Navier-Stokes equation for a stationary cylindrical coordinate system is shown in equation 9.2-21.

$$\rho \left(\frac{\partial u_r}{\partial t} + u_r \frac{\partial u_r}{\partial r} + \frac{u_\theta}{r} \frac{\partial u_r}{\partial \theta} - \frac{u_\theta^2}{r} + u_z \frac{\partial u_r}{\partial z} + \right) = \quad 9.2-21$$

$$-\frac{\partial p}{\partial r} + \mu \left[\frac{\partial}{\partial r} \left(\frac{1}{r} \frac{\partial}{\partial r} (r u_r) \right) + \frac{1}{r^2} \frac{\partial^2 u_r}{\partial \theta^2} - \frac{2}{r^2} \frac{\partial u_\theta}{\partial \theta} + \frac{\partial^2 u_r}{\partial z^2} \right] + F_r$$

If the three simplifying assumptions of no body force, steady state, and azimuthal symmetry are applied, equation 9.2-21 simplifies to equation 9.2-22.

$$\rho \left(u_r \frac{\partial u_r}{\partial r} - \frac{u_\theta^2}{r} + u_z \frac{\partial u_r}{\partial z} + \right) = -\frac{\partial p}{\partial r} + \mu \left[\frac{\partial}{\partial r} \left(\frac{1}{r} \frac{\partial}{\partial r} (r u_r) \right) + \frac{\partial^2 u_r}{\partial z^2} \right] \quad 9.2-22$$

For reasons related to the previous mention of accuracy to $(H/r)^2$, the first two terms on the RHS of equation 9.2-22 are temporarily ignored, leaving equation 9.2-23.

$$u_r \frac{\partial u_r}{\partial r} - \frac{u_\theta^2}{r} - u_z \frac{\partial u_r}{\partial z} = \frac{\mu}{\rho} \frac{\partial^2 u_r}{\partial z^2} \quad 9.2-23$$

Equations 9.2-2 to 9.2-4, 9.2-17, and 9.2-19 are substituted into equation 9.2-23 yielding a nondimensional but inertially-correct momentum equation in the radial direction. To understand fully what these researchers accomplished, one must “do the math”. The first term in equation 9.2-23 is partially nondimensionalized as shown in the following steps indicated by equations 9.2-24 to 9.2-28.

$$u_r \frac{\partial u_r}{\partial r} = \omega r \delta^2 u \frac{\partial(\omega r \delta^2 u)}{\partial r} \quad 9.2-24$$

$$= \omega^2 r \delta^4 u \frac{\partial(r u)}{\partial r} \quad 9.2-25$$

$$= \omega^2 r \delta^4 u \left[r \frac{\partial u}{\partial r} + u \right] \quad 9.2-26$$

$$= \omega^2 \delta^4 r \left[u r \frac{\partial u}{\partial r} + u^2 \right] \quad 9.2-27$$

$$= \delta^4 \omega^2 r \left[u \frac{\partial u}{\partial x} + u^2 \right] \quad 9.2-28$$

The next term in equation 9.2-23 will be transformed into partial nondimensional form as shown by equations 9.2-29 to 9.2-30.

$$\frac{u_\theta^2}{r} = \frac{(\omega r + \omega r \delta^2 v)^2}{r} \quad 9.2-29$$

$$= \omega^2 r (1 + 2\delta^2 v + \delta^4 v^2) \quad 9.2-30$$

The third term in equation 9.2-23 will be transformed into partial nondimensional form as shown by equations 9.2-31 to 9.2-33.

$$u_z \frac{\partial u_r}{\partial z} = \omega H_0 \delta^2 w \frac{\partial(\omega r \delta^2 u)}{\partial z} \quad 9.2-31$$

$$= \delta^4 \omega^2 r w H_0 \frac{\partial u}{\partial z} \quad 9.2-32$$

$$= \delta^4 \omega^2 r w \frac{\partial u}{\partial y} \quad 9.2-33$$

Finally, the term on the right hand side of equation 9.2-23 will be transformed into partial nondimensional form as shown by equations 9.2-34 to 9.2-36.

$$\frac{\mu}{\rho} \frac{\partial^2 u_r}{\partial z^2} = \frac{\mu}{\rho} \frac{\omega r \delta^2}{H_0^2} \frac{\partial^2 u}{\partial y^2} \quad 9.2-34$$

$$= \frac{\mu}{\rho} \frac{\omega r}{H_0^2} \frac{\omega H_0^2}{v} \frac{\partial^2 u}{\partial y^2} \quad 9.2-35$$

$$= \omega^2 r \frac{\partial^2 u}{\partial y^2} \quad 9.2-36$$

If equations 9.2-28, 9.2-30, 9.2-33, and 9.2-36 are combined into a partial nondimensional version of equation 9.2-23, the result is equation 9.2-37.

$$\delta^4 \omega^2 r \left[u \frac{\partial u}{\partial x} + u^2 \right] - (\omega^2 r (1 + 2\delta^2 v + \delta^4 v^2)) + \delta^4 \omega^2 r w \frac{\partial u}{\partial y} = \omega^2 r \frac{\partial^2 u}{\partial y^2} \quad 9.2-37$$

If the term $\omega^2 r$ is divided out of each term, the result is equation 9.2-38.

$$\frac{\partial^2 u}{\partial y^2} + 1 + \delta^2 2v - \delta^4 \left[u \frac{\partial u}{\partial x} + w \frac{\partial u}{\partial y} + u^2 - v^2 \right] = 0 \quad 9.2-38$$

If a similar process is applied to the θ momentum equation, the result is shown in equation 9.2-39.

$$\frac{\partial^2 v}{\partial y^2} - \delta^2 2u - \delta^4 \left[u \frac{\partial v}{\partial x} + w \frac{\partial v}{\partial y} + 2uv \right] = 0 \quad 9.2-39$$

The continuity equation, 9.2-23, the radial momentum equation, 9.2-38, and the azimuthal momentum equation, 9.2-39, are the nondimensional equations obtained by Sisoiev et al [54]. They are repeated altogether as equations 9.2-40 to 9.2-42.

$$\frac{\partial u}{\partial x} + 2u + \frac{\partial w}{\partial y} = 0 \quad 9.2-40$$

$$\frac{\partial^2 u}{\partial y^2} + 1 + \delta^2 2v - \delta^4 \left[u \frac{\partial u}{\partial x} + w \frac{\partial u}{\partial y} + u^2 - v^2 \right] = 0 \quad 9.2-41$$

$$\frac{\partial^2 v}{\partial y^2} - \delta^2 2u - \delta^4 \left[u \frac{\partial v}{\partial x} + w \frac{\partial v}{\partial y} + 2uv \right] = 0 \quad 9.2-42$$

In these equations, if terms of δ^2 and higher are neglected, then the analyses of Hinze and Milborn [34], and Sun [32] are obtained. In Sisoiev et al, the authors mentioned the accuracy of equations 9.2-40 to 9.2-42 is of the order $(H_0/r)^2$ without considering boundary conditions, however, this is not obvious until the two terms of equation 9.2-22 that were temporarily ignored are reconsidered.

First, the pressure term of equation 9.2-22 is recast into a partial nondimensional form using equation 9.2-5 and shown as equation 9.2-43.

$$\frac{1}{\rho} \frac{\partial p}{\partial r} = \frac{1}{\rho} \frac{\partial (p_n \rho \omega^2 H_0^2)}{\partial r} \quad 9.2-43$$

A form of equation 9.2-17 is substituted into 9.2-43 yielding expression 9.2-44.

$$= \frac{\omega^2 H_0^2}{r} \frac{\partial p_n}{\partial x} \quad 9.2-44$$

The second term on the RHS of equation 9.2-22 is cast into a partial nondimensional form as shown by equation 9.2-45.

$$\frac{\mu}{\rho} \frac{\partial}{\partial r} \left(\frac{1}{r} \frac{\partial (r u_r)}{\partial r} \right) = \frac{\mu}{\rho} \frac{\partial}{\partial r} \left(\frac{1}{r} \frac{\partial (r \omega r \delta^2 u)}{\partial r} \right) \quad 9.2-45$$

The steps that lead to the final form of 9.2-45 are shown as expressions 9.2-46 to 9.2-50.

It is implied these are equal to the LHS of 9.2-45.

$$= \frac{\mu}{\rho} \omega \delta^2 \frac{\partial}{\partial r} \left(\frac{1}{r} \frac{\partial (r^2 u)}{\partial r} \right) \quad 9.2-46$$

$$= \omega^2 H_0^2 \frac{\partial}{\partial r} \left(r \frac{\partial u}{\partial r} + 2u \right) \quad 9.2-47$$

$$= \omega^2 H_0^2 \left(r \frac{\partial^2 u}{\partial r^2} + \frac{\partial u}{\partial r} + 2 \frac{\partial u}{\partial r} \right) \quad 9.2-48$$

$$= \omega^2 H_0^2 \left(\frac{\partial^2 u}{r \partial x^2} + 3 \frac{\partial u}{r \partial x} \right) \quad 9.2-49$$

$$= \frac{\omega^2 H_0^2}{r} \left(\frac{\partial^2 u}{\partial x^2} + 3 \frac{\partial u}{\partial x} \right) \quad 9.2-50$$

If equations 9.2-44 and 9.2-50 are summed, expression 9.2-51 is obtained.

$$\frac{\omega^2 H_0^2}{r} \frac{\partial p_n}{\partial x} + \frac{\omega^2 H_0^2}{r} \left(\frac{\partial^2 u}{\partial x^2} + 3 \frac{\partial u}{\partial x} \right) \quad 9.2-51$$

Equation 9.2-51 is simplified further yielding expression 9.2-52.

In equation 9.2-37, the entire equation was divided by $\omega^2 r$. When the term in 9.2-52 is

$$\frac{\omega^2 H_0^2}{r} \left[\frac{\partial^2 u}{\partial x^2} + 3 \frac{\partial u}{\partial x} - \frac{\partial p_n}{\partial x} \right] \quad 9.2-52$$

divided by this same term, expression 9.2-53 is obtained. It is the neglected term in equations 9.2-40 to 9.2-42 and accounts for the order of error.

$$\frac{H_0^2}{r^2} \left[\frac{\partial^2 u}{\partial x^2} + 3 \frac{\partial u}{\partial x} - \frac{\partial p_n}{\partial x} \right] \quad 9.2-53$$

The azimuthal analysis will not be carried out in the same level of detail. The corresponding nondimensional terms were paired with the dimensional terms; the substitutions are the same as for the radial equation. The azimuthal, or theta, momentum equation in stationary coordinates is shown as equation 9.2-54.

$$\begin{aligned} \rho \left(\frac{\partial u_\theta}{\partial t} + u_r \frac{\partial u_\theta}{\partial r} + \frac{u_\theta}{r} \frac{\partial u_\theta}{\partial \theta} + \frac{u_r u_\theta}{r} + u_z \frac{\partial u_\theta}{\partial z} \right) = & \quad 9.2-54 \\ - \frac{1}{r} \frac{\partial p}{\partial \theta} + \mu \left[\frac{\partial}{\partial r} \left(\frac{1}{r} \frac{\partial}{\partial r} (r u_\theta) \right) + \frac{1}{r^2} \frac{\partial^2 u_\theta}{\partial \theta^2} + \frac{2}{r^2} \frac{\partial u_r}{\partial \theta} + \frac{\partial^2 u_\theta}{\partial z^2} \right] + F_\theta \end{aligned}$$

If body forces are neglected, and it is assumed in steady state with axisymmetric flow, equation 9.2-54 simplifies to equation 9.2-55. Equation 9.2-55 is “inertially correct” after the substitution of equation 9.2-3.

$$u_r \frac{\partial u_\theta}{\partial r} + \frac{u_r u_\theta}{r} + u_z \frac{\partial u_\theta}{\partial z} = \frac{\mu}{\rho} \left[\frac{\partial}{\partial r} \left(\frac{1}{r} \frac{\partial}{\partial r} (r u_\theta) \right) + \frac{\partial^2 u_\theta}{\partial z^2} \right] \quad 9.2-55$$

The dimensional terms, and the corresponding nondimensional terms, from the LHS of 9.2-55 are listed as expressions 9.2-56 to 9.2-58; however, no calculations are included.

$$u_r \frac{\partial u_\theta}{\partial r} \Leftrightarrow [\omega^2 r] \delta^2 u + [\omega^2 r] \delta^4 u \frac{\partial v}{\partial x} + [\omega^2 r] \delta^4 uv \quad 9.2-56$$

$$\frac{u_r u_\theta}{r} \Leftrightarrow [\omega^2 r] \delta^2 u + [\omega^2 r] \delta^4 uv \quad 9.2-57$$

$$u_z \frac{\partial u_\theta}{\partial z} \Leftrightarrow [\omega^2 r] \delta^4 \frac{\partial v}{\partial y} \quad 9.2-58$$

Corresponding to second term on the RHS of 9.2-55 leads to expression 9.2-59.

$$\frac{\partial^2 u_\theta}{\partial z^2} \Leftrightarrow [\omega^2 r] \frac{\partial^2 v}{\partial y^2} \quad 9.2-59$$

The first term on the right hand side of 9.2-55 leads to expression 9.2-60.

$$\frac{\mu}{\rho} \left[\frac{\partial}{\partial r} \left(\frac{1}{r} \frac{\partial}{\partial r} (r u_\theta) \right) \right] \Leftrightarrow \frac{\mu}{\rho} \frac{\omega \delta^2}{r} \left[\frac{\partial^2 v}{\partial x^2} + 3 \frac{\partial v}{\partial x} \right] = \frac{\omega^2 H_0^2}{r} \left[\frac{\partial^2 v}{\partial x^2} + 3 \frac{\partial v}{\partial x} \right] \quad 9.2-60$$

Equation 9.2-42 consists of the terms found in expressions 9.2-56 to 9.2-60. When this equation is divided through by $\omega^2 r$, the expression in equation 9.2-60 becomes proportional to H_0^2/r^2 . If this term is neglected, that is the order of error.

Although the error term was stated, its derivation was not included in publications by Sisoiev et al. This section has covered the derivation of the error term and the order of terms in powers of δ . The next section depends on the nondimensional groups and changes of variables that were fully developed in this section.

9.3 Curvilinear Coordinates

In sections 9.3 through 9.6, the mathematical minimum is derived for comprehending a formulation of the Navier-Stokes equations in curvilinear coordinates as derived in an article by Mogilevskii and Shkadov [71]. Their formulation is brief and built on a set of nondimensional variables. The mathematics is tedious; however, the reward is an understanding of curvilinear coordinates and realizing the case for a blended curve high-speed bell is the “most reduced” form of their equations.

The phrase “blended curve” is chosen over “arbitrary curve” since the formulation is for a thin film with the advice that the film thickness is much less than the radius of curvature of any point on the bell surface. Most industrial bells are conical, or are conical and blended into a concave curve; in all cases, the bells are assumed axisymmetric.

The simplest formulation for eventually describing the fluid thickness on a bell is a force balance at any point, along with the assumption of a thin film. This leaves a singularity at the origin where there is an infinite line source; however, due to fluid distribution geometry, bells do not form a film at the origin, therefore, that issue can be neglected.

One of the novel result in this dissertation was realizing the approximate formulation for high-a speed bell is equivalent to the “most reduced” form of the elegant curvilinear formulation of Mogilevskii and Shkadov.

The starting point of the curvilinear formulation is defining a coordinate system. In this case, the coordinates are defined as an arc length along the wetted profile that starts from the axis of rotation, a normal to the bell surface at the said arc length, and an azimuthal angle. Another method of visualizing this is defining a curve in any plane that contains the

axis of rotation, and then rotating that curve by two pi radians, or a complete circle, thus forming an axisymmetric surface of revolution. This coordinate system is partially shown in Figure 9.3-1 as a plane curve. The azimuthal angle around the z -axis is not shown.

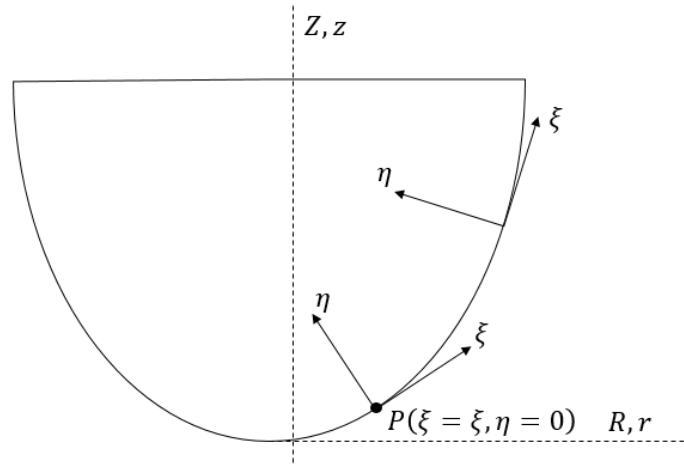


Figure 9.3-1 Curvilinear Coordinates ξ, η

If the neighborhood of point P from Figure 9.3-1 is enlarged to illustrate differential quantities, Figure 9.3-2 shows how the curvilinear coordinates are directed.

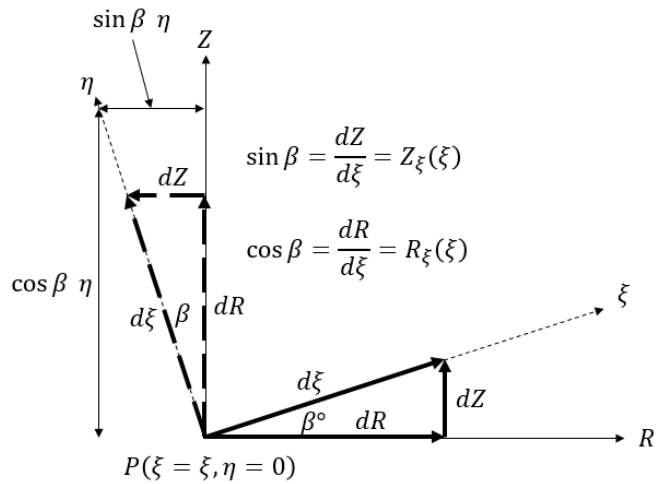


Figure 9.3-2 Differential quantities define proportions

Finally, combining Figure 9.3-1 and Figure 9.3-2 to produce Figure 9.3-3 shows the coordinate equations in the curvilinear system and generic position, $(r(\xi, \eta), z(\xi, \eta))$ in a plane.

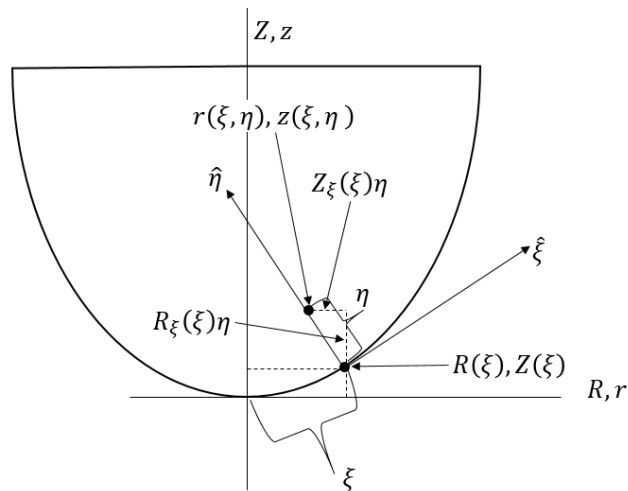


Figure 9.3-3 Curvilinear Coordinates

In Figure 9.3-3, a revolution of a planar curve drawn in a cylindrical coordinate system (r, φ, z) forms the bell solid surface. The curvilinear coordinates (ξ, θ, η) are formed by arc length along the bell surface and scaled values of the normal distances from the bell surface, thus establishing r and z positions. The angle of revolution, or azimuthal angle, is the same value in both coordinate systems. The radial and vertical cylindrical positions on the bell surface in the arc length coordinate are defined by equations 9.3-1 and 9.3-2.

$$r = R(\xi) \quad 9.3-1$$

$$z = Z(\xi) \quad 9.3-2$$

The radial, azimuthal, and vertical positions as a function of curvilinear coordinates are defined by equations 9.3-3, 9.3-4, and 9.3-5.

$$r(\xi, \eta) = R(\xi) - Z_{\xi}\eta \quad 9.3-3$$

$$z(\xi, \eta) = Z(\xi) + R_{\xi}\eta \quad 9.3-4$$

$$\theta = \varphi \quad 9.3-5$$

The film thickness, h , is assumed much less than the radius of curvature of the bell surface. This assumption ensures the origin of the radius of curvature is outside the film thickness, in equation form, it is expressed as 9.3-6.

$$h(r) \ll r_c \quad 9.3-6$$

9.4 Metric Tensor Coefficients

The next step in developing the Navier-Stokes equations based on these curvilinear coordinates is deriving the metric coefficients that appear in various vector operators. In a Cartesian coordinate system the dot products of unit vectors is a Kronecker delta as shown in equation 9.4-1.

$$\mathbf{e}_i \cdot \mathbf{e}_j = \delta_{ij} \quad i, j = 1, 2, 3 \quad 9.4-1$$

The curvilinear coordinate system (ξ, θ, η) is mutually orthogonal. The fully expanded dot product relationships are shown in equation 9.4-2.

$$\mathbf{e}_i \cdot \mathbf{e}_j = \begin{bmatrix} \mathbf{e}_\xi \cdot \mathbf{e}_\xi = 1 & \mathbf{e}_\xi \cdot \mathbf{e}_\theta = 0 & \mathbf{e}_\xi \cdot \mathbf{e}_\eta = 0 \\ \mathbf{e}_\theta \cdot \mathbf{e}_\xi = 0 & \mathbf{e}_\theta \cdot \mathbf{e}_\theta = 1 & \mathbf{e}_\theta \cdot \mathbf{e}_\eta = 0 \\ \mathbf{e}_\eta \cdot \mathbf{e}_\xi = 0 & \mathbf{e}_\eta \cdot \mathbf{e}_\theta = 0 & \mathbf{e}_\eta \cdot \mathbf{e}_\eta = 1 \end{bmatrix} \quad 9.4-2$$

In fact, the current system of (ξ, θ, η) is by definition and visual inspection mutually orthogonal since ξ, η are at right angles in a plane that contains the axis of rotation and θ is perpendicular to that plane, hence, perpendicular to ξ, η .

If a curvilinear coordinate system is mutually orthogonal, any problem analyzed in that system becomes less complex because the metric tensor is diagonal. If the Jacobian determinant, equation 9.4-3, shown in index and expanded notation, is non-vanishing, the Cartesian coordinate system (x_j) and the curvilinear system (q_i) can transform coordinate triplets from one system to the other.

$$\frac{\partial q_i}{\partial x_j} = \begin{bmatrix} \frac{\partial q_1}{\partial x_1} & \frac{\partial q_1}{\partial x_2} & \frac{\partial q_1}{\partial x_3} \\ \frac{\partial q_2}{\partial x_1} & \frac{\partial q_2}{\partial x_2} & \frac{\partial q_2}{\partial x_3} \\ \frac{\partial q_3}{\partial x_1} & \frac{\partial q_3}{\partial x_2} & \frac{\partial q_3}{\partial x_3} \end{bmatrix} \quad i, j = 1, 2, 3 \quad 9.4-3$$

In a Cartesian system, the square of the length is defined by equation 9.4-4.

$$ds^2 = dx_i \cdot dx_i \quad 9.4-4$$

The same length terms are expressed in the curvilinear system as shown by equation 9.4-5.

$$ds^2 = \frac{\partial x_i}{\partial q_l} \frac{\partial x_i}{\partial q_m} dq_l dq_m = g_{lm} dq_l dq_m \quad 9.4-5$$

The coefficients g_{lm} are the components of the metric tensor, or metric coefficients. They are defined by equation 9.4-6.

$$\frac{\partial x_i}{\partial q_l} \frac{\partial x_i}{\partial q_m} = g_{lm} \quad 9.4-6$$

Orthogonality dictates there are only three diagonal coefficients in this metric tensor, therefore, length of a vector is defined by equation 9.4-7, where $h_{(i)}$ are referred to as scale factors. This h is not the same as the previous h designating film thickness.

$$ds^2 = h_1^2 dq_1^2 + h_2^2 dq_2^2 + h_3^2 dq_3^2 \quad 9.4-7$$

Equations 9.4-6 and 9.4-7 lead to an indicial notation representation, equation 9.4-8, of the three metric coefficients. These are also referred to as Lamé' coefficients.

$$g_{ii} = h_{(i)}^2 \quad 9.4-8$$

Expansion of the indicial notation, as shown by equations 9.4-9 to 9.4-11, leads to coefficients, or scale factors, that can be used in the Del and Laplace operators in the $(q_1 = \xi, q_2 = \theta, q_3 = \eta)$ curvilinear coordinate system.

$$h_{(1)} = \sqrt{g_{11}} = \sqrt{\frac{\partial x_1}{\partial q_1} \frac{\partial x_1}{\partial q_1} + \frac{\partial x_2}{\partial q_1} \frac{\partial x_2}{\partial q_1} + \frac{\partial x_3}{\partial q_1} \frac{\partial x_3}{\partial q_1}} \quad 9.4-9$$

$$h_{(2)} = \sqrt{g_{22}} = \sqrt{\frac{\partial x_1}{\partial q_2} \frac{\partial x_1}{\partial q_2} + \frac{\partial x_2}{\partial q_2} \frac{\partial x_2}{\partial q_2} + \frac{\partial x_3}{\partial q_2} \frac{\partial x_3}{\partial q_2}} \quad 9.4-10$$

$$h_{(3)} = \sqrt{g_{33}} = \sqrt{\frac{\partial x_1}{\partial q_3} \frac{\partial x_1}{\partial q_3} + \frac{\partial x_2}{\partial q_3} \frac{\partial x_2}{\partial q_3} + \frac{\partial x_3}{\partial q_3} \frac{\partial x_3}{\partial q_3}} \quad 9.4-11$$

Parenthesis is used on the indices of each h to associate the scale factor with a particular coordinate not included in indicial operations. Armed with definitions of scale factors, the actual scale factors used in the (ξ, θ, η) system can be calculated.

First, a set of Cartesian coordinates in terms of (ξ, θ, η) is obtained from Figure 9.3-3. Although this figure does not illustrate an (x, y) plane, it is a plane perpendicular to the z -axis in Figure 9.3-3. The reflection of the distance, equation 9.3-3, from the axis of rotation to a point in space can be reflected onto this plane, the x component is the distance multiplied by the cosine of θ , and the y component is the same distance multiplied by the

sin of θ . The x and y coordinates are given by equations 9.4-12 and 9.4-13. The z coordinate was stated in equation 9.3-4 and is shown again as equation 9.4-14.

$$x(\xi, \eta) = x_1 = (R(\xi) - Z_\xi \eta) \cos \theta \quad 9.4-12$$

$$y(\xi, \eta) = x_2 = (R(\xi) - Z_\xi \eta) \sin \theta \quad 9.4-13$$

$$z(\xi, \eta) = Z(\xi) + R_\xi \eta \quad 9.4-14$$

Next, calculate the derivative of each Cartesian term with respect to each curvilinear coordinate, essentially calculating the terms of a Jacobian transformation. For the θ and η coordinates, these are straightforward calculations. On the other hand, the ξ coordinate is a calculation, followed by an order of magnitude simplification, and finally, followed again by a simplification obtained from applying the binomial theorem.

The derivatives of the Cartesian terms with respect to η are given by equations 9.4-15 through 9.4-17.

$$\frac{\partial x}{\partial \eta} = -Z_\xi \cos \theta \quad 9.4-15$$

$$\frac{\partial y}{\partial \eta} = -Z_\xi \sin \theta \quad 9.4-16$$

$$\frac{\partial z}{\partial \eta} = R_\xi \quad 9.4-17$$

Equations 9.4-18 through 9.4-20 are the Cartesian partial derivatives with respect to θ .

$$\frac{\partial x}{\partial \theta} = -(R(\xi) - Z_{\xi}\eta) \sin \theta \quad 9.4-18$$

$$\frac{\partial y}{\partial \theta} = (R(\xi) - Z_{\xi}\eta) \cos \theta \quad 9.4-19$$

$$\frac{\partial z}{\partial \theta} = 0 \quad 9.4-20$$

Finally, equations 9.4-21 through 9.4-23 are the Cartesian partial derivatives with respect to ξ .

$$\frac{\partial x}{\partial \xi} = (R_{\xi} - Z_{\xi\xi}\eta) \cos \theta \quad 9.4-21$$

$$\frac{\partial y}{\partial \xi} = (R_{\xi} - Z_{\xi\xi}\eta) \sin \theta \quad 9.4-22$$

$$\frac{\partial z}{\partial \xi} = Z_{\xi} + R_{\xi\xi}\eta \quad 9.4-23$$

The calculation for h_3 is shown by equation 9.4-24.

$$h_3 = \sqrt{(-Z_{\xi} \cos \theta)^2 + (-Z_{\xi} \sin \theta)^2 + R_{\xi}^2} \quad 9.4-24$$

Equation 9.4-24 reduces to equation 9.4-25.

$$h_3 = \sqrt{Z_{\xi}^2((\cos \theta)^2 + (\sin \theta)^2) + R_{\xi}^2} \quad 9.4-25$$

Equation 9.4-25 reduces further, by means of a trigonometric identity, to equation 9.4-26.

$$h_3 = \sqrt{Z_{\xi}^2 + R_{\xi}^2} \quad 9.4-26$$

Equation can be simplified further; however, it requires interpreting these derivatives based on Figure 9.3-2. In that figure, the angle β is the angle of the slope, or derivative, where R_ξ is the cosine of β and Z_ξ is the sine of β , therefore, h_3 is identically equal to one.

$$h_3 = \sqrt{(\sin \beta)^2 + (\cos \beta)^2} = 1 \quad 9.4-27$$

The calculation for h_2 is shown by equation 9.4-28.

$$h_2 = \sqrt{(-(R(\xi) - Z_\xi \eta) \sin \theta)^2 + ((R(\xi) - Z_\xi \eta) \cos \theta)^2} \quad 9.4-28$$

Equation 9.4-28 can be reduced to equation 9.4-29, which returns the radial position from equation 9.3-3.

$$h_2 = \sqrt{(R(\xi) - Z_\xi \eta)^2 (\sin^2 \theta + \cos^2 \theta)} = R(\xi) - Z_\xi \eta = r(\xi, \eta) \quad 9.4-29$$

The case for h_1 has several steps. The initial calculation begins with equation 9.4-30.

$$h_1 = \sqrt{((R_\xi - Z_{\xi\xi} \eta) \cos \theta)^2 + ((R_\xi - Z_{\xi\xi} \eta) \sin \theta)^2 + (Z_\xi + R_{\xi\xi} \eta)^2} \quad 9.4-30$$

Using a common trigonometric identity, equation 9.4-30 reduces to equation 9.4-31.

$$h_1 = \sqrt{(R_\xi - Z_{\xi\xi} \eta)^2 + (Z_\xi + R_{\xi\xi} \eta)^2} \quad 9.4-31$$

The terms in equation 9.4-31 are expanded, yielding equation 9.4-32.

$$h_1 = \sqrt{R_\xi^2 - 2R_\xi Z_{\xi\xi}\eta + Z_{\xi\xi}^2\eta^2 + Z_\xi^2 + 2Z_\xi R_{\xi\xi}\eta + R_{\xi\xi}^2\eta^2} \quad 9.4-32$$

If terms of equation 9.4-32 are rearranged, equation 9.4-33 is obtained.

$$h_1 = \sqrt{R_\xi^2 + Z_\xi^2 + 2(Z_\xi R_{\xi\xi} - R_\xi Z_{\xi\xi})\eta + (Z_{\xi\xi}^2 + R_{\xi\xi}^2)\eta^2} \quad 9.4-33$$

The sum of first two terms under the radical sign is identically one. Since η , a typical dimension of film thickness in the high-speed case is on order of $10^{-5,6}$ and the curvature of R and Z is on order of 10^{-2} , the entire last term under the radical that is multiplied by η^2 can be neglected.

Equation 9.4-33 can be simplified further into equation 9.4-34.

$$h_1 = \sqrt{1 + 2(Z_\xi R_{\xi\xi} - R_\xi Z_{\xi\xi})\eta} = (1 + 2(Z_\xi R_{\xi\xi} - R_\xi Z_{\xi\xi})\eta)^{1/2} \quad 9.4-34$$

The binomial theorem, shown in equation 9.4-35 can approximate equation 9.4-34 under certain conditions.

$$(1 + bx)^\alpha \cong 1 + \alpha bx \quad \alpha bx \ll 1 \quad 9.4-35$$

If the binomial theorem is applied to equation 9.4-35, equation 9.4-36 is obtained.

$$1 + (Z_\xi R_{\xi\xi} - R_\xi Z_{\xi\xi})\eta \quad 9.4-36$$

Equation 9.4-36 is rewritten in a slightly different form as equation 9.4-37.

$$1 - (R_\xi Z_{\xi\xi} - Z_\xi R_{\xi\xi})\eta = 1 - \mathcal{K}\eta \quad 9.4-37$$

The three metric coefficients, or scale factors, are gathered in one place, and given as equations 9.4-38 through 9.4-40.

$$h_3 = 1 \quad 9.4-38$$

$$h_2 = r(\xi, \eta) \quad 9.4-39$$

$$h_1 = 1 - \mathcal{K}\eta \quad 9.4-40$$

These are the same scale factors, or Lamé' coefficients, presented by Mogilevskii et al [71].

9.5 Unit Vector Derivatives in Curvilinear Coordinates

This section will derive the derivatives of unit vectors with respect to coordinates. These derivatives are needed to create the vector invariant operators in a coordinate system. Most relevant to this dissertation are the radial components of the momentum equation found in Mogilevskii et al. The mathematics is tedious; however, stepping into learning the art of curvilinear coordinates is worth the effort of this exercise many times over.

The order of magnitude analysis of the previous section, though done on a disk in cylindrical coordinates, is applicable in other coordinate system and bell profile shapes that are similar in size and operating characteristics. However, this dissertation does not quantify the extent of similarity.

The order of magnitude analysis and deciphering the Navier-Stokes equations in their curvilinear coordinates enables finding the terms that substantiate an approximation for calculating film thickness on an arbitrary bell profile surface. The first step in formulating the Navier-Stokes equations in curvilinear coordinates was shown in section 9.3, namely, calculating the metric coefficients. Although the coordinate system in their publication was curvilinear, it was also mutually orthogonal, meaning the intersection of coordinates axes are at mutual right angles. In this case, the metric tensor is diagonal, and the coefficients are referred to as the Lamé' coefficients.

The next step is formulating the spatial derivatives of unit vectors with respect to each coordinate. In a Cartesian system, the derivatives of the unit vectors are all zero since the vectors are constant in magnitude and direction. On the other hand, for example, in cylindrical or spherical systems the unit vectors change in direction depending on their

location in space. However, the derivatives are reasonably obvious and a simple geometric interpretation leads to the correct derivative. This is due to surfaces of constant curvature. If the curvature was to vary, as in the case of an arbitrary bell profile, the derivatives would have a general geometric behavior but the components would be less obvious and require calculation.

The function of the metric coefficients can be best described with an example contrasting Cartesian and cylindrical coordinates. In a Cartesian system, if position vector is changed by dx , the distance moved is dx . On the other hand, in a cylindrical system, if the angle is changed by $d\theta$, the distance is $dl = rd\theta$. A reciprocal example is if the distance is dl , the change in the coordinate is $\frac{1}{r}d\theta$.

Continuing with a cylindrical example, the change in the radial unit vector with respect to changes in theta is $\frac{\partial \hat{r}}{\partial \theta} = \hat{\theta} = -\sin \theta \hat{i} + \cos \theta \hat{j}$; on the other hand $\frac{\partial \hat{r}}{\partial r} = 0$. Both can be geometrically derived from a diagram. As a coordinate system becomes more complex, its characteristics need to be obtained analytically instead of by a visual/geometric interpretation.

Happel and Brenner published probably the most teachable [88] general derivation of the derivatives of unit vectors that begins with defining the metric coefficients in a differential relationship as shown by equation 9.5-1. Their method of derivation was faithfully followed along with helpful narration. It should be noted they worked with a reciprocal formulation.

$$h_k = \left| \frac{dq_k}{dl_k} \right| \quad 9.5-1$$

In equation 9.5-1, dl_k is a distance and dq_k is the change in coordinate that produces that distance, and h_k scales this relationship as explained in the previous cylindrical example. At the same point in space, unit tangent vectors tangent to the coordinate axes can be described by equation 9.5-2 where \mathbf{R} is a position vector.

$$\hat{i}_k = \frac{\partial \vec{R}}{\partial l_k} \quad 9.5-2$$

Though the magnitude of the unit vector at any point is unity, their direction can change throughout the domain. Equation of 9.5-2 is multiplied by the reciprocal of corresponding, and equivalent sides of equation 9.5-1 yielding equation 9.5-3.

$$\frac{1}{h_k} \hat{i}_k = \frac{\partial \vec{R}}{\partial l_k} \frac{dl_k}{dq_k} \quad 9.5-3$$

Applying the “reverse” of the chain rule to the RHS of equation 9.5-3 and isolating the unit vector yields equation 9.5-4.

$$\hat{i}_k = h_k \frac{\partial \vec{R}}{\partial q_k} \quad 9.5-4$$

In an orthogonal coordinate system, the dot product of unit vector is equation 9.5-5.

$$\hat{i}_k \cdot \hat{i}_j = \delta_{ij} \quad 9.5-5$$

Equation 9.5-5 is differentiated while $j = k$, yielding equation 9.5-6.

$$\frac{\partial}{\partial q_l} (\hat{i}_k \cdot \hat{i}_k) = \frac{\partial \hat{i}_k}{\partial q_l} \cdot \hat{i}_k + \hat{i}_k \cdot \frac{\partial \hat{i}_k}{\partial q_l} = 2\hat{i}_k \cdot \frac{\partial \hat{i}_k}{\partial q_l} = 0 \quad 9.5-6$$

Equation 9.5-6 shows that $\partial \hat{i}_k / \partial q_l$ is zero or, less obvious, but a result of the dot product, is perpendicular to \hat{i}_k .

A consequence of equation 9.5-2 and 9.5-5 is shown in equation 9.5-7.

$$\frac{\partial}{\partial q_j} \left(\frac{\partial \vec{R}}{\partial q_k} \cdot \frac{\partial \vec{R}}{\partial q_l} \right) = 0 \quad (k \neq l) \quad 9.5-7$$

Since i, j, k are index placeholders, three relationships can be obtained from equation 9.5-7 through cyclic permutation of these indices, as shown in equations 9.5-8 through 9.5-10.

$$\frac{\partial}{\partial q_j} \left(\frac{\partial R}{\partial q_k} \cdot \frac{\partial R}{\partial q_l} \right) = \frac{\partial^2 R}{\partial q_j \partial q_k} \cdot \frac{\partial R}{\partial q_l} + \frac{\partial^2 R}{\partial q_j \partial q_l} \cdot \frac{\partial R}{\partial q_k} = 0 \quad k \neq l \quad 9.5-8$$

$$\frac{\partial}{\partial q_l} \left(\frac{\partial R}{\partial q_j} \cdot \frac{\partial R}{\partial q_k} \right) = \frac{\partial^2 R}{\partial q_l \partial q_j} \cdot \frac{\partial R}{\partial q_k} + \frac{\partial^2 R}{\partial q_l \partial q_k} \cdot \frac{\partial R}{\partial q_j} = 0 \quad j \neq k \quad 9.5-9$$

$$\frac{\partial}{\partial q_k} \left(\frac{\partial R}{\partial q_l} \cdot \frac{\partial R}{\partial q_j} \right) = \frac{\partial^2 R}{\partial q_k \partial q_l} \cdot \frac{\partial R}{\partial q_j} + \frac{\partial^2 R}{\partial q_k \partial q_j} \cdot \frac{\partial R}{\partial q_l} = 0 \quad l \neq j \quad 9.5-10$$

Since the order of differentiation and dot product are interchangeable, equation 9.5-9 is subtracted from equation 9.5-8, the result is added to equation 9.5-10, yielding equation 9.5-11.

$$\frac{\partial^2 R}{\partial q_k \partial q_j} \cdot \frac{\partial R}{\partial q_l} = 0 \quad j \neq k \neq l \quad 9.5-11$$

If equation 9.5-4 is substituted, along with the change in index, into the second term on the LHS of equation 9.5-11, equation 9.5-12 is obtained.

$$\frac{\partial}{\partial q_j} \left(\frac{i_k}{h_k} \right) \cdot \frac{i_l}{h_l} = \frac{\partial}{\partial q_j} \left(\frac{i_k}{h_k} \right) \cdot i_l = 0 \quad j \neq k \neq l \quad 9.5-12$$

Differentiating equation 9.5-12 as indicated yields equation 9.5-13.

$$\left(i_k \frac{\partial}{\partial q_j} \left(\frac{1}{h_k} \right) + \frac{1}{h_k} \frac{\partial i_k}{\partial q_j} \right) \cdot i_l = 0 \quad j \neq k \neq l \quad 9.5-13$$

Since $j \neq k \neq l$, the first term in equation 9.5-13, $i_k \cdot i_l$, is eliminated, leaving equation 9.5-14.

$$\left(\frac{1}{h_k} \frac{\partial i_k}{\partial q_j} \right) \cdot i_l = \frac{\partial i_k}{\partial q_j} \cdot i_l = 0 \quad j \neq k \neq l \quad 9.5-14$$

Equation 9.5-14 proves that $\frac{\partial i_k}{\partial q_j}$ is orthogonal to i_l and does not have a component in the i_l direction. If equation 9.5-5 is differentiated with respect to q_j when the unit vector indices are the same, equation 9.5-15 is obtained.

$$\frac{\partial i_k}{\partial q_j} \cdot i_k = 0 \quad 9.5-15$$

Equation 9.5-15 proves that $\frac{\partial i_k}{\partial q_j}$ is orthogonal to i_k and does not have a component in the i_k direction either. Therefore, $\frac{\partial i_k}{\partial q_j} \parallel i_j$ when $j \neq k$. This result does not show its importance until the equality in equation 9.5-16 is analyzed further. This equality is true because the order of differentiation is interchangeable.

$$\frac{\partial}{\partial q_j} \left(\frac{\partial \mathbf{R}}{\partial q_k} \right) = \frac{\partial}{\partial q_k} \left(\frac{\partial \mathbf{R}}{\partial q_j} \right) \quad 9.5-16$$

Equation 9.5-4 is restated differently in equation 9.5-17.

$$\frac{i_k}{h_k} = \frac{\partial \vec{R}}{dq_k} \quad 9.5-17$$

If equation 9.5-16 is substituted into equation 9.5-17, equation 9.5-18 is obtained.

$$\frac{\partial}{\partial q_j} \left(\frac{i_k}{h_k} \right) = \frac{\partial}{\partial q_k} \left(\frac{i_j}{h_j} \right) \quad 9.5-18$$

If both sides of equation 9.5-18 are differentiated as indicated, equation 9.5-19 is obtained.

At first glance, equation 9.5-19 seems nonsensical since it contains terms with and without a unit vector; however, a unit vector is implied in the terms without an explicit unit vector.

$$\frac{1}{h_k} \frac{\partial i_k}{\partial q_j} + i_k \frac{\partial}{\partial q_j} \left(\frac{1}{h_k} \right) = \frac{1}{h_j} \frac{\partial i_j}{\partial q_k} + i_j \frac{\partial}{\partial q_k} \left(\frac{1}{h_j} \right) \quad 9.5-19$$

The conclusions of equation 9.5-14 and 9.5-15 can be stated as equation 9.5-20. In other words, if the derivative is parallel to i_j , then it means the only component of it is in the i_j direction.

$$\frac{\partial i_k}{\partial q_j} \parallel i_j = \frac{\partial i_k}{\partial q_j} i_j \quad j \neq k \quad 9.5-20$$

The leading derivative terms on each side of equation 9.5-19 can be replaced with equation 9.5-20 as shown in equation 9.5-21, thus, the latent unit vector is now patent.

$$\frac{1}{h_k} \frac{\partial i_k}{\partial q_j} i_j + i_k \frac{\partial}{\partial q_j} \left(\frac{1}{h_k} \right) = \frac{1}{h_j} \frac{\partial i_j}{\partial q_k} i_k + i_j \frac{\partial}{\partial q_k} \left(\frac{1}{h_j} \right) \quad j \neq k \quad 9.5-21$$

Equation 9.5-21 separates into two scalar equations, although the unit vectors are still present, as indicated by equation 9.5-22. These equations are symmetrical relationships and only one is needed for the calculating derivatives of unit vectors.

$$\begin{aligned} \frac{1}{h_k} \frac{\partial i_k}{\partial q_j} i_j &= i_j \frac{\partial}{\partial q_k} \left(\frac{1}{h_j} \right) \quad j \neq k \quad (a) \\ i_k \frac{\partial}{\partial q_j} \left(\frac{1}{h_k} \right) &= \frac{1}{h_j} \frac{\partial i_j}{\partial q_k} i_k \quad j \neq k \quad (b) \end{aligned} \quad 9.5-22$$

After one of the equations from 9.5-22 is solved for the derivative term, the result is shown as equation 9.5-23. This equation is for calculating mixed index derivatives of unit vectors.

$$\frac{\partial i_k}{\partial q_j} i_j = i_j h_k \frac{\partial}{\partial q_k} \left(\frac{1}{h_j} \right) \quad j \neq k \quad 9.5-23$$

The remaining case is when the indices in the derivative term are equal. The derivation begins with rules of cross products in right-handed coordinate systems. Right-handed cyclic permutation creates three cross product relationships as shown in equations 9.5-24.

$$i_j = i_k \times i_l \quad i_k = i_l \times i_j \quad i_l = i_j \times i_k \quad 9.5-24$$

Since the cross product does not commute, reversal of the crossed terms causes a sign change in the product. The first cross product from equation 9.5-24 is differentiated as shown in equation 9.5-25.

$$\frac{\partial i_j}{\partial q_j} = (i_j \times i_l)h_k \frac{\partial}{\partial q_k} \left(\frac{1}{h_j} \right) + (i_k \times i_j)h_l \frac{\partial}{\partial q_l} \left(\frac{1}{h_j} \right) \quad 9.5-25$$

If the anti-commutative cross product terms in equation are computed and replaced with their product, the result is equation 9.5-26.

$$\frac{\partial i_j}{\partial q_j} = -i_k h_k \frac{\partial}{\partial q_k} \left(\frac{1}{h_j} \right) - i_l h_l \frac{\partial}{\partial q_l} \left(\frac{1}{h_j} \right) \quad 9.5-26$$

From equation 9.5-1 through 9.5-26, along with explanatory narration is the complete recreation of the derivation of Happel and Brenner. However, it should be noted that their derivation is based on reciprocals of the metric coefficients derived in section 9.3. This inversion is shown as equations 9.5-27.

$$\lambda(\xi, \eta) = \frac{1}{h_1} \quad r(\xi, \eta) = \frac{1}{h_2} \quad h_3 = 1 \quad h_1 = \frac{1}{\lambda(\xi, \eta)} \quad h_2 = \frac{1}{r(\xi, \eta)} \quad h_3 = 1 \quad 9.5-27$$

Applying these derivative formulas to the coordinate system of will yield a listing of nine unit vector derivatives with respect to each coordinate. Additionally, a change in nomenclature includes (ξ, θ, η) being substituted for the generic coordinates (q_1, q_2, q_3) , and $\hat{\xi}, \hat{\theta}, \hat{\eta}$ substituted for i , a placeholder unit vector. These nine derivatives comprise equations 9.5-28 through 9.5-36.

$$\frac{\partial \hat{\xi}}{\partial \xi} = -\hat{\theta} \frac{1}{r} \frac{\partial}{\partial \theta} (\lambda) - \hat{\eta} \frac{1}{\lambda} \frac{\partial}{\partial \eta} (\lambda) = -\lambda_{\eta} \hat{\eta} \quad 9.5-28$$

$$\frac{\partial \hat{\xi}}{\partial \theta} = \hat{\theta} \frac{1}{\lambda} \frac{\partial}{\partial \xi} (r) = \hat{\theta} \frac{1}{\lambda} r_{\xi} \quad 9.5-29$$

$$\frac{\partial \hat{\xi}}{\partial \eta} = \hat{\eta} \frac{1}{\lambda} \frac{\partial}{\partial \xi} (1) = 0 \quad 9.5-30$$

$$\frac{\partial \hat{\theta}}{\partial \xi} = \hat{\xi} \frac{1}{r} \frac{\partial}{\partial \theta} (\lambda) = 0 \quad 9.5-31$$

$$\frac{\partial \hat{\theta}}{\partial \theta} = -\hat{\xi} \frac{1}{\lambda} \frac{\partial}{\partial \xi} (r) - \hat{\eta} \frac{1}{\lambda} \frac{\partial}{\partial \eta} (r) = -\hat{\xi} \frac{1}{\lambda} r_{\xi} - \hat{\eta} r_{\eta} \quad 9.5-32$$

$$\frac{\partial \hat{\theta}}{\partial \eta} = \hat{\eta} \frac{1}{r} \frac{\partial}{\partial \theta} (1) = 0 \quad 9.5-33$$

$$\frac{\partial \hat{\eta}}{\partial \xi} = \hat{\xi} \frac{1}{\lambda} \frac{\partial}{\partial \eta} (\lambda) = \hat{\xi} \lambda_{\eta} \quad 9.5-34$$

$$\frac{\partial \hat{\eta}}{\partial \theta} = \hat{\theta} \frac{1}{\lambda} \frac{\partial}{\partial \eta} (r) = \hat{\theta} r_{\eta} \quad 9.5-35$$

$$\frac{\partial \hat{\eta}}{\partial \eta} = -\hat{\xi} \frac{1}{\lambda} \frac{\partial}{\partial \xi} (1) - \hat{\theta} \frac{1}{r} \frac{\partial}{\partial \theta} (1) = 0 \quad 9.5-36$$

9.6 Vector Invariants

In this dissertation, the Navier-Stokes equations have been shown in cylindrical and spherical coordinate systems. The effects of rotation around a vertical axis were included by using the Greenspan formulation or a kinematic substitution for tangential velocity. The kinematic substitution is the difference between bell surface tangential velocity and fluid tangential velocity, thereby, forming a velocity referenced to an inertial observer.

A form of the Navier-Stokes equations is shown in equation 9.6-1 without any reference to the coordinate system. A “coordinate specific” formulation can be obtained by applying Newton’s Law to a differential parcel of fluid in the coordinates of the analysis, or by applying the vector operators that correspond to the coordinate system of analysis. The vector invariants are shown in this section; however, they are not derived, moreover, they could have several form; general vector invariants can be found in the literature. The invariants that correspond to Cartesian, cylindrical, and spherical coordinates are ubiquitous.

$$\rho \left(\frac{\partial \mathbf{u}}{\partial t} + \mathbf{u} \cdot \nabla \mathbf{u} \right) = -\nabla p + \mu \nabla^2 \mathbf{u} + \mathbf{F} \quad 9.6-1$$

In equation 9.6-1, the LHS is the inertial force. On the RHS, the first term is the pressure force, the second term is the viscous force, and the third term is the body force such as gravity. Equation 9.6-1 shows a more common form of the Navier-Stokes equation for an incompressible fluid with the viscous term written as the Laplacian of velocity.

The gradient, divergence, and Laplacian operators are shown by equations 9.6-2 through 9.6-6. They are written in terms of derivative operators and metric coefficients. The derivatives of unit vectors appear as the derivative operators are applied.

Equation 9.6-2 is the gradient operator.

$$\nabla = \frac{1}{h_1} \frac{\partial}{\partial q_1} \hat{q}_1 + \frac{1}{h_2} \frac{\partial}{\partial q_2} \hat{q}_2 + \frac{1}{h_3} \frac{\partial}{\partial q_3} \hat{q}_3 \quad 9.6-2$$

Equation 9.6-3 is the divergence operator.

$$\nabla \cdot = \frac{1}{h_1 h_2 h_3} \left\{ \frac{\partial}{\partial q_1} (h_2 h_3) + \frac{\partial}{\partial q_2} (h_1 h_3) + \frac{\partial}{\partial q_3} (h_1 h_2) \right\} \quad 9.6-3$$

Equation 9.6-4 [89],[90] is a formulation of the convective derivative.

$$[u \cdot \nabla u]_i = \frac{u_j}{h_j} \frac{\partial u_i}{\partial q^j} + \frac{u_j}{h_j h_i} \left(u_i \frac{\partial h_i}{\partial q^j} - u_j \frac{\partial h_j}{\partial q^i} \right) \quad 9.6-4$$

Equation 9.6-5 is the Laplacian operator.

$$\Delta = \frac{1}{h_1 h_2 h_3} \left\{ \frac{\partial}{\partial q_1} \left(\frac{h_2 h_3}{h_1} \frac{\partial}{\partial q_1} \right) + \frac{\partial}{\partial q_2} \left(\frac{h_1 h_3}{h_2} \frac{\partial}{\partial q_2} \right) + \frac{\partial}{\partial q_3} \left(\frac{h_1 h_2}{h_3} \frac{\partial}{\partial q_3} \right) \right\} \quad 9.6-5$$

Equation 9.6-6 is alternative [90], though tedious, formulation of the Laplacian operator applied to a generic vector \mathbf{A} .

$$\begin{aligned}
(\nabla^2 A)_i &= \nabla^2 A_i + \frac{2}{h_i h_j} \left(\frac{1}{h_i} \frac{\partial h_i}{\partial u_j} \frac{\partial}{\partial u_i} - \frac{1}{h_j} \frac{\partial h_j}{\partial u_i} \frac{\partial}{\partial u_j} \right) A_j & 9.6-6 \\
&+ \frac{h}{h_i h_j^2} \left[\frac{A_j}{h_i^2} \frac{\partial h_j}{\partial u_i} \frac{\partial}{\partial u_j} \left(\frac{h_i^2}{h} \right) - \frac{A_i}{h_j^2} \frac{\partial h_i}{\partial u_j} \frac{\partial}{\partial u_i} \left(\frac{h_j^2}{h} \right) \right] \\
&+ \frac{A_j}{h_i} \frac{h}{h_j^3} \left[\frac{1}{h_j} \frac{\partial h_j}{\partial u_i} \frac{\partial}{\partial u_j} \left(\frac{h_j^2}{h} \right) + \frac{h}{h_j^2} \frac{\partial}{\partial u_i} \left(\frac{h_j^2}{h} \right) \frac{\partial}{\partial u_j} \left(\frac{h_j^2}{h} \right) - \frac{\partial^2}{\partial u_i \partial u_j} \left(\frac{h_j^2}{h} \right) \right] \\
&- \frac{A_i}{h_i h_j^2} \left[\frac{2}{h_i} \left(\frac{\partial h_j}{\partial u_i} \right)^2 - \frac{\partial^2 h_i}{\partial u_j^2} \right] \quad h = h_1 h_2 h_3
\end{aligned}$$

The contents of sections 9.3 through 9.6 were necessary learning that enabled understanding the formulation and implications of the work by Mogilevskii and Shkadov. In the next section, parts of their radially outward, or ξ component of momentum conservation are derived.

9.7 Navier-Stokes in a Curvilinear System

The ξ momentum equation from the work of Mogilevskii and Shkadov [71] is a lengthy equation, shown as equation 9.7-1.

$$\begin{aligned}
 & u_{yy} + \lambda^{-1}\beta F^2 r_\xi + \beta Fr^{-1}r_\eta e^{-x} + 2v\lambda^{-1}\beta E^{-1}Fr_\xi & 9.7-1 \\
 & -E^{-2}[u_t + uu_x\lambda^{-1}R_\xi + wu_y + \lambda^{-1}(u^2R_\xi - v^2r_\xi\beta + uw\lambda_y)] \\
 & -\varepsilon\{\lambda^{-1}R_\xi(p + p_x) + u_y(\beta r_\eta + \lambda^{-1}\varepsilon^{-1}\lambda_y)\} \\
 & +u\left[R_\xi\lambda^{-1}(\varepsilon\lambda^{-1}r_\xi)_x + \beta((\varepsilon\lambda\beta)^{-1}\lambda_y)_y\right] \\
 & +\varepsilon^2\lambda^{-2}\{(u_{xx} + u_x)R_\xi^2 + (u_x + u)[RR_{\xi\xi} + R_\xi(\beta r_\xi - R_\xi\lambda^{-1}\lambda_x)] \\
 & +2w_xR_\xi\lambda_y + wR_\xi[\varepsilon\lambda\beta(\lambda r)_\eta]\} = 0
 \end{aligned}$$

Their continuity equation is shown as equation 9.7-2.

$$R_\xi\left(u_x + u\left(1 + \beta\frac{1}{R_\xi}r_\xi\right)\right) + \lambda w_\eta + w\varepsilon\beta(r\lambda)_\eta = 0 \quad 9.7-2$$

In this section, the mathematics developed in sections 9.3 through 9.6 , and the order of magnitude analysis from section 9.2 , are the tools to derive and simplify equations 9.7-1 and 9.7-2. Many, but not all, of the algebraic steps will be shown. Some of the terms from line 4 of equation 9.7-1 are derivatives and the product rule expands them into other terms. These were ignored since they were insignificant based on a magnitude order analysis, moreover, authors' purpose for this additional complexity was not immediately apparent.

In an incompressible fluid that is described by an orthogonal coordinate system, the continuity equation in terms of the curvilinear coordinates of Mogilevskii et al is derived by starting with an invariant form of the divergence of velocity. The invariant form is

expanded to include the effects of the metric coefficients and derivatives of unit vectors. The divergence equation can be written as equation 9.7-3. Since the flow is axisymmetric, the derivatives with respect to θ vanish.

$$\nabla \cdot \mathbf{q} = 0 \quad 9.7-3$$

Equation 9.7-3 written in terms of the metric coefficients and non-dimensional velocities is shown by equation 9.7-4.

$$\frac{1}{h_1 h_2 h_3} \left(\frac{\partial}{\partial \xi} (h_2 h_3 (V^\xi)) + \frac{\partial}{\partial \eta} (h_1 h_2 (V^\eta)) \right) = 0 \quad 9.7-4$$

The non-dimensional velocities of Mogilevskii et al in the arc length direction and “normal to the bell surface” direction are equations 9.7-5 and 9.7-6 in which V^ξ, V^η represent dimensional velocities and u, w represent non-dimensional velocities.

$$V^\xi = \omega R \left(\frac{H^2 \omega}{v} \right) u \quad 9.7-5$$

$$V^\eta = \omega H \left(\frac{H^2 \omega}{v} \right) w \quad 9.7-6$$

When metric coefficients, equations 9.7-5 and 9.7-6 are substituted into equation 9.7-4, 9.7-7 is obtained.

$$\frac{1}{\lambda r} \left(\frac{\partial}{\partial \xi} \left(r \left(\omega R \frac{H^2 \omega}{v} u \right) \right) + \frac{\partial}{\partial \eta} \left(\lambda r \left(\omega H \frac{H^2 \omega}{v} w \right) \right) \right) = 0 \quad 9.7-7$$

After derivative operations and grouping of constants in 9.7-7, equation 9.7-8 is obtained.

$$\frac{1}{\lambda} \frac{H^2 \omega^2}{\nu} \left(\frac{1}{r} \frac{\partial r}{\partial \xi} R u + \frac{\partial R}{\partial \xi} u + R \frac{\partial u}{\partial \xi} + \frac{1}{r} H \frac{\partial \lambda}{\partial \eta} r w + \frac{1}{r} H \lambda \frac{\partial r}{\partial \eta} w + H \lambda \frac{\partial w}{\partial \eta} \right) = 0 \quad 9.7-8$$

Mogilevskii et al introduced non-dimensional lengths and several scaled relationships; these are shown in equations 9.7-9 through 9.7-12. Equation 9.7-10 is obtained by taking the derivative of 9.7-9; derivative forms of 9.7-9 and 9.7-11 are used in changes of variables.

$$x = \ln \left(\frac{R(\xi)}{R_0} \right) \quad 9.7-9$$

$$\frac{dx}{d\xi} = \frac{1}{R} \frac{dR}{d\xi} \quad 9.7-10$$

$$y = \frac{\eta}{H} \quad 9.7-11$$

$$\beta = \frac{R}{r} \quad 9.7-12$$

$$\varepsilon = \frac{H}{R} \quad 9.7-13$$

Equation 9.7-12 is substituted into the first two terms of equation 9.7-8 yielding equation 9.7-14.

$$R_\xi \left(u \left(1 + \beta \frac{1}{R_\xi} r_\xi \right) \right) \quad 9.7-14$$

Equation 9.7-10 substituted into term 3 of equation 9.7-8 and when added to 9.7-14, yields 9.7-15.

$$R_{\xi} \left(u_x + u \left(1 + \beta \frac{1}{R_{\xi}} r_{\xi} \right) \right) \quad 9.7-15$$

Terms 4 and 5 in equation 9.7-8 can be combined, yielding equation 9.7-16.

$$w \frac{1}{r} H \left(\frac{\partial \lambda}{\partial \eta} r + \lambda \frac{\partial r}{\partial \eta} \right) = w \varepsilon \beta (r \lambda)_{\eta} \quad 9.7-16$$

Equation 9.7-11 is substituted into term 6 of equation 9.7-8, yielding equation 9.7-17.

$$H \lambda \frac{\partial w}{\partial \eta} = \lambda \frac{\partial w}{\partial y} = \lambda w_y \quad 9.7-17$$

When equations 9.7-14 through 9.7-17 are combined, the outcome is equation 9.7-18.

$$R_{\xi} \left[u_x + u \left(1 + \beta \frac{1}{R_{\xi}} r_{\xi} \right) \right] + w_y \lambda + w \varepsilon \beta (r \lambda)_{\eta} = 0 \quad 9.7-18$$

Equation 9.7-18 is the continuity equation as described by equation 9.7-2.

The steps covered in equations 9.7-1 through 9.7-18 are similar to the process of deriving other terms in the publication by Mogilevskii et al; however, they have the added complication of derivatives of unit vectors.

The material derivative consists of temporal and convective terms. The convective components in the ξ direction $[u \cdot \nabla u]_i$, are obtained from equation 9.6-4. First, the temporal time require the introduction of non-dimensional time, t , as shown in equation 9.7-19. Although none of the formulations in this dissertation includes transient behavior,

however, the temporal derivative, being the simplest, indicates the common terms that will be factored out of almost all the other terms in the Navier-Stokes equations.

$$\frac{t}{\omega \left(\frac{H^2 \omega}{\nu} \right)} = t' \quad 9.7-19$$

The non-dimensional temporal term is obtained as shown in equation 9.7-20.

$$\frac{\partial V^\xi}{\partial t'} = \frac{\partial \left[\omega R \left(\frac{H^2 \omega}{\nu} \right) u \right]}{\partial \left[\frac{t}{\omega \left(\frac{H^2 \omega}{\nu} \right)} \right]} = \omega^2 R \left(\frac{H^2 \omega}{\nu} \right)^2 \frac{\partial u}{\partial t} = \omega^2 R E^{-2} \frac{\partial u}{\partial t} \quad 9.7-20$$

Equation 9.7-20 indicates that a common factor of $\omega^2 R$ will appear in all the terms except the body forces which will be divided by $\omega^2 R$ and lead to a Froude number.

The convective terms in the material derivative are obtained using equations 9.6-3 and 9.6-4. The latter, an indicial equation, has a methodical application of operations, and is the preferred approach. Equation 9.6-4 is expanded for the index $i = 1$, or the ξ direction.

The expanded version is shown as equation 9.7-21.

$$[\mathbf{u} \cdot \nabla \mathbf{u}]_1 = \frac{u_1}{h_1} \frac{\partial u_1}{\partial q^1} + \frac{u_2}{h_2} \frac{\partial u_1}{\partial q^2} + \frac{u_3}{h_3} \frac{\partial u_1}{\partial q^3} + \frac{u_1}{h_1 h_1} \left(u_1 \frac{\partial h_1}{\partial q^1} - u_1 \frac{\partial h_1}{\partial q^1} \right) \quad 9.7-21$$

$$+ \frac{u_2}{h_2 h_1} \left(u_1 \frac{\partial h_1}{\partial q^2} - u_2 \frac{\partial h_2}{\partial q^1} \right) + \frac{u_3}{h_3 h_1} \left(u_1 \frac{\partial h_1}{\partial q^3} - u_3 \frac{\partial h_3}{\partial q^1} \right)$$

In equation 9.7-21, the generic indices are replaced with the corresponding coordinate and metric coefficient from the (ξ, θ, η) system.

$$[\mathbf{u} \cdot \nabla \mathbf{u}]_1 = \frac{u}{\lambda} \frac{\partial u}{\partial \xi} + \frac{v}{r} \frac{\partial u}{\partial \theta} + \frac{w}{1} \frac{\partial u}{\partial \eta} + \frac{u}{\lambda^2} \left(u \frac{\partial \lambda}{\partial \xi} - u \frac{\partial \lambda}{\partial \xi} \right) + \frac{v}{r\lambda} \left(u \frac{\partial \lambda}{\partial \theta} - v \frac{\partial r}{\partial \xi} \right) + \frac{w}{\lambda} \left(u \frac{\partial \lambda}{\partial \eta} - w \frac{\partial 1}{\partial \xi} \right) \quad 9.7-22$$

In equation 9.7-22, several terms can be neglected; they are listed as equations 9.7-23 through 9.7-25.

$$u \frac{\partial \lambda}{\partial \xi} - u \frac{\partial \lambda}{\partial \xi} = 0 \quad 9.7-23$$

$$u \frac{\partial \lambda}{\partial \theta} = 0 \quad 9.7-24$$

$$w \frac{\partial 1}{\partial \xi} = 0 \quad 9.7-25$$

$$\frac{v}{r} \frac{\partial u}{\partial \theta} = 0 \quad 9.7-26$$

Thus, equation 9.7-22 is reduced to equation 9.7-27.

$$[\mathbf{u} \cdot \nabla \mathbf{u}]_1 = \frac{u}{\lambda} \frac{\partial u}{\partial \xi} + w \frac{\partial u}{\partial \eta} - \frac{v^2}{r\lambda} \frac{\partial r}{\partial \xi} + u \frac{w}{\lambda} \frac{\partial \lambda}{\partial \eta} \quad 9.7-27$$

The non-dimensional velocity in the θ direction is given by equation 9.7-28. The non-dimensional velocities in the ζ and η directions were previously given by equations 9.7-4 and 9.7-5.

$$V^\theta = \omega R \left(F + \frac{H^2 \omega}{\nu} v \right) \quad 9.7-28$$

After substitution of non-dimensional variables, the first term on the RHS of 9.7-27 generates two components as, shown by expression 9.7-29. These are (a) the fourth term and (b) the second term, both on line 2 in equation 9.7-1.

$$\omega^2 R E^{-2} \lambda^{-1} u^2 R_\xi \quad (a) \quad 9.7-29$$

$$\omega^2 R E^{-2} \lambda^{-1} u R_\xi u_x \quad (b)$$

After substitution of non-dimensional variables, the second term on the RHS of 9.7-27 creates the third term on line 2 of equation 9.7-1; this is given by expression 9.7-30.

$$\omega^2 R E^{-2} w u_y \quad 9.7-30$$

After substitution of non-dimensional variables, the third term on the RHS of 9.7-27 creates three components as shown by expression 9.7-31. In equation 9.7-1, these were (a) the fourth terms on line 1, (b) the fifth term on line 2, and (c) the second term, or centrifugal term, of line 1.

$$-\omega^2 R 2v\lambda^{-1}\beta E^{-1} F r_\xi \quad (a) \quad 9.7-31$$

$$-\omega^2 R E^{-2} \lambda^{-1} v^2 r_\xi \beta \quad (b)$$

$$-\omega^2 R \lambda^{-1} \beta F^2 r_\xi \quad (c)$$

Finally, after substitution of non-dimensional variables, the last term on the RHS of 9.7-27 generates expression 9.7-32, the sixth term on line 2 of equation 9.7-1.

$$\omega^2 R E^{-2} \lambda^{-1} u w \lambda_y \quad 9.7-32$$

The remaining terms from equation 9.7-1 are found by applying a similar process; however, on line 4 the terms are an expansion of a derivative. Since the only viscous force that is important to this dissertation is the second derivative of ξ velocity with respect to η , that term is stated as equation 9.7-33, or the first term on the first line of equation 9.7-1. The

jump to this result does not reveal the tedious algebra required to derive other terms in equation 9.7-1. If derivations of the other terms were included and it included pages of algebra, distraction, rather than further learning would probably be one of the results.

$$\omega^2 R u_{yy} \qquad 9.7-33$$

At this point, sufficient working knowledge of the curvilinear system of Mogilevskii et al has been achieved. The publication that originally seemed cryptic was decrypted with definitions of the metric tensor, derivatives of unit vector with respect to coordinates, and vector operators derived for the specific coordinate system.

Although the ζ momentum equation found in Mogilevskii et al was essentially derived while preparing this dissertation, most of the terms obtained from the Laplacian were left out of to maintain brevity. The other equations found in the paper were not derived and were assumed to result from the same procedure of applying the appropriate vector operators. The hurdle of “breaking into” the art of curvilinear coordinates was overcome.

9.8 Convergence of High Speed Cases

In this section, the “high speed thin film formulation” simplification of equation 9.7-1 is derived. The order of magnitude analysis for the radial coordinate in a cylindrical coordinate system, equation 9.2-41, leaves the viscous force term from the second derivative of radial velocity with respect to the surface normal and the inertial force from the centrifugal term. Although equation 9.2-41 was developed for a disk, it is assumed for a reasonably similar bell profile, the orders of magnitude remain relevant when applied to equation 9.7-1.

The centrifugal term enters the analysis either through the Greenspan [86] formulation or through a kinematic substitution [59], [58]. The constant polar angle spherical kinematic formulation of the fluid velocity as seen by the rotating observer is shown as equation 9.8-1, earlier as equation 8.6-1.

$$v'_{\phi} = -v_{\phi} + \omega r \sin \beta \quad 9.8-1$$

In a curvilinear system the perpendicular distance to the differential parcel of fluid on the bell surface is $R(\xi)$. The inertially-correct velocity in the curvilinear system is described by equation 9.8-2.

$$v'_{\theta} = -v_{\theta} + \omega R(\xi) \quad 9.8-2$$

If v_{θ}^2 is entered into the convective derivative term responsible for describing the centrifugal force within the third term on the RHS of equation 9.7-27, the terms in expression 9.8-3 are obtained.

$$-\rho \frac{1}{r\lambda} (v_{\theta}'^2 - 2v_{\theta}' R(\xi)\omega + R(\xi)^2\omega^2) \frac{\partial r}{\partial \xi} \quad 9.8-3$$

The component of expression 9.8-3 that survives the order of magnitude analysis is the third term.

The only component of viscous force that survives the order of magnitude analysis is generated inside the first term on the RHS of equation 9.6-6 or the third term of the LHS of 9.6-5, both of which are equal to the $\frac{\partial^2}{\partial \eta^2}$ term of the Laplacian acting on v_{ξ} . This term is given by equation 9.8-4, which is further simplified for a thin film because λr is essentially constant in the film.

$$\frac{\mu}{\lambda r} \frac{\partial}{\partial \eta} \left(\lambda r \frac{\partial v_{\xi}}{\partial \eta} \right) = \mu \frac{\partial^2 v_{\xi}}{\partial \eta^2} \quad 9.8-4$$

If the other surviving components of the order of magnitude analysis are substituted back into the Navier-Stokes equation in the ξ direction, equation 9.8-5 is obtained.

$$-\frac{\rho}{\mu} \frac{1}{r(\xi, \eta)\lambda} R(\xi)^2 \omega^2 \frac{\partial r}{\partial \xi} = \frac{\partial^2 v_{\xi}}{\partial \eta^2} \quad 9.8-5$$

On, or near the surface of a bell is a thin film condition, i.e. where $\eta \ll R$, λ approaches 1, $r(\xi, \eta) \approx r(\xi, 0) = R(\xi)$, and $r_{\xi} = R_{\xi}$. Equation 9.8-5 simplifies further to equation 9.8-6.

$$-\frac{\rho}{\mu}R\omega^2R\xi = \frac{\partial^2 v_\xi}{\partial \eta^2} \quad 9.8-6$$

Recalling the thin film formulations in the spherical and cylindrical coordinate systems of Table 8.7-1, the bell cross sectional profiles were defined by a coordinate axis. Moreover, the most reduced equation of motion consists of a “centrifugal force” with a component parallel to the surface of the bell and a viscous force proportional to the second derivative of velocity parallel to the bell surface with respect to a normal to the bell surface. In the case of a disk, the equation of motion is equation 9.8-7; and Figure 9.8-1 illustrates the centrifugal force and the velocity parallel to the bell surface.

$$-\frac{\rho\omega^2}{\mu}R = \frac{\partial^2 v_r}{\partial z^2} \quad 9.8-7$$

On a disk, they are collinear as illustrated by Figure 9.8-1.

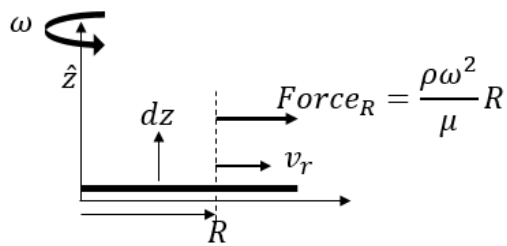


Figure 9.8-1 Cylindrical System

In the case of a cone, the equation of motion is equation 9.8-8 , and illustrates the forces and geometry.

$$-\frac{\rho\omega^2}{\mu} R \sin \beta \sin \beta = \frac{\partial^2 v_r}{r^2 \partial \theta^2} \quad 9.8-8$$

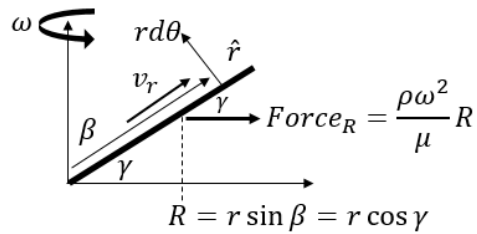


Figure 9.8-2 Spherical System: Constant Polar Angle

Finally, in the case of a constant radius in a spherical system, the equation of motion is 9.8-9, and Figure 9.8-3 illustrates the angle between the centrifugal force and the surface tangent, along with the interpretation of the cosine of γ .

$$-\frac{\rho\omega^2}{\mu} R \frac{\sqrt{\mathcal{R}^2 - R^2}}{\mathcal{R}} = \frac{\partial^2 v_\theta}{\partial r^2} \quad 9.8-9$$

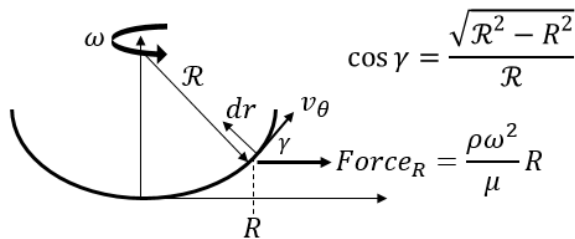


Figure 9.8-3 Spherical System: Constant Radius

A distinct pattern exists in equations 9.8-7 through 9.8-9 even though they are in different coordinate systems or different configurations of the same coordinate system and are expressed with different coordinates. In each case, a centrifugal term that is a function of fluid properties of density and absolute viscosity is multiplied by a distance perpendicular to the axis of rotation; this product is multiplied by the cosine of the angle between the said perpendicular and the bell surface tangent in an outward direction. The pattern in the thin film equations of motion at a point on the surface of the bell is summarized by equation 9.8-10.

$$-\frac{\rho\omega^2}{\mu}R \cos\gamma = \frac{\partial^2 v_{tangent}}{\partial n_{normal}^2} \quad 9.8-10$$

In the case of an arbitrary bell, but within the norms of the art, the equations of motion could be applied as a piecewise radial or conical analysis with different variables and coordinates depending on the location in the bell profile. What is proposed in this dissertation is to define the bell profile as a function of x in a Cartesian system as shown in Figure 9.8-4.

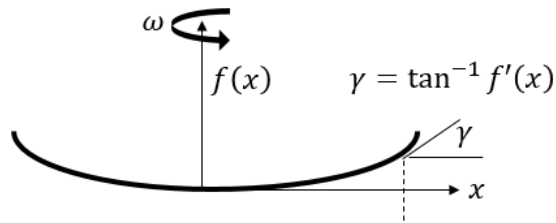


Figure 9.8-4 Bell profile as $f(x)$

With the visualization of Figure 9.8-4 “substituted” into equation 9.8-10, equation 9.8-11 results, which describes the equation of motion in a thin fluid film on an arbitrary profile bell.

$$-\frac{\rho\omega^2}{\mu}R \cos(\tan^{-1}(f'(x))) = \frac{\partial^2 v_{tangent}}{\partial n_{normal}^2} \quad 9.8-11$$

Equation 9.8-11 is not a “Navier-Stokes equation”. It can be described as the product of pattern matching, or an industrial approximation, but it is not rigorous physics. A Production Engineer, with a calculus background, could integrate this equation and, thereby, calculate the film thickness on an arbitrary bell profile. In other words, the IR4TD mission of harvesting basic research and bringing it to the production environment has been accomplished for this task. The Production Engineer knowledge can extend beyond the confines of cones, disks, or spheres; instead, their mental model could include a bell with a blended profile. However, even with the benefit of this result, it is not without baggage. Under certain circumstances, a thickening film could be calculated, but it may not reflect the reality and complexity of nature. In the next chapter, publications will be presented that support a relatively short region on the bell where the film thickens.

The overlap between the Cartesian system and the curvilinear system of is shown in Figure 9.8-5.

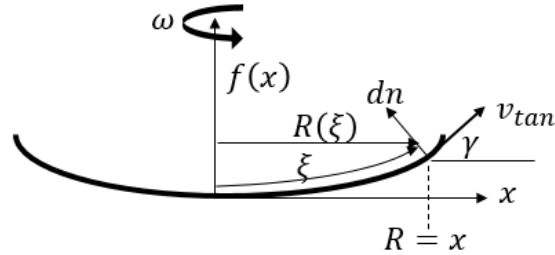


Figure 9.8-5 Cartesian & Curvilinear Systems

A statement of synthesis from Figure 9.8-5 is expressed by equation 9.8-12 and simplified further in equation 9.8-13.

$$\cos \gamma = \cos(\tan^{-1}(f'(x))) = \frac{\partial r(\xi, \eta = 0)}{\partial \xi} = \frac{\partial r}{\partial \xi} = r_{\xi} = \frac{\partial R}{\partial \xi} = R_{\xi} \quad 9.8-12$$

$$\cos(\tan^{-1}(f'(x))) = R_{\xi} \quad 9.8-13$$

Therefore the question - “is there a reduced formulation of the Navier-Stokes equation that is equal to equation 9.8-11?” has been answered. Equation 9.8-6 is equal to equation 9.8-11 and this is given by equation 9.8-14.

$$-\frac{\rho}{\mu} R \omega^2 R_{\xi} = \frac{\partial^2 v_{\xi}}{\partial \eta^2} = -\frac{\rho \omega^2}{\mu} R \cos(\tan^{-1}(f'(x))) = \frac{\partial^2 v_{tangent}}{\partial n_{normal}^2} \quad 9.8-14$$

The key to equation 9.8-14 is the trigonometric relationship shown by equation 9.8-15.

$$R_{\xi} = \cos(\tan^{-1}(f'(x)))$$

9.8-15

Equation 9.8-6 is the most reduced case of continuous curvilinear implementation of the Navier-Stokes equation describing a thin film on a high-speed bell. On the other hand, equation 9.8-11 is an approximation only applicable for a thin film.

Therefore, equation 9.8-11 is proven as an acceptable approximation for describing the radial momentum of a thin film of fluid on a rotary bell. The unknown film thickness is found by integrating the velocity profile and then equating it to the centrally supplied flow.

Further research or work in this area that includes free surface boundary conditions, initial fluid velocity conditions from a radial inlet, and transient behavior would overshadow the work contained in this dissertation.

10.1 Film thickness Calculation

This section references two publications that included numerical modeling of paint atomization by means of a rotary bell. Geometry and film thicknesses data are referenced; however, illustrations are redrawn to protect copyrights. Equation 9.8-11 is shown again as equation 10.1-1, and includes more compact notation.

$$-K = -\frac{\rho\omega^2}{\mu}R \cos \gamma = \frac{\partial^2 v_{tangent}}{\partial n_{normal}^2} = v_{nn} \quad 10.1-1$$

After integrating equation 10.1-1 with no slip and no shear boundary conditions, equation 10.1-2 that describes the outward velocity profile is obtained.

$$v = K \left(hn - \frac{n^2}{2} \right) \quad v'(h) = 0, v(0) = 0 \quad 10.1-2$$

If the outward velocity profile is integrated over a surface at the radial position, R , and over the unknown height, h , and then equated to the flow, Q , as indicated by equation 10.1-3, the film thickness normal to the bell surface can be found.

$$Q = 2\pi RK \int_0^h \left(hn - \frac{n^2}{2} \right) dn = 2\pi RK \frac{h^3}{3} \quad 10.1-3$$

An equation for the film thickness, h , as function of flow parameters and bell profile is shown as equation 10.1-4.

$$h = \sqrt[3]{\frac{3Q\mu}{\rho 2\pi R^2 \omega^2 \cos \gamma}}$$

A bell profile was scaled from an illustration found in Domnick et al [91]. It consists of a conical section with a slope angle of about 28 degrees up to a radius of about 30 mm, and then blends into another conical section with slope of about 60 degrees out to a radius of about 31.5 mm. The fluid had a viscosity of about .086 Pa-s viscosity, and a density approximated as 1.0 gram per cc. Two RPM's are shown in Figure 10.1-1, one at 40,000 and another at 60,000; this plot agrees exactly with the Domnick et al data.

Another publication by Shen et al [83] did not contain enough details to recreate their work, however, their thickness measurements illustrated a film that was increasing in thickness within the concave profile near the periphery of the bell.

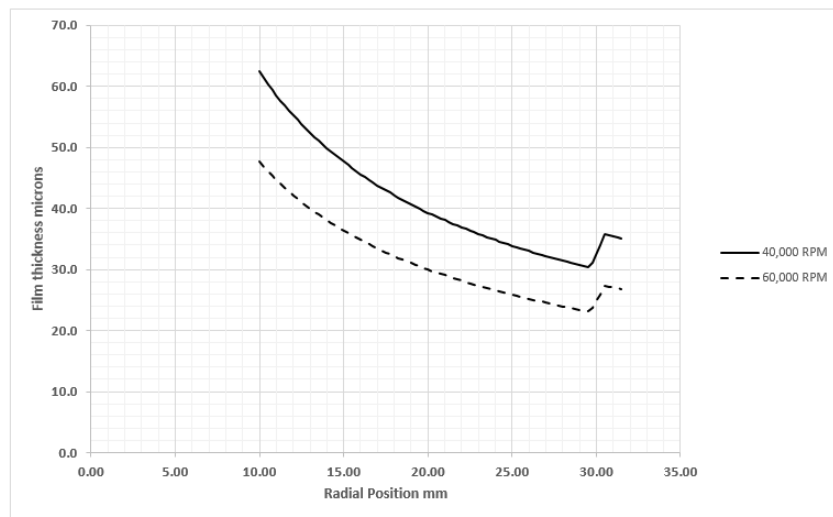


Figure 10.1-1 Film Thickness Example

The agreement between Figure 10.1-1 and the work of Domnick et al [91] indicates the analytical solution they used produced similar results as the approximation developed in this dissertation; however, their solution was not disclosed in their publication. On the other hand, the reference cited by Domnick et al for their analytical solution [92] of film thickness at the edge of the bell, uses a film thickness equation for a “cup atomizer” that is geometrically and algebraically equal to equation 10.1-4, though in a different form. This shows that other researchers are using the same approximation as pointed out in this dissertation. This dissertation proved that a simplified case of the Navier-Stokes equations that were cast into a surface following coordinate system yields the same solution; however, the surface following case has the ability to be “reversed” into the full Navier-Stokes equations. The advantage of the approximation developed in this dissertation is the bell profile is expressed as a function of the abscissa in a Cartesian coordinate system, whereas other formulations are expressed as functions of the cone angle.

Furthermore, in this same paper by Domnick et al, a Volume of Fluid (VOF) calculation performed using the commercial CFD code FLUENT generated film thickness results for the edge of the bell under the same conditions. In the case of 60,000 RPM, the calculated film thickness was 22 microns, and in the case of 40,000 RPM, the calculated film thickness was 30 microns. Both FLUENT cases reasonably agree with the analytical calculations.

Recalling a reference from the literature review, Symons and Bizard [81] validate equation 10.1-4, although expressed in a different form in their work, with experimental measurements. In their paper, the analytical solution and measurement data are well within reasonable agreement. However, in their experiments, RPM’s were lower, and the radial

positions were larger, than rotary bells used in automotive painting applications. Their work was a unique non-contact method.

Hinze and Milborn [34] experimentally validated their theoretical work, which includes a form of equation 10.1-4, however, their analysis generated models for other behaviors, such as the of spiral fluid flow inside the cup. In their paper, they show photographs where they correctly predicted the pitch of the spiral pattern by means of an injected dye.

10.2 Conclusion

At the start of the research for this dissertation, a stated goal was difficult to enunciate; hence, at the beginning, it was necessary to become immersed into the art and science of fluid atomization, from which a constant though was to be on the lookout for opportunities to contribute.

Although solutions for fluid film characteristics on a spinning object are ubiquitous in the literature, however, conical or disk geometries seemed to be most common while spherical applications were found in the area of optical coatings. On the other hand, some bells seemed to have blended profiles that were conical and variable concave. A natural follow on question seemed obvious: how are the film characteristics defined when the bell profile does not fit one of the convenient common coordinate systems?

Based on the models found in the literature, equation 9.8-11 seemed obvious and yielded the correct answer for one published bell profile. However, it is an approximation or maybe a pattern match, an industrial shortcut or an extrapolation, but it is not strictly black letter fluid mechanics.

As it turns out, this approximation is the most reduced case of an outstanding analysis and publication that defined the bell by a unique curvilinear coordinate system. Unfortunately, a significant mathematical hurdle had to be overcome on the path to understanding this work. Once this hurdle was overcome, the analysis seemed trivial and illuminated the real issue with film models that predict an increasing film thickness because of a varying profile. Unlike cones and disk, which have constant geometry theoretically extending to infinity, the effects of an “arbitrary” profile cannot be generalized. Regardless, the film

properties on an “arbitrary” bell can be modelled, but the allowable extent of increasing thickness is unknown. Bell designs that are essentially conical, and typically near the periphery, a short concave radius exists. This approximation from this dissertation offers a solution in the relatively short distance where the film thickens.

Therefore, probably the most significant contribution to the body of knowledge from this dissertation is the development and justification for use of the approximation model of a thin film on an arbitrary bell that proves it is the reduced formulation of the Navier-Stokes formulation. A collateral result is a trail of learning for myself and others that want to explore this type of continuum mechanics problem. The metric tensor, general derivatives of unit vectors and general vector invariants did not seem trivial on the other side of the learning hurdle.

The next significant contribution was a publication on the reduction of order achieved by understanding the complex plane symmetry for solutions of velocity profiles on a spinning cone that include centrifugal and Coriolis forces. In the past, several publications had referenced this technique as a procedure; however, none had explained it. In reality, the underlying mathematical explanation was more interesting than the solution.

The remaining teachable contributions such as a MatLab solution of the Von Karman problem or formulations of the absolute velocity on a spinning device, or cross product intricacies in a spherical system, all have presence in the literature. The solutions detailed in this dissertation are based on the assumption that the next reader is new to the field and would appreciate the more detailed explanation.

11.1 Publication I

Reduction of Order: Analytical Solution of Film Formation in the Electrostatic Rotary Bell Sprayer

Abstract: This brief paper explains the slight differences in governing equations for a fluid film in a spinning cone, and the mechanism that reduces the order of a solution. Spinning cones with a centrally supplied fluid that spreads over its inner surface as a thin film have been the subject of interest for many years. Though often cast as a mathematical analysis, understanding this process is important, especially in the application of automotive painting. The analysis consists of a system of equations obtained from the Navier–Stokes equations along with simple boundary conditions that describe radial and tangential momentum conservation. Solutions to this system of equations are shown using several techniques. The connection between these techniques is slightly subtle. However, the conditions that enable reduction of order are clear once they are exposed. Directional velocity profiles in the film can be a combination of four roots in the complex plane. This system of roots also contains two diagonal axes of symmetry that are offset by 90 degrees. Alternatively, if the radial and tangential velocity profiles are expressed as a single complex function, a reduced order solution that is a combination of one set of diagonal set of roots can be found.

11.2 Publication II

Spatial Positioning and Operating Parameters of an Electrostatic Rotary Bell Sprayer (ERBS): a 3D Mapping of Droplet Size Distributions

Abstract: The fundamental physical behavior during droplet formation and flow from a rotary bell spray in the absence of an electrostatic field were measured and evaluated. The impact of a wide range of operating parameters of the rotary bell spray on the droplet sizes and size distributions using a three-dimensional (3-D) mapping technique were determined. The effects of fluid flow rates and rotational speed of the rotary bell on the spray profiles at various vertical and horizontal locations within the spray flowfield were measured. The results showed that increasing the rotational speed caused the Sauter mean diameter of the droplets to decrease significantly. The high-speed rotary bell atomizer produced an axisymmetric spray cross-section that was donut-shaped (toroidal) closer to the bell cup; this shape was a consequence of the interaction between liquid droplet motions at the cup edge with the shaping airflow. This interaction created a vortex motion, which then formed a toroid-shaped vortex ring which momentarily trapped larger droplets. Hence, a noticeable increase in droplet sizes was measured toward the edge of the spray field in its radial direction for locations close to the cup.

11.3 Publication III

Advances in Automotive Conversion Coatings during Pretreatment of the Body Structure: A Review

Abstract: Automotive conversion coatings consist of layers of materials that are chemically applied to the body structures of vehicles before painting to improve corrosion protection and paint adhesion. These coatings are a consequence of surface-based chemical reactions and are sandwiched between paint layers and the base metal; the chemical reactions involved distinctly classify conversion coatings from other coating technologies. Although the tri-cationic conversion coating bath chemistry that was developed around the end of the 20th century remains persistent, environmental, health, and cost issues favor a new generation of greener methods and materials such as zirconium. Environmental forces driving lightweight material selection during automobile body design are possibly more influential for transitioning to zirconium than the concerns regarding the body coating process. The chemistry involved in some conversion coatings processing has been known for over 100 years. However, recent advances in chemical processing, changes in the components used for vehicle body structures, environmental considerations and costs have prompted the automobile industry to embrace new conversion coatings technologies. These are discussed herein along with a historical perspective that has led to the use of current conversion coatings technologies. In addition, future directions for automobile body conversion coatings are discussed that may affect conversion coatings in the age of multi-material body structures.

REFERENCES

1. Omar, M.; Hassan, M.I.; Saito, K.; Alloo, R. Ir self-referencing thermography for detection of in-depth defects. *Infrared Physics and Technology* **2005**, *46*, 283-289.
2. Omar, M.; Gharaibeh, B.; Salazar, A.J.; Saito, K. Infrared thermography and ultraviolet fluorescence for the nondestructive evaluation of ballast tanks' coated surfaces. *The NDT and E International Journal* **2007**, *40*, 62-70.
3. Salaimeh, A.; Gharaibeh, B.; Campion, J.; Evans, M.; Saito, K. Real-time quantification of viable bacteria in liquid medium using infrared thermography. *Infrared Physics and Technology* **2011**, *54*.
4. Salaimeh, A.; Gharaibeh, B.; Campion, J.; Evans, M.; Saito, K. Real-time quantification of staphylococcus aureus in liquid medium using infrared thermography. *Infrared Physics and Technology* **2012**, *55*, 17-172.
5. Poozesh, S.; Akafuah, N.K.; Saito, K.; Grana, J. Comprehensive examination of a new mechanism to produce small droplets in droplet-on-demand inkjet technology. *Applied Physics A* **2016**, *122* 1-12
6. Poozesh, S.; Setiawan, N.; Akafuah, N.K.; Saito, K.; Marsac, P. Assessment of predictive models for characterizing the atomization process in a spray dryer's bi-fluid nozzle. *Chemical Engineering Science* **2018**, *180*, 42-51
7. Toda, K.; Salazar, A.J.; Saito, K. *Automotive painting technology: A monozukuri-hitozukuri perspective*. 2012.
8. Srinivasan, V.; Salazar, A.J.; Saito, K. Modeling the disintegration of modulated liquid jets using volume-of-fluid (vof) methodology. *Applied Mathematical Modeling* **2011**, *35*, 3170-3130.
9. Srinivasan, V.; Salazar, A.J.; Saito, K. Numerical simulation of the disintegration of forced liquid jets using volume-of-fluid (vof) method. *Computational Fluid Dynamics* **2010**, *24*, 317-333.
10. Akafuah, N.K.; Salazar, A.J.; Saito, K. Infrared thermography-based visualization of droplet transport in liquid sprays. *Infrared Physics and Technology* **2010**, *53*, 218-226.
11. Akafuah, N.K.; Salazar, A.J.; Saito, K. Estimation of liquid volume fraction and droplet number density in automotive paint spray using infrared thermography-based visualization technique. *Atomization and Sprays* **2009**, *19*, 847-861.
12. Srinivathan, V.; Salazar, A.J.; Saito, K. Numerical investigation on the disintegration of round turbulent liquid jets using les/vof techniques. *Computer Modeling and Simulation in Engineering* **2008**, *18*, 1-47.
13. Viti, V.; Salazar, A.J.; Saito, K. A numerical study of the coupling between the flow field and the electrostatic field inside an automobile spray paint booth. *IASME Transactions* **2005**, *2*, 261-269
14. Salazar, A.J.; McDonough, J.M.; Saito, K. Computational fluid dynamics simulation of automotive spray painting process. *Computer Modeling and Simulation in Engineering* **1997**, *2*, 131-133.
15. Doerre, M.; Hibbitts, L.; Patrick, G.; Akafuah, N. Advances in automotive conversion coatings during pretreatment of the body structure: A review. *Coatings* **2018**, *8*.

16. Darwish Ahmad, A.; Singh, B.B.; Doerre, M.; Abubaker, A.M.; Arabghahestani, M.; Salaimah, A.A.; Akafuah, N.K. Spatial positioning and operating parameters of a rotary bell sprayer: 3d mapping of droplet size distributions. *Fluids* **2019**, *4*, 165.
17. Wilson, J.E.; Grib, S.W.; Darwish Ahmad, A.; Renfro, M.W.; Adams, S.A.; Salaimah, A.A. Study of near-cup droplet breakup of an automotive electrostatic rotary bell (esrb) atomizer using high-speed shadowgraph imaging. *Coatings* **2018**, *8*, 174.
18. Darwish Ahmad, A.; Abubaker, A.M.; Salaimah, A.A.; Akafuah, N.K. Schlieren visualization of shaping air during operation of an electrostatic rotary bell sprayer: Impact of shaping air on droplet atomization and transport. *Coatings* **2018**, *8*, 279.
19. Williams, F.A. The role of theory in combustion science. In *Twenty-Fourth Symposium (International) on Combustion*, The Combustion Institute: 1992.
20. Feynman, R. *The feynman lectures on physics*. Basic Books: New York City, USA, 2010; Vol. 1.
21. Moore, C. Insect destroyer. 656,774, 1900.
22. Crosbie, S. 1,149,810 1915.
23. Hopkins, R.Z. Method of applying lacquer on the like. 1,861,475, 1929.
24. Hadley, W.E. Portable tar spaying machine. 2,151,100, 1939.
25. Salsas-Serra, F. Atomizer for liquids. 2,166,772, 1939.
26. Smart, W.L. Liquid feeding apparatus. 2,728,607, 1955.
27. Sedlassik, J. Dual atomization and electrostatic deposition means. 3,000,574, 1961.
28. Mitsui, M. Improved rotary paint atomizing device. 4,458,844, 1984.
29. Vetter, K. Sprayer. 4,518,119, 1985.
30. Metcalfe, R.; Bordeau, R. Rotary atomization means for the production of metal powder. 4,207,040, 1980.
31. Matsumoto, S.; Saito, K.; Takashima, Y. Phenomenal transition of liquid atomization from disk *Journal of Chemical Engineering Japan* **1974**, *7*, 13-19.
32. Sun, H.; Chen, G.; Wang, L.n.; FeiWang. Ligament and droplet generation by oil film on a rotating disk. *International Journal of Aerospace Engineering* **2015**, *2015*, 14.
33. Walton, W.H.; Prewett, W.C. The production of sprays and mists of uniform drop size by means of spinning disc type sprayers. *Proceedings of the Physical Society* **1949**, *62*, 341-350.
34. Hinze, J.O.; Milborn, H.J. The atomization of liquids by means of a rotating cup. *Journal of Applied Mechanics* **1950**, *17*, 147-153.
35. Dixon, B.E.; Russell, A.A.W.; Swallow, J.E.L. Liquid films formed by means of rotating disks. *British Journal of Applied Physics* **1952**, *3*, 115-119.
36. Fraser, R.P.; Dombrowski, N.; Routley, J.H. The production of uniform liquid sheets from spinning cups. *Chemical Engineering Science* **1963**, *18*, 315-321.
37. Dombrowski, N.; Johns, W.R. The aerodynamic instability and disintegration of viscous liquid sheets. *Chemical Engineering Science*, **1963**, *18*, 203-214.
38. Dombrowski, N.; Johns, W.R. The aerodynamic instability and disintegration of viscous liquid sheets - erratum. *Chemical Engineering Science* **1963**, *18*, 470.
39. Chuech, S.G. Spatial instability of a viscous liquid sheet. *International Journal for Numerical Methods In Fluids* **2006**, *50*, 1461-1474.

40. Kamiya, T.; Kayano, A. Disintegration of viscous fluid in the ligament state purged from a rotating disk. *Journal of Chemical Engineering Japan* **1971**, *4*, 364-369.
41. Kamiya, T.; Kayano, A. Film-type disintegration by rotating disk. *Journal of Chemical Engineering of Japan* **1972**, *5*, 174-182.
42. T. Kamiya. An analysis of the ligament-type disintegration of thin liquid film at the edge of a rotating disk. *Journal of Chemical Engineering Japan* **1972**, *5*, 391-396.
43. Rauscher, J.W.; Kelly, R.E.; Cole, J.D. An asymptotic solution for the laminar flow of a thin film on a rotating disk. *Journal of Applied Mechanics* **1973**, *March*, 43-47.
44. Dombrowski, N.; Lloyd, T.L. Atomisation of liquids by spinning cups. *The Chemical Engineering Journal* **1974**, *8*, 63-81.
45. Dombrowski, N.; Boize, L. The atomization characteristics of a spinning disk ultra low volume applicator. *Journal Agricultural Research Engineering* **1976**, *21*, 87-99.
46. Frost, A.R. Rotary atomization in the ligament formation mode. *Journal Agricultural Research Engineering* **1981**, *26*, 63-78.
47. Li, Y.; Sisoiev, G.M.; Shikhmurzaev, Y.D. Spinning disk atomization: Theory of the ligament regime. *PHYSICS OF FLUIDS* **2018**, *30*.
48. Dombrowski, N.; Lloyd, T.L. Atomisation of liquids by spinning cups. *The Chemical Engineering Journal*, **1974**, *8*.
49. Kawase, Y.; De, A. Ligament-type disintegration of non-newtonian fluid in spinning disk atomization. *Journal of Non-Newtonian Fluid Mechanics*, **1982**, *10*, 367-371.
50. Hina, S.; Shafique, A.; Mustafa, M. Numerical simulations of heat transfer around a circular cylinder immersed in a shear-thinning fluid obeying cross model. *Physica A* **2020**, *540*.
51. Dunsikii, V.F.; N. V. Nikitin; Shul'ginova, G.A. Atomization by a rotating disk of liquids which poorly wet its surface. *Translated from Inzhenerno-Fizicheskii Zhurnal* **1985**, *48*.
52. Alcock, R.; Froehlich, D. Analysis of rotary atomizers. *Transactions of the ASAE* **1986**, *29*, 1514-1519.
53. Yangisawa, M. Slip effect for thin film liquid on a rotating disk. *American Institute of Physics* **1986**, *61*, 1034-1037.
54. Sisoiev, G.M.; Taldrik, A.F.; Shkadov, V.Y. Flow of a viscous liquid film on the surface of a rotating disk. *Translated from Inzhenerno-Fizicheskii Zhurnal* **1987**, *51*, 571-575.
55. Sisoiev, G.M.; Shkadov, V.Y. Flow stability of a film of viscous liquid on the surface of a rotating disk. *Translated from Inzhenerno-Fizicheskii Zhurnal* **1987**, *51*, 571-575.
56. Middleman, S. The effect of induced air-flow on the spin coating of viscous liquids. *Journal of Applied Physics* **1987**, *62*, 2530-2532.
57. Sato, M. Formation of uniformly sized liquid droplets using a spinning disk under applied electrostatic field. *IEEE Transaction on Industry Applications* **1991**, *27*, 316-322.

58. Makarytchev, S.V.; Xue, E.; Langrish, T.A.G.; Prince, R.G.H. On modelling fluid flow over a rotating conical surface. *Chemical Engineering Science* **1997**, *52*, 1055-1057,.
59. Bruin, S. Velocity distributions in a liquid film flowing over a rotating conical surface. *Chemical Engineering Science* **1969**, *24*, 1647-1654.
60. Birnie, D.P.; Manley, M. Combined flow and evaporation of fluid on a spinning disk. *Physics of Fluids* **1996**, *9*, 870-875.
61. Momoniat, E.; Mason, D.P. Investigation of the effect of the coriolis force on a thin fluid film on a rotating disk. *International Journal of Non-Linear Mechanics* **1999**, *13*, 1069-1087.
62. Leneweit, G.; Roesner, K.G.; Koehler, R. Surface instabilities of thin liquid film flow on a rotating disk. *Experiments in Fluids* **1999**, *26*.
63. Wang, C.Y. Flow over a surface with parallel grooves. *Physics of Fluids* **2003**, *15*, 1114-1121.
64. Domnick, J.; Scheibe, A.; Ye, Q. The electrostatic spray painting process with high-speed rotary bell atomizers: Influences of operating conditions and target geometries In *International Conference on Liquid Atomization and Spray Systems (ICLASS) Europe, I.f.L.A.a.S.S.-I.-.* Ed. Sorrento, Italy, 2003.
65. Domnick, J.; Scheibe, A.; Ye, Q. The simulation of the electrostatic spray painting process with high-speed rotary bell atomizers. Part i: Direct charging. *Particle & Particle System Characterization* **2005**, *22*, 141-150.
66. Domnick, J.; Scheibe, A.; Ye, Q. The simulation of the electrostatic spray painting process with high-speed rotary bell atomizers. Part i: External charging. *Particle & Particle System Characterization* **2006**, *23*, 408-416.
67. Matar, O.K.; Lawrence, C.J. The effect of surfactant on the flow of a thin liquid film over a spinning disc. *Chemical Engineering Science* **2006**, *61*, 1074-1091.
68. Chuech, S.G. Spatial instability of a viscous liquid sheet. *International Journal for Numerical Methods in Fluids* **2006**, *50*, 1461-1474.
69. Ogasawara, S.; Daikou, M.; Hachinohe, A.; Inamura, T.; Hirosaki, A.; Saito, Y.; Matsuhita, Y.; Aoki, H.; Miura, T.; Sendai, M. Atomization of liquid issued from an ultra high-speed rotary bell. In *International Conference On Liquid Atomization & Spray Systems, ICLASS, Ed. Vail, Colorado, 2009*.
70. Fukuta, K.; Murate, M.; Ohashi, Y.; Toda, K. New rotary bell for metallic paint application. *Metal Finishing* **1993**, *October*, 39-42.
71. Mogilevskii, E.I.; Shkadov, V.Y. Thin viscous fluid film flows over rotating curvilinear surfaces. *Fluid Dynamics* **2009**, *44*, 189-201.
72. Kim, T.-S.; Kim, M.-U. The flow and hydrodynamic stability of a liquid film on a rotating disc. *Fluid Dynamics Research* **2009**, *41*, 28.
73. Sisoiev, G.M.; Goldgof, D.B.; Korzhova, V.N. Stationary spiral waves in film flow over a spinning disk. *Physics of Fluids* **2010**, *22*.
74. Ogasawara, S.; Daikoku, M.; Shirota, M.; Inamura, T.; Saito, Y.; Yasumura, K.; Shoji, M.; Aoki, H.; Miura, T. Liquid atomization using a rotary bell cup atomizer. *Journal of Fluid Science and Technology* **2010**, *5*, 464-474.
75. Ahmed, M.; Youssef, M.S. Characteristics of mean droplet size produced by spinning disk atomizers. *Journal of Fluids Engineering* **2012**, *134*, 071103-071101-071103-071109.

76. Junxiang, L.; Qingbo, Y.; Qiang, G. Experimental investigation of liquid disintegration by rotary cups. *Chemical Engineering Science* **2012**, *73*, 44-50.
77. Tirumkudulu, M.S.; Paramati, M. Stability of a moving radial liquid sheet: Time-dependent equations. *Physics of Fluids* **2013**, *25*.
78. Ahmed, M.; M.S.Youssef. Influence of spinning cup and disk atomizer configurations on droplet size and velocity characteristics. *Chemical Engineering Science* **2014**, *107*, 149-157.
79. Bizjan, B.; Širok, B.; Hočevár, M.; AlenOrbanić. Ligament-type liquid disintegration by a spinning wheel. *Chemical Engineering Science* **2014**, *116*, 172-182.
80. Yang, S.; Bayanheshig; Zhao, X.L.; Xing, S.; Jiang, Y.X.; Wu, N.; Jiao, Q.B.; Li, W.H.; Tan, X. Establishment and experimental verification of the photoresist model considering interface slip between photoresist and concave spherical substrate. *AIP ADVANCES* **2015**, *5*.
81. Symons, D.D.; Bizard, A.F.M. Measurement of fluid flow thickness within a rotating cone. *Journal of Fluids Engineering* **2015**, *137*.
82. Constantin, A.; Johnson, R.S. An exact, steady, purely azimuthal equatorial flow with a free surface. *American Meteorological Society* **2016**, *June*.
83. Shen, B.; Ye, Q.; Tiedje, O.; Domnick, J. Primary breakup of liquids using a high-speed rotary bell atomizer for spray painting processes. In *28th Conference on Liquid Atomization and Spray Systems*, 2017, I.E., Ed. Valencia, Spain, 2017.
84. Constantin, A.J., R S. An exact, steady, purely azimuthal equatorial flow with a free surface. *Journal of Physical Oceanography* **2016**, *46*, 1935-1945.
85. Stewart, R.H. *Introduction to physical oceanography*. Department of Oceanography, Texas A&M University: Texas A&M University, 2009.
86. Greenspan, H.P. *The theory of rotating fluids*. University Printing House, Cambridge: Cambridge, 1968.
87. Doerre, M.; Akafuah, N. Reduction of order: Analytical solution of film formation in the electrostatic rotary bell sprayer. *Symmetry* **2019**, *11*.
88. Happel, J.; Brenner, H. *Low reynolds number hydrodynamics*. Martinus Nijhoff Publishers: Boston, 1983.
89. Weisstein, E.W. Weisstein, eric w. "Convective operator." From mathworld--a wolfram web resource. <http://mathworld.Wolfram.Com/convectiveoperator.Html>
90. Fitzpatrick, R. *Theoretical fluid mechanics*. IOP Publishing Ltd 2017.
91. Domnick, J.; Scheibe, A.; Ye, Q. Simulation of the film formation at a high-speed rotary bell atomizer used in the automotive spray painting process. In *ILASS 2008*, ILASS: Como Lake, Italy, 2008.
92. Bayvel, L.; Orzechowski, Z. *Liquid atomization* Taylor & Francis: Washington DC, USA, 1993.

VITA

Mark Doerre

Education

PhD Mechanical Engineering - April 2020
University of Kentucky, Lexington, KY

MS Mechanical Engineering - September 1984
Massachusetts Institute of Technology, Cambridge, MA

BS Mechanical Engineering - July 1981
Worcester Polytechnic Institute, Worcester, MA

Publications

Advances in Automotive Conversion Coatings during Pretreatment of the Body Structure: A Review [15]

Reduction of Order: Analytical Solution of Film Formation in the Electrostatic Rotary Bell Sprayer [87]

Spatial Positioning and Operating Parameters of an Electrostatic Rotary Bell Sprayer (ERBS): a 3D Mapping of Droplet Size Distributions [16]

Professional Experience

Mark worked as an Engineer for General Electric Turbine Business Group, IBM Office Products Division, and Lexmark, formerly IBM, for a total of 36 years. He retired in 2016 and obtained a PhD in 2020. Future second career interests include teaching engineering.